AD-A159 770 NONLINEAR MOTIONS AND FORCES ON TENSION LEG PLATFORMS 1/2
(U) SCIENCE APPLICATIONS INC ANNAPOLIS MD
N SALVESEN ET AL. MAY 84 USCG-M-84-4 DTCG23-83-C-20064
UNCLASSIFIED F/G 13/10 NL

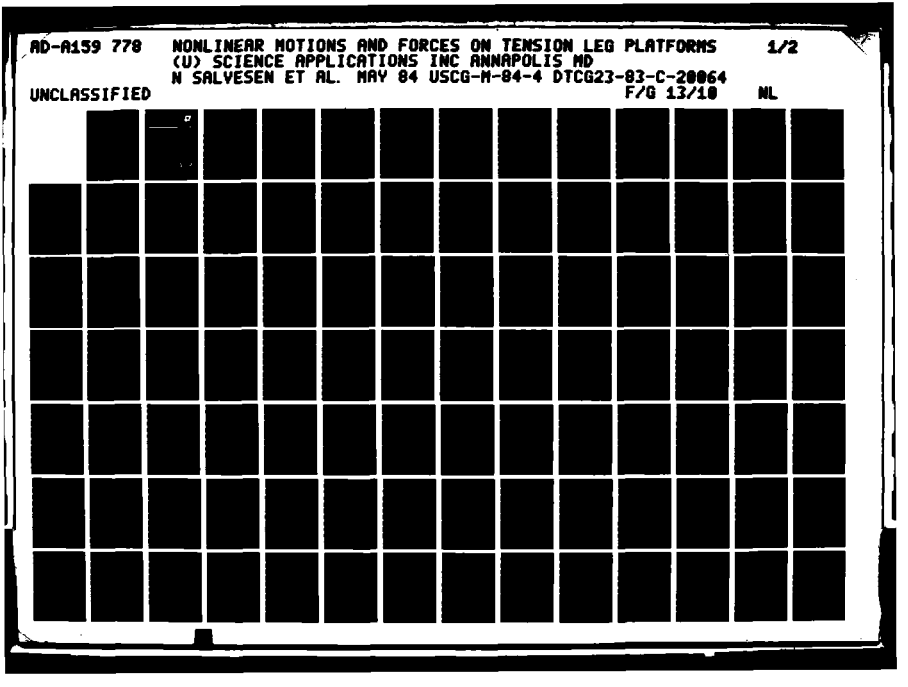

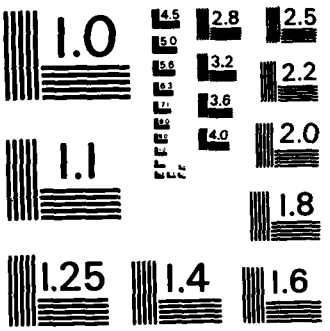

MICROCOPY RESOLUTION TEST CHART
NATIONAL BUREAU OF STANDARDS - 1963 - A

U.S. Department
of Transportation

**United States
Coast Guard**

NONLINEAR MOTIONS AND FORCES ON TENSION LEG PLATFORMS

Nils Salvesen
Michael J. Meinhold
Dick K. Yue

Science Applications, Inc.

Office of Merchant Marine Safety
Washington, D.C. 20593

May 1984
Final Report

USCG-M-84-4(16718)

Technical Report Documentation Page

1. Report No.	2. Government Accession No.	3. Recipient's Catalog No.
USCG-M-84-4 (16718)	AD-A159 778	

4. Title and Subtitle
Nonlinear Motions and Forces on Tension Leg Platforms

5. Report Date
August 1984

6. Performing Organization Code

8. Performing Organization Report No.

7. Author(s)
N. Salvesen, M.J. Meinhold, D.K. Yue

9. Performing Organization Name and Address
Science Applications, Inc.
134 Holiday Court, Suite 318
Annapolis, MD 21401

10. Work Unit No. (TRAIS)

11. Contract or Grant No.
DTCG 23-83-C-20064

13. Type of Report and Period Covered
FINAL REPORT
Sept 1983- May 1984

12. Sponsoring Agency Name and Address
U.S. Coast Guard (G-MTH-5/13)
2100 Second Street, SW
Washington, D.C. 20593

14. Sponsoring Agency Code

15. Supplementary Notes

16. Abstract

New computational methods have been applied in an investigation of the nonlinear surge motions and springing loads in the tendons of tension leg platforms (TLPs). The second-order wave drift forces as well as the linear hydrodynamic coefficients and the wave-induced exciting forces are computed by a three-dimensional hybrid-finite-element method (HFEM). Both a new formula for predicting the viscous drag forces and the conventional Morison drag formula have been used in a time-domain computational procedure to predict the nonlinear surge motions for two TLP configurations due to wind, current and wave excitations. The wave-induces first-and second-order pitch springing exciting moments and the resulting springing tension loads in the tendons are computed for regular waves, two waves (wave groups) and irregular waves using a short-wave approximation method. Upper bound estimates of the surge motions and the tendon springing loads are computed for some selected extreme environmental conditions. "Average" surge displacements and "average" springing loads are also computed for some selected typical operational conditions. Finally, the surge motions and the springing loads of a TLP with one tendon removed have been predicted and compared to the results for the same TLP with all of the tendons intact.

17. Key Words	18. Distribution Statement
Tension Leg Platform (TLP) Nonlinear Surge Motion Springing Loads Tendon Tension	Document is available to the public through the National Technical Information Service, Springfield, VA 22161

19. Security Classif. (of this report)	20. Security Classif. (of this page)	21. No. of Pages	22. Price
Unclassified	Unclassified	120	

Form DOT F 1700.7 (8-72) REPRODUCTION OF THIS FORM IS AUTHORIZED

TABLE OF CONTENTS

TABLE OF CONTENTS
(continued)

TABLE OF CONTENTS
(continued)

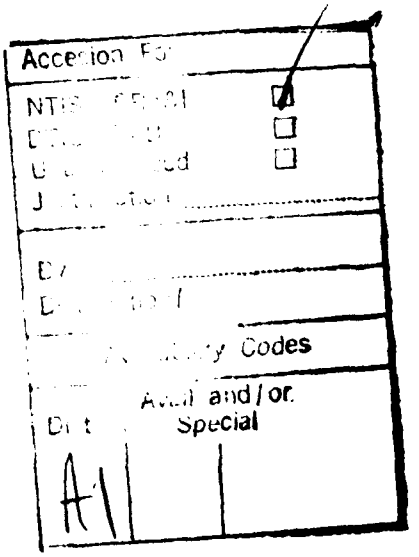

ABSTRACT

New computational methods have been applied in an investigation of the nonlinear surge motions and springing loads in the tendons of tension leg platforms (TLPs). The second-order wave drift forces as well as the linear hydrodynamic coefficients and the wave-induced exciting forces are computed by a three-dimensional hybrid-finite-element method (HFEM). Both a new formula for predicting the viscous drag forces and the conventional Morison drag formula have been used in a time-domain computational procedure to predict the nonlinear surge motions for two TLP configurations due to wind, current and wave excitations. The wave-induced first- and second-order pitch springing exciting moments and the resulting springing tension loads in the tendons are computed for regular waves, two waves (wave groups) and irregular waves using a short-wave approximation method. Upper bound estimates of the surge motions and the tendon springing loads are computed for some selected extreme environmental conditions. "Average" surge displacements and "average" springing loads are also computed for some selected typical operational conditions. Finally, the surge motions and the springing loads of a TLP with one tendon removed have been predicted and compared to the results for the same TLP with all of the tendons intact.

1.0 INTRODUCTION

1.1 Objectives

The main objectives of this project have been to investigate the following nonlinear TLP responses:

- surge motions due to nonlinear wave-induced drift forces, wind loading and viscous interactions between current and oscillatory motions

- additional tension loads in the tendons due to nonlinear wave-induced springing loads, and

- motions and loads for reduced number of tendons.

1.2 Background

1.2.1 Tension Leg Platform Concept

In order to minimize the wave-induced tension loads and the wave-induced surge displacements, TLPs are designed in such a way that the natural periods of oscillations for the vertical heave and pitch motions and for the horizontal surge and yaw motions are far outside the range in which the wave energy of the ocean is a maximum. TLPs usually have a natural period in heave of about 2-3 seconds and a natural period in surge of about 100-140 seconds.

When waves pass a floating body, it will be excited by two types of forces:

- The primary linear exciting forces which have the same period as the wave period, and

- The secondary nonlinear exciting forces which have steady and oscillatory components with periods far outside the range of the typical wave periods. These nonlinear forces are often referred to as the slowly-varying drift and high-frequency springing exciting forces.

An important design aspect of the TLP is that the nonlinear springing and drift forces may introduce excitation at the natural heave and surge frequencies of the TLP. Therefore, it is possible that the high-frequency springing forces can cause additional tension loads in the tendons and that the slowly-varying drift forces can cause surge displacements which are as large if not larger than the loads and displacements caused by the primary linear wave-induced exciting forces.

1.2.2 Prediction of TLP Responses

It is relatively easy to predict the primary linear exciting forces and the resulting motions and tension loads. Since these primary motions occur at frequencies far removed from the TLPs natural frequencies, they can be predicted accurately using a frequency domain approach with linear coupled differential equations ignoring the nonlinear viscous damping.

On the other hand, the secondary motions and loads caused by the nonlinear wave-induced excitation is very difficult to predict accurately. The major problem areas are the three following:

- Accurate prediction of the nonlinear drift and springing exciting forces in regular waves. (Prediction methods only exist for the second-order forces.)

- Accurate prediction of the slowly-varying surge responses and the high-frequency springing responses which both occur at the natural

TLP frequencies and hence are governed by the nonlinear viscous damping forces. (The accuracy of existing methods for predicting the viscous damping for TLPs is questionable.)

- Accurate predictions of drift and springing responses in irregular seas is a very complicated problem. Not only is the viscous damping nonlinear with complicated interaction effects between the steady current and the oscillatory motions, but more importantly, the nonlinear forces in irregular seas is due to nonlinear interactions between the different wave components.

1.2.3 The TLP Motion and Load Computer Code System

A large-scale computer code system has been developed by SAI specifically for the purpose of analyzing the nonlinear dynamics of TLPs. Figure 1-1 shows a schematic layout of the TLP Motion and Load Computer Code System. The system consists of a total of seven individual computer codes which are grouped in three major parts:

Part I: Potential-Flow Predictions by a Hybrid-Finite-Element Method (HFEM) Computer Program

Part II: Surge-Response Predictions by Time-Domain Integrations Method

Part III: Springing-Response Predictions by a New High-Frequency Method

This computer code system is a result of several man-years of research work and code development. It is probably one of the most advanced TLP dynamic response prediction systems presently in existence.

Figure 1-1. TLP Motions and Loads Computer Code System

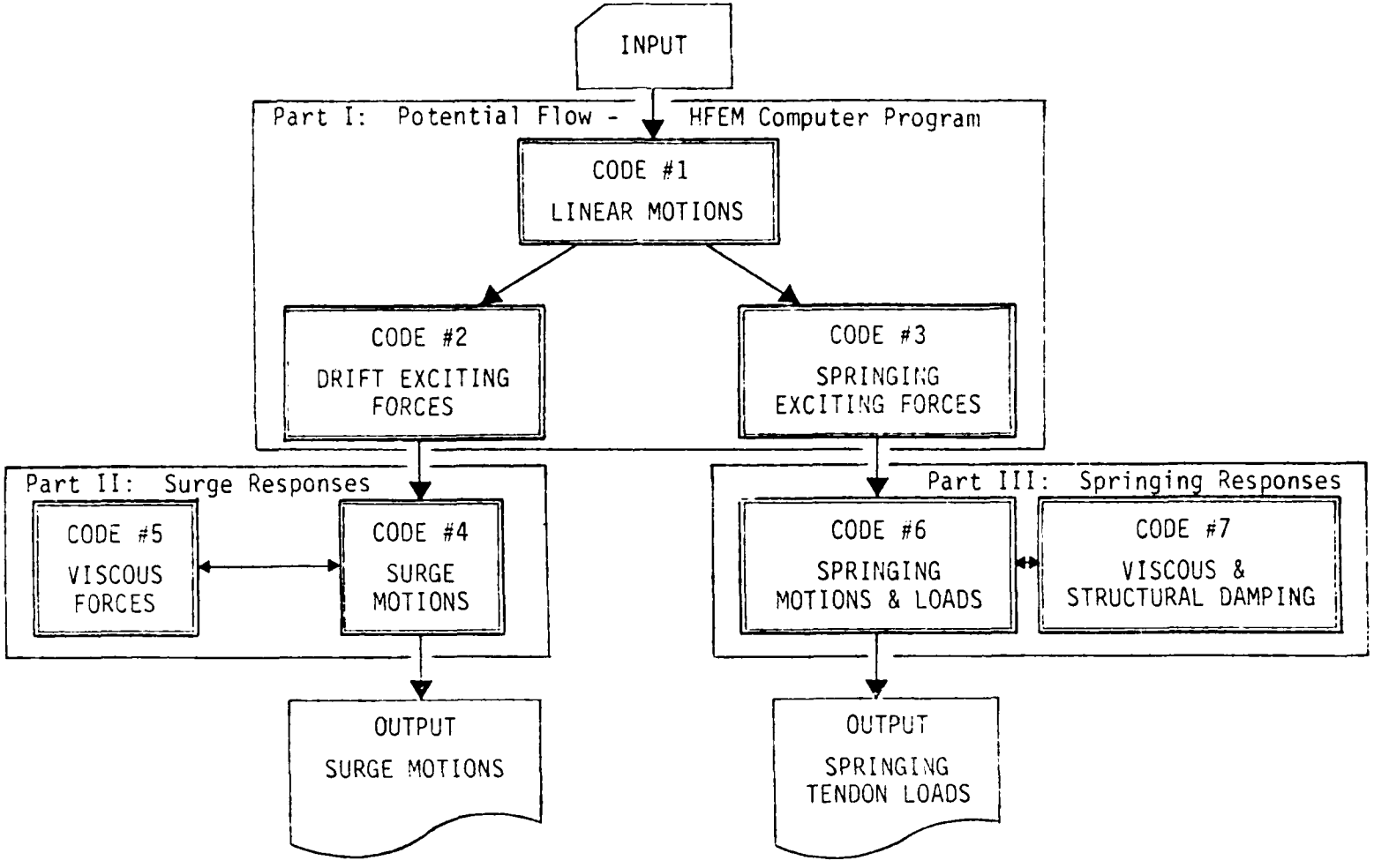

1.3 Summary of Results

Surge motions and tendon tension springing loads have been computed for two TLPs. TLP #1 is a 2000-foot depth design and TLP #2 is a 3000-foot depth design. More detailed descriptions of their geometry are given in Appendix A. The main underwater structure of both of the platforms consists of four vertical corner legs and four horizontal pontoons. Both platforms have four vertical tendons at each of the four legs.

Motions and loads have been predicted for extreme environmental conditions as well as for a typical operational condition.

1.3.1 Surge Motion Results

The surge motions were computed by the nonlinear time-domain surge motion code for a large number of wave, wind and current conditions. The most important findings are as follows:

(a) Upper bound estimates

For TLP #1 it was found that for the environmental conditions considered here the maximum surge displacement is 152.3 feet (166.6 feet)*. This maximum surge displacement will occur in a condition consisting of maximum unsteady wind, maximum steady current and regular waves with period T = 9.5 seconds. This is the wave period for which the steady wave-induced drift force is maximum. It is here assumed that the wave steepness measured as the ratio between the wave height and the wave length, H/λ, is 0.10.

---

* In this section, the results given in parentheses have been obtained by the conventional Morison drag formula, whereas the results not in parentheses have been obtained by a new drag formula.

It should be emphasized that the surge displacement is smaller for the maximum design wave condition (H = 80 feet and T = 14.0 seconds) than it is for the condition stated above. Our computations show that the maximum surge displacement is 102.4 feet (127.4 feet) for the maximum design wave condition with maximum current and maximum unsteady wind.

These are extreme upper bound estimates which will only occur under extreme and rare conditions. Further investigations of the probability of the occurrance of such rare events is needed.

(b) Typical operational estimates

The surge motions have also been computed for a "typical" irregular wave condition with significant wave height, $H_{1/3}$, equal to 10 feet and with steady current and steady wind of a strength typical for this sea condition. For TLP #1 the total "average" surge displacement is estimated to be about 26 feet. Note that the estimates show that the amplitudes of the wave frequency and the slowly-varying components are less than two and four feet respectively and that the steady surge can be expected to be about 20 feet.

Also it should be pointed out that the investigation revealed a large difference between the surge results obtained using the two viscous drag formulas. The large difference between the two formulas is due to the fact that the conventional Morison quadratic formula predicts a very large additional steady displacement due to interaction effects between the wave frequency components and the steady current. It is believed that this interaction effect is overpredicted by the conventional quadratic drag formula.

such large slowly-varying motions, we need to know more about the probability and statistics of such events (or events close to these events). For typical general irregular sea conditions it can be expected that the slowly-varying motions are quite small, probably less than say 4 feet.

The steady surge displacements, on the other hand, can be expected to be much larger than the unsteady motions. For some of the conditions investigated, we have the following results for the steady surge.

	Steady Surge
• Maximum current	
(a) with zero unsteady surge	14.4
(b) with maximum wave-freuqency surge	42.3*
• Maximum steady wind	52.5
• Steady wave-induced drift	
(a) regular wave with maximum drift	64.1
(b) typical irregular sea ($H_{1/3}$ = 10')	2.3

Hence, for typical environmental conditions one may expect up to about 20 feet of steady surge. However, the extreme steady surge displacement may be considerably larger.

2.2 HFEM Potential Flow Calculations

The three-dimensional linear diffraction analyses were performed using the SAI Hydro-Finite-Element Method (HFEM) code utilizing the vertical (perpendicular) planes of symmetry. The HFEM diffraction code is a powerful numerical method for calculating the hydrodynamic forces and the wave-induced responses and loads of three-dimensional offshore structures. The

---

* As predicted by Morison quadratic drag formula.

These results show that large wave-frequency surge motions can only be expected for very extreme wave conditions as, for example, the maximum design regular wave. For typical wave conditions it can be expected that the amplitude of the wave-frequency component will be less than two feet.

The amplitudes of the slowly-varying surge motions are given below for several environmental conditions:

	Surge Amplitude
• Unsteady wind	
(a) zero current	40.9'
(b) maximum current	$\approx$ 20'
• Two regular waves (wave grouping)	
(a) zero current	$\approx$ 58'
(b) maximum current	$\approx$ 25'
• Typical irregular waves ($H_{1/3}$ = 10')	2.6'

These results show that large slowly-varying natural-frequency surge motions can be expected under "ideal" severe conditions when the excitation frequency is precisely equal to the natural frequency. For the unsteady wind case it is assumed that the unsteady part of the wind has one single frequency component with amplitude equal to 10% of the maximum steady wind speed and frequency equal to the natural frequency. For the two-wave case, it is assumed that the difference frequency for the two wave components is equal to the natural frequency:

$$\omega_2 - \omega_1 = \omega_n.$$

This implies that there will be a second-order slowly-varying wave-exciting force with excitation frequency equal to the difference frequency. Both of these natural-frequency excitation conditions are very "idealistic" conditions. Before we can make any predictions about the probability of

to these viscous interaction effects can typically reduce the amplitude of the slowly-varying motions by as much as a factor of four.

The steady surge displacement is due to

- steady wind forces,
- steady nonlinear wave-induced drift forces,
- steady current forces, and
- nonlinear interaction between current and wave-frequency motions and slowly-varying motions.

In this project we have computed the surge displacement due to all of the above-stated steady forces; however, of main interest in this study is the computation of the steady surge due to the nonlinear wave-drift force and the nonlinear viscous interaction.

We shall now present some results for the different surge displacement components so that we can get a better feeling for the order of magnitude of the different components and their relative importance. First, we shall consider the wave-frequency surge displacement components. The amplitude of the wave-frequency component for three wave conditions is given below.

	Surge Amplitude
• Maximum regular wave ($H = 80'$, $\lambda = 1000'$ and $T = 14$ sec)	22.1'
• Steep regular wave with typical wave length ($H = 46'$, $\lambda = 462'$ and $T = 9.5$ sec)	1.7'
• Typical irregular waves ($H_{1/3} = 10'$)	0.9'

We shall now take a look at the different components of the surge displacement. The surge motion of a TLP can be separated into three main parts:

$$x(t) = X_0 + \sum_i X_i \cos\omega_i t + \sum_j X_j \cos\omega_j t$$

The first term, X_0, is the mean steady displacement. The second term, $\sum_i X_i \cos\omega_i t$, consists of first-order frequency components which have frequencies identical to the wave frequencies. We shall refer to these as the linear wave-frequency components. The third and final term, $\sum_j X_j \cos\omega_j t$, consists of frequency components which have frequencies near or equal to the natural surge frequency. Note that the natural frequency components are far removed from the wave-frequency components. We shall refer to these as the nonlinear slowly-varying components.

It is important to recognize that the linear wave-frequency components are caused by linear wave-induced excitation and that the motions at these frequencies are governed by the inertia forces and, furthermore, that viscous damping has practically no effect on these frequency components. Hence, the wave frequency motion can easily be predicted by the well established linear superposition approach.

On the other hand, the slowly-varying components at or near the natural frequency are caused by nonlinear wave-induced excitation and/or wind excitation.* Furthermore, since these motions are at or near the natural frequency, they are to a large extent governed by nonlinear viscous damping forces. Note that the damping of the slowly-varying motions is very much affected by nonlinear viscous interactions between the slowly-varying motion, the steady current and the wave-frequency motions. The damping due

* Note that nonlinear viscous interactions between the steady current and the wave-frequency components may also result in slowly-varying excitation which has not been considered in this investigation.

The results presented in Table 2-1 show that for the maximum regular wave condition with maximum steady wind and current, the maximum surge displacement computed by the SAI drag formula is 92.7 feet and computed by the quadratic drag formula is 118.8 feet. The large difference between the two drag formulas is due to the fact that the quadratic formula predicts a very large additional steady displacement due to interaction effects between wave frequency and current. It is believed that this interaction effect is overpredicted by the quadratic drag formula. Furthermore, for the maximum regular wave condition it is seen in Table 2-1 that the unsteady wind increases the surge by 9.7 feet when the SAI drag formula is used, whereas it increases by only 8.9 feet when the quadratic drag formula is used.

The second wave condition presented in Table 2-1 is the regular wave condition which will result in the maximum drift force. The results presented in Section 2.2 show that the maximum drift force will occur for a regular wave with T = 9.5 seconds. Our predictions show that the surge displacement for this wave condition with maximum steady wind and current will be 133.5 feet when using the SAI drag formula and 153.8 when using the quadratic formula. The unsteady wind results show 152.3-foot surge displacement for the SAI drag case and 166.6 feet for the quadratic drag case. Note that the surge displacements are substantially larger for the maximum drift wave case than for the maximum wave condition.

Significant surge displacements are also shown in Table 2-1 for the typical irregular case as computed by the SAI drag formula. With zero current the surge displacement is only 11.6 feet and with maximum current it is 25 feet. Therefore, for typical general irregular wave conditions, the surge displacements can be expected to be very small.

Total surge displacements were not computed for the two regular wave case (wave grouping). For this case only the slowly-varying wave excitation and response were investigated since these are the most important aspects of wave grouping excitation.

- Typical irregular wave condition ($H_{1/3}$ = 10 ft)

Different combinations of wind and current conditions have been used with these wave conditions.

A summary of the total surge displacements for the maximum regular wave, the regular wave with maximum drift and the typical irregular wave conditions is presented in Table 2-1 for the TLP #1 configuration (see Appendix A for TLP dimensions). Results are shown as obtained by the new SAI drag formula and by the quadratic Morison drag formula.

Table 2-1. Total surge displacements for TLP #1 for two regular wave conditions and a typical irregular wave condition.

	Maximum Surge Displacement (in feet)	
	SAI Drag	Quadratic Drag
Maximum Regular Wave Conditions		
Wave: Maximum Regular Wave (H = 80 and T = 14.0)		
Current: Maximum Steady		
Wind: (a) Maximum Steady	92.7	118.8
(b) Unsteady	102.4	127.7
Regular Wave with Maximum Wave Drift		
Wave: Regular Maximum Drift (H = 46.4 and T = 9.5)		
Current: Maximum Steady		
Wind: (a) Maximum Steady	133.5	153.8
(b) Unsteady	152.3	166.6
Typical Irregular Wave Conditions		
Wave: Irregular Waves ($H_{1/3}$ = 10)		
Wind: Steady (39 ft/sec)		
Current: (a) Zero Current	11.6*	
(b) Maximum Steady	25.0*	

* This is the significant surge displacement, $x_{1/3}$.

the linear wave-exciting forces and the second-order wave-drift forces are computed by the hybrid-finite-element method. These quantities are then used as input for the nonlinear time-domain surge-motion computations.

Computations have shown that three-dimensional hydrodynamic interaction effects between the legs and the pontoons have an important influence on the values of the predicted added mass, wave damping and exciting forces. Hence, the complete three-dimensional computation has to be performed. Computations of hydrodynamic quantities that are made for the legs and for the pontoons separately and then simply added will not be sufficiently accurate to correctly predict the surge motion of the TLP.

The viscous forces are predicted by a new drag formula as well as by the conventional quadratic Morison drag formula. This new formula has been developed because it is believed that the Morison drag formula overpredicts the magnitude of the viscous interaction effects between current, wave-frequency motions and slowly-varying motions. The surge motions due to simultaneous action of the wind, current and wave excitation are predicted by a numerical time-integration procedure which includes all of the important nonlinear effects.

2.1.2 Summary of Surge Motion Results

In this study, we have investigated the surge motions for four different wave conditions:

- Maximum regular-wave condition ($H = 80$ ft, $\lambda = 1000$ ft and $T = 14$ sec)
- Regular wave with maximum steady drift force ($H = 46.4$ ft, $\lambda = 462$ ft and $T = 9.5$ sec)
- Two regular waves (Wave grouping) ($T_1 = 9.7$ sec and $T_2 = 8.9$ sec)

2.0 SURGE MOTION INVESTIGATION

2.1 Introduction

2.1.1 Objective and Approach

The main objective of this part of the project has been to investigate the surge motions due to nonlinear wave-induced drift forces, nonlinear wind loading and nonlinear viscous interactions between current and oscillatory motions. Two TLP configurations are analyzed for selected severe and typical average wind, wave and current conditions. An extensive evaluation and comparison of the surge displacements due to the important nonlinear viscous interaction effects between current, wave-frequency motions and slowly-varying motions as predicted by a new viscous force formula and by the conventional Morison force formula are presented. Unfortunately, there are practically no experimental ersults available for these important nonlinear viscous interaction effects. There is also a lack of experimental data for the nonlinear surge motions under controlled environmental conditions for which computations can be performed. (See Appendix D for a discussion of comparisions between theory and experiments.)

A new computational method developed by SAI (Salvesen, et al., 1982) is here used to investigate the nonlinear surge motions for TLPs. The computations consist of three main parts:

- potential-flow computations;
- viscous-force predictions; and
- nonlinear time-domain surge computations.

The potential-flow calculations are performed first by a three-dimensional hybrid-finite-element method. The added mass, the wave-damping coefficients,

In this investigation we have only considered additional natural frequency tendon loads due to periodic springing excitation. Wave impact excitation may also result in large natural frequency tendon loads often referred to as "ringing" loads. It is recommended that an investigation of the wave-impact "ringing" problem should be conducted in order to establish the magnitude of these loads and establish a general procedure for predicting such loads.

loads will occur in regular waves in the tank which are of the same magnitude as predicted by the theory. Also we need to determine experimentally the springing loads for wave groups and irregular sea waves. The springing experiment could be conducted quite inexpensively by using a vertical cylinder which can pitch about a fixed horizontal axis at the pitch center. The proper restoring coefficient can be modelled by a stiff horizontal spring attached at the top. The most important aspect, at least for the initial experiment, is to model correctly the physical concept of the springing problem and to do it in a simple way so that the correct conditions can easily be modelled and controlled.

Furthermore, improvements are needed in the prediction of the extreme values for both the surge displacements and the tendon tension springing loads. Both of these responses are natural frequency responses which are governed by nonlinear viscous damping and caused by nonlinear exciting forces with frequencies at or very close to the natural frequency. Any conventional extreme statistics approach as used for linear responses are not applicable.

Therefore, it is strongly recommended that a new general procedure should be developed for predicting more accurately the extreme values of the slowly-varying surge motions and the tendon tension springing loads. It is anticipated that such a procedure would consist of the two following parts:

- A method for predicting the probability and the statistics for extreme events which can cause linear or nonlinear excitation at or near prescribed high or low frequency values.

- Nonlinear methods which can predict with sufficient accuracy the slowly-varying horizontal responses and the high frequency springing loads due to events as described by the above-stated method.

It is believed that the methods presented here or similar methods could be used as a starting point for general extreme value prediction methods; however, a considerable amount of improvements and extensions would be required.

On the other hand, the maximum springing loads for the three tendons supporting the one leg may for natural frequency regular wave excitation be twice as large as it is for a TLP with all sixteen tendons intact.

1.4 Concluding Remarks and Recommendations

The TLP surge-motion investigation conducted under this project seems to show that the accuracy of surge displacement computations could be improved by a better viscous force model. In particular, we need to improve the accuracy of the prediction of the nonlinear viscous forces due to interactions between the different modes of motion. At least, improvements are needed for the three following components:

- Additional steady surge displacement due to viscous interactions between the steady current and the oscillatory motions.

- Additional viscous damping of the slowly-varying natural frequency surge motions due to viscous interactions between these motions and the steady current and the wave-frequency motions.

- Steady and slowly-varying nonlinear viscous "drift" excitation due to viscous interactions between the different wave components.

It is recommended that experiments should be conducted with a single large vertical cylinder in a towing tank. Tests should be conducted schematically for a large combination of current speeds, wave-frequency motions and slowly-varying motions. Most importantly, the results should be made generally available.

Similarly, single vertical cylinder experiments are also recommended for the springing problem. We need a much better basic understanding of this problem. It is believed that a single cylinder test would give much more useful data than a test conducted with a complete TLP model. It is extremely important to determine experimantally if tendon tension springing

(c) Sea-state investigations

Computations performed for different irregular wave conditions seem to indicate that the second-order springing loads will be substantially larger in a partially developed sea state than in a fully developed sea state with the same significant wave height.

(d) Pitch center investigation

The pitch center investigation results show that a very effective way to reduce the second-order tendon tension springing loads is to move the pitch center closer to the free surface level. However, the study shows that the first-order low-frequency tendon loads may increase by moving the pitch center closer to the free surface. Therefore, a careful investigation of the first- and second-order tendon load results is required before any judgment can be made with regard to the pitch center location.

(e) *TLP size investigation*

Springing loads were predicted both for the 2000-foot TLP #1 design and for the 3000-foot TLP #2 design. A comparison of these results seems to indicate that the springing problem is much more critical for a deep-water TLP which typically has a higher natural period.

1.3.3 Results for Reduced Number of Tendons

The investigations presented here show that a TLP with one tendon removed can only experience an external load 50-56% as large as a TLP with all of the tendons intact if it is assumed that the maximum design load for a tendon is twice the original pretension value.

The surge motion characteristics for a TLP with one less tendon can be expected to be quite the same as for an intact TLP.

Note that the tendon tension load due to first-order regular wave excitation with wave frequency equal to the natural frequency is only 470 kips per tendon.

If TLP #1 is excited by two simultaneous regular waves with sum frequency precisely equal to the natural frequency

$$\omega_1 + \omega_2 = \omega_n = 2.508 \text{ rad/sec}$$

the additional tendon tension load due to second-order wave excitation is

$$\tau^{(2)} = 780 \text{ kips per tendon}$$

Again we must stress that these values must only be considered as upper bound estimates. It is very unlikely that such precise regular wave events will ever occur. We need to investigate the probability and the statistics of such events in order to make better estimates of the extreme springing loads.

(b) Typical operational estimates

For a typical partially-developed irregular sea condition with significant wave height, $H_{1/3} = 10'$, the significant amplitude of the wave-induced nonlinear tendon tension load is

$$\tau_{1/3} = 102 \text{ kips per tendon.}$$

This value has been obtained by a new irregular-wave method which includes the second-order springing excitation due to the interactions between the different wave components. It is believed that this method will give reasonable estimates of the "average" tendon tension loads for typical irregular-wave conditions. However, it is believed that extreme values may not be accurately estimated by this approach.

Furthermore, it is of interest to note that the predictions show that if wave groups with perfect tuning do occur in the ocean, they may result in slowly-varying surge motions of considerable magnitude and probably larger than those due to the maximum unsteady wind conditions considered here.

1.3.2 Springing Load Results

We shall here refer to springing loads as the additional tendon loads caused by wave-induced vertical motions at or near the natural frequency of the TLP. The high-frequency vertical motions at the tendons is due to natural-frequency pitch motions about the virtual mass center. The pitch exciting moment is caused by linear and nonlinear wave-induced horizontal forces acting on the four legs at a location close to the undisturbed free-surface level.

Note that all of the springing load results presented here are for zero degree heading. It follows from the geometry considerations that it can be expected that the springing loads will be approximately $\sqrt{2}$ times larger at 45 degree heading than at zero degree heading.

(a) Upper bound estimates

For TLP #1 excited by regular waves with period precisely equal to twice the natural period

$$T_w = 2T_n = 5.012 \text{ sec},$$

the additional tendon tension load due to natural frequency pitch motions caused by second-order wave-induced excitation is

$$\tau^{(2)} = 1020 \text{ kips per tendon.}$$

fundamental idea is to use conventional finite elements to approximate the hydrodynamic solution in a fluid region near the body, whereas analytical representations are employed outside this region. By using a variation formulation, finite elements are necessary only in a region very close to the body resulting in significant savings in computational effort (see Figure 2-1). The flexibility and versatility of the finite element approach and the virtual absence of tedious analytical preparation make the HFEM a viable and, in many applications, superior alternative to the traditional integral equation method using Green function (source-distribution method).

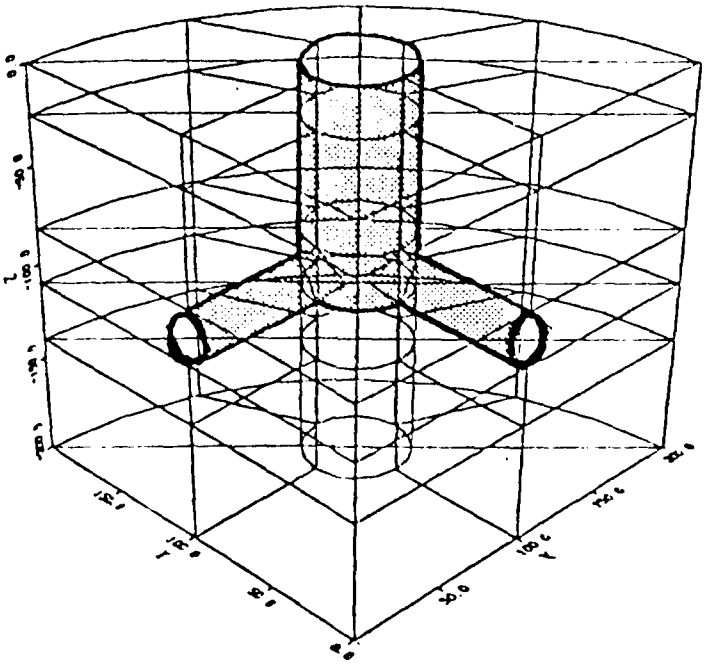

Figure 2-1. Typical HFEM grid for a sample TLP configuration.

The various theoretical and application aspects of the HFEM are well established (Yue, Chen and Mei, 1976; Yue, Chen and Mei, 1978; Aranha, Mei and Yue, 1979), and the method is now widely accepted among offshore engineers. Further verification of the improved SAI HFEM code is also available in SAI Capability Report #SAI-83-463-07.

The second-order steady surge drift force is formulated using momentum conservation relationships expressed in terms of the far-field radiated or scattered velocity potential. The original idea is due to Maruo (1960) and our derivation follows closely to that of Newman (1967).

HFEM Result

The HFEM computer program has been used for all of the results presented in this section. The TLP has in these computations been represented by the four vertical legs and the four horizontal pontoons. Special attention has been given to three-dimensional effects and interactions between the major members (legs and pontoons). Only 0^{o} heading has been considered. All of the HFEM results presented in this section are for TLP #1.

Aside from the four vertical legs and four horizontal pontoons, all other small submerged structural members and risers are ignored in the diffraction theory. Such members constitute only about 5% of the total submerged volume and their typical dimensions are so small compared to incident wave lengths that diffraction effects can be ignored. (A term corresponding to the hydrodynamic added mass of these small members is, however, included in the equation of motion as a small correction.) Since the vertical displacement of the TLP is much smaller than that in surge, its contribution to horizontal drift forces is unimportant and is neglected in our drift calculations.

The following HFEM results for TLP #1 are presented as function of incident wave period:

- Figure 2-2a. Added mass in surge.
- Figure 2-2b. Wave radiation damping in surge.
- Figure 2-3a. First-order surge exciting force, RAO.

- Figure 2-3b. First-order surge exciting force amplitudes for H/λ as given by Figure 2-5.

- Figure 2-4a. Second-order drift force, RAO.

- Figure 2-4b. Second-order drift force amplitudes for H/λ as given by Figure 2-5.

- Figure 2-5. Assumed relationship between maximum wave steepness, H/λ, and wave period, T.

The following are main highlights of our computer results.

- For moderately long waves ($T \sim 20$ seconds), the surge added mass based on displaced mass (Morison's formula with inertia coefficient, $C_m = 2.0$) is almost 30% larger than predicted by the HFEM code. This is mainly due to three-dimensional and interaction effects.

- For exciting force and linear surge motion, most of the effect of multiple legs can be accounted for by relative phasing, and the effect of hydrodynamic interaction is relatively small. The presence of the pontoons is important for longer waves, $T > 8$ sec. For example, for $T = 14$ sec, the pontoons increase the exciting force by almost 20%.

- For the surge drift forces, the effect of hydrodynamic interaction is significant, and the results based on a single leg calculation are inadequate. The drift force is not greatly changed by allowing the body to surge, and the pontoons have almost negligible contribution. The heading angle of the TLP is found to have an important effect on the drift force, but this aspect has not been further investigated in this study.

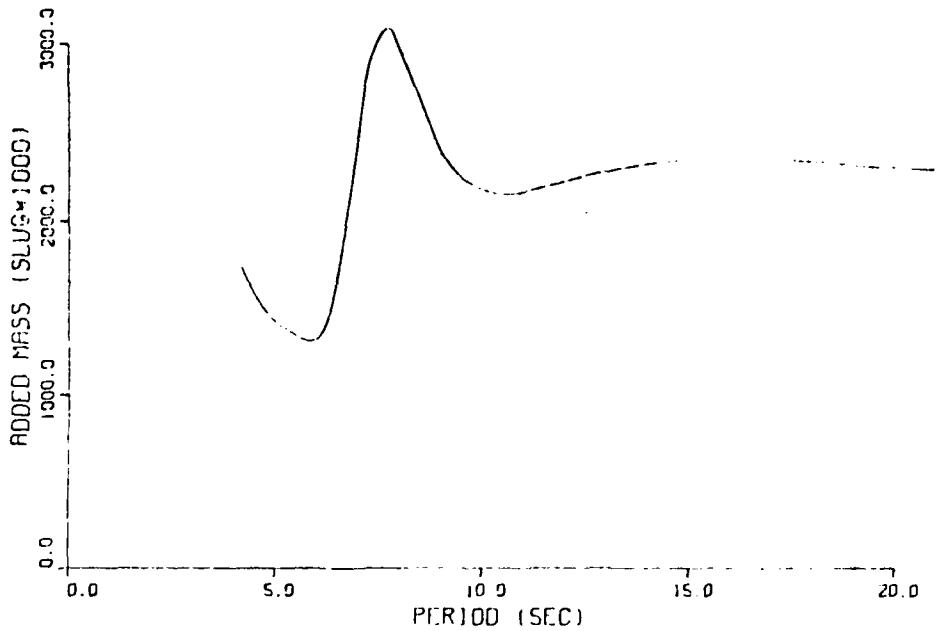

Figure 2-2a. Added mass in surge.

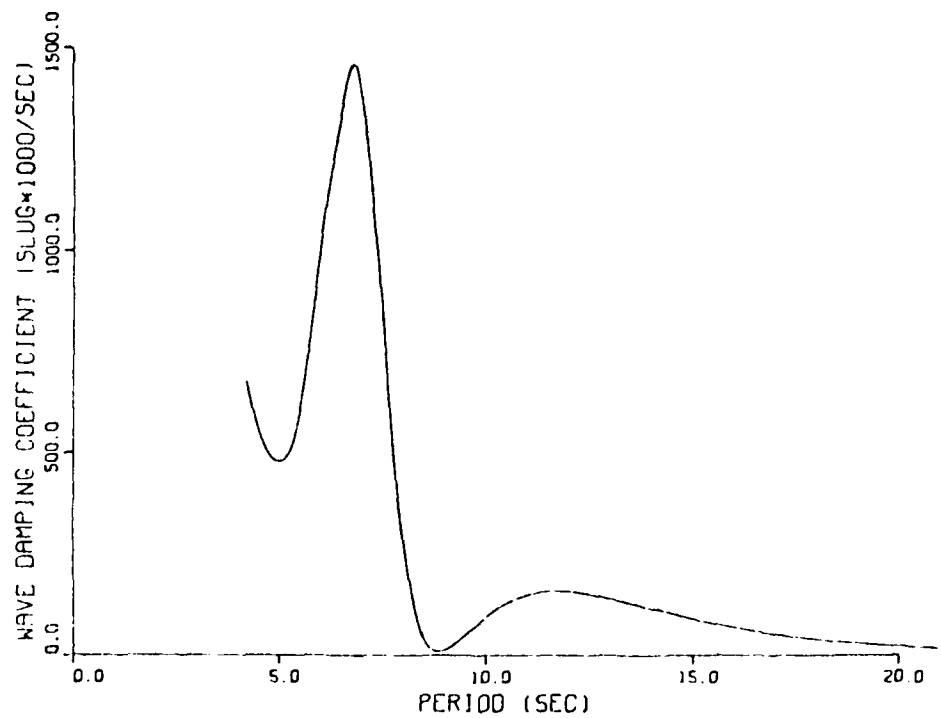

Figure 2-2b. Wave radiation damping in surge.

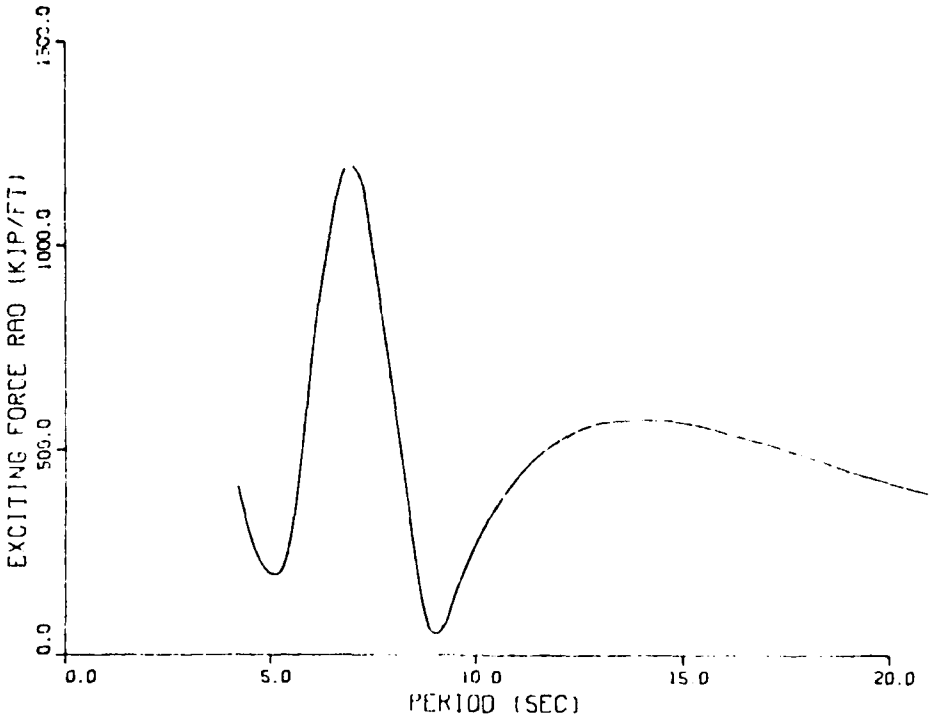

Figure 2-3a. First-order surge exciting force, RAO.

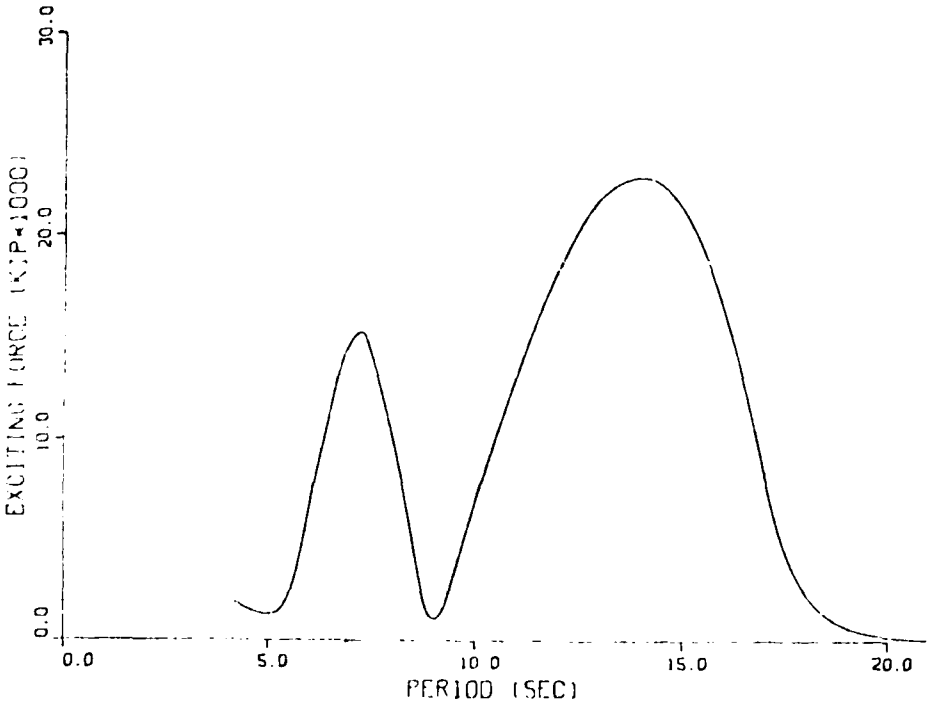

Figure 2-3b. First-order surge exciting force amplitudes for H/λ as given by Figure 2-5.

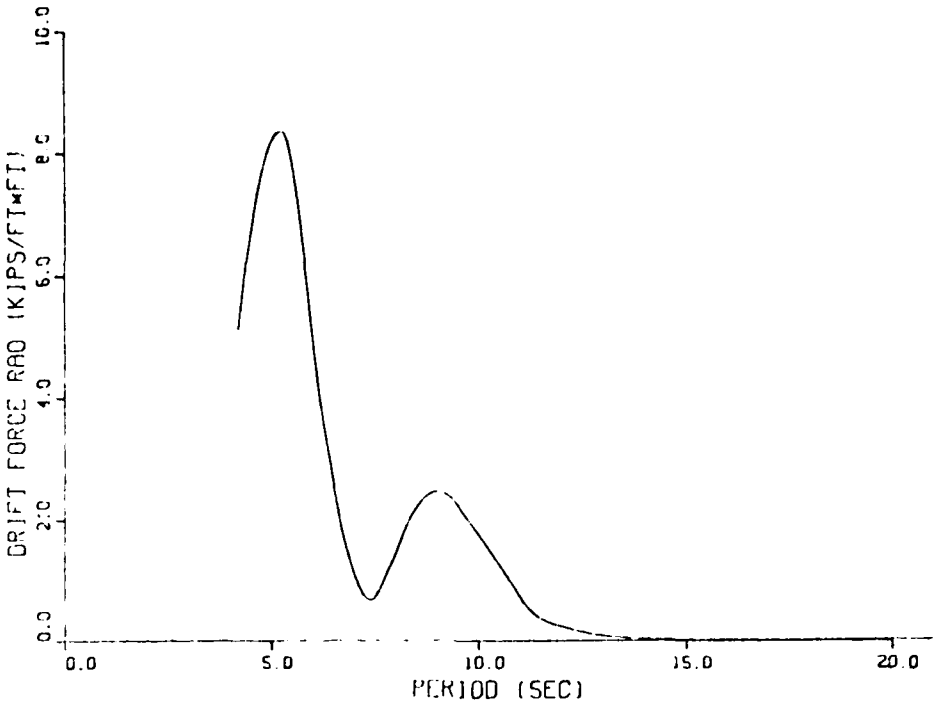

Figure 2-4a. Second-order drift force, RAO.

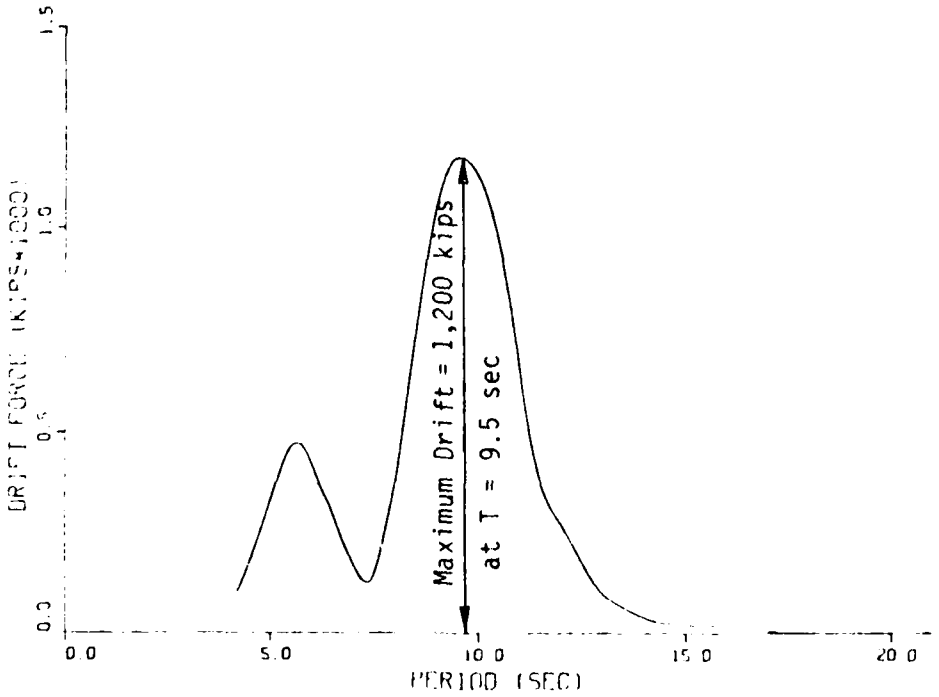

Figure 2-4b. Second-order drift force amplitudes for H/λ as given by Figure 2-5.

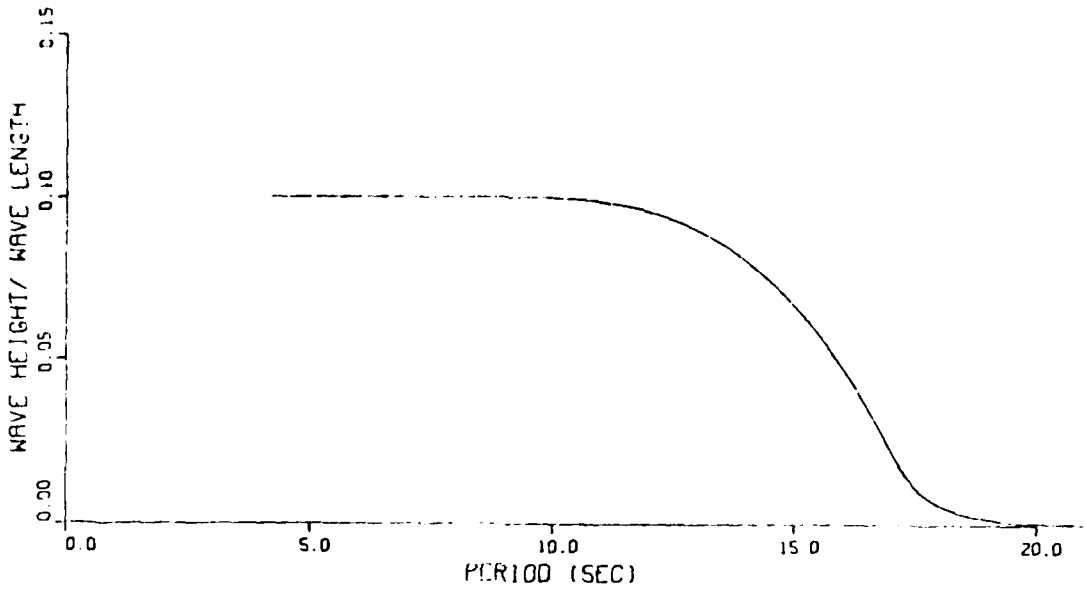

Figure 2-5. Assumed relationship between maximum wave steepness, H/λ, and wave period, T.

2.3 Equation of Motion

A computer program has been developed which predicts the nonlinear surge motions in the time domain. A numerical time-stepping procedure is used in which the time, t, is advanced in small time steps, Δt. The equation of motion which is solved at each time step is

$$(M + A)\ddot{x} + B\dot{x} + Cx = f_V + f_W + f_E \qquad (2\text{-}1)$$

where
- M = total body mass
- A = surge added mass
- B = surge wave-radiation damping coefficient
- C = nonlinear surge restoring coefficient
- $\ddot{x}$ = surge acceleration
- $\dot{x}$ = surge velocity
- x = surge displacement
- f_V = total hydrodynamic viscous force
- f_W = viscous wind-drag force
- f_E = total wave-induced exciting force

The total mass of the TLP #1 design, including tendons and risers, is (see Appendix A)

$$M = 2{,}600 * 10^3 \text{ slugs.}$$

The linear spring constant, the value of C as $x \to 0$, is

$$C_L = 18.32 \text{ kips/ft.}$$

The added mass, A, and wave damping coefficient, B, have been computed by the HFEM code (see Section 2.2). For the computations presented here the infinite period values ($T \to \infty$) have been used:

$$A(T \to \infty) = 2{,}630 * 10^3 \text{ slugs}$$

and

$$B(T \to \infty) = 0.$$

The total hydrodynamic viscous force, $f_V(t)$, is computed at each time step by the SAI drag formula

$$\begin{aligned} f_V(t) = \sum \tfrac{1}{2}\rho D \Big\{ & C_{Ds} |V_s| V_s [1 + f(\bar{V}_1/|V_s|, K_{C1}) + f(\bar{V}_2/|V_s|, K_{C2})] \\ & + C_{D1} |V_1| V_1 \beta(\gamma_1, K_{C1}) \\ & + C_{D2} |V_2| V_2 \beta(\gamma_2, K_{C2}) [1 + f(\bar{V}_1/\bar{V}_2, K_{C1})] \Big\} \end{aligned} \tag{2-2}$$

See Salvesen, et al. (1982) for more details. Note that the drag coefficients, C_D, and the relative velocity components vary for the different sections and that the summation is over all of the sections which the different members are divided into. For comparison purposes, the viscous drag forces are also computed by the "quadratic drag formula",

$$f_V(t) = \sum \tfrac{1}{2} \rho D \, C_D |V| V \tag{2-3}$$

where V is the fluid relative velocity at each section. The above formula is often referred to as the Morison drag force.

The viscous wind-drag force is predicted by

$$f_W(t) = \sum \tfrac{1}{2} \rho C_p A \cdot W|W| \tag{2-4}$$

where W is the wind speed. The maximum steady wind speed is

$$W_o = 70 \text{ knots},$$

and the most severe unsteady wind is assumed to be

$$W(t) = 70 + 7 \cdot \cos\omega_n t \text{ (knots)}. \tag{2-5}$$

Here ω_n is the surge natural frequency of the system. The maximum steady wind force is

$$f_W = 960 \text{ kips}$$

and the maximum unsteady wind force is

$$f_W(t) = 960 \text{ kips} + 190 \text{ kips} \cdot \cos\omega_n t. \tag{2-6}$$

The total wave-induced exciting force is

$$f_E(t) = F_o^E + \sum_i F_i^E \cos(\omega_i t + \varepsilon_i) + \sum_j F_j^E \cos(\omega_j t + \varepsilon_j) \tag{2-7}$$

where F_o^E = steady wave drift force

F_i^E = amplitude of the primary wave exciting force components which has the same frequency ω_i as the frequency of wave components

F_j^E = amplitude of the slowly-varying wave-drift exciting force components.

For regular waves the steady drift force is

$$F_0^E = F^{(2)}(\omega) \cdot [A(\omega)]^2 \tag{2-8}$$

where $F^{(2)}(\omega)$ is the second-order steady drift force per unit wave amplitude for regular waves

and where $A(\omega)$ is the wave amplitude.

The amplitude of the primary wave-exciting force is

$$F_i^E(\omega) = F^{(1)}(\omega) \cdot A(\omega) \tag{2-9}$$

where $F^{(1)}(\omega)$ is the first-order exciting force per unit wave amplitude in regular waves.

Note that the slowly-varying drift force is zero in regular waves.

2.4 Regular-Wave Surge Displacement Results for TLP #1

The surge displacement in regular waves as computed here will finally come to a steady-state condition after the initial transient motions have died out. The final steady-state surge motions x(t) in regular waves may be expressed as

$$x(t) = X_0 + X_1 \cos\omega_1 t + X_2 \cos\omega_2 t \tag{2-10}$$

where X_0 = mean displacement due to wind, wave drift and current (including body and wave velocity interactions)

X_1 = amplitude of the frequency components of the primary first-order motions due to primary wave excitation only (primary motions are dominated by inertia effects and are not affected by current, wind or the slowly-varying motions)

X_2 = amplitude of the slowly-varying motion components due to unsteady wind (its magnitude is affected by current and the primary motions through the viscous damping force).

The mean displacement X_o and the amplitude of the slowly-varying motions X_2 shall be further divided into parts which describe the separate contirbutions due to wind, wave drift, current and current-motion interactions. The mean surge displacement can be divided into the following five components:

$$X_o = X_o^W + X_o^D + X_o^C + X_o^{CP} + X_o^{CS} \qquad (2\text{-}11)$$

where X_o^W = displacement due to steady wind

X_o^D = displacement due to steady wave-drift

X_o^C = displacement due to current alone

X_o^{CP} = displacement due to steady viscous force caused by interaction between current, primary body and wave particle velocities

X_o^{CS} = additional displacement due to steady viscous force caused by interactions between current and the slowly-varying body motions.

The amplitude of the slowly-varying motions, X_2, can be divided into the following three components

$$X_2 = X_2^{WD} + X_2^{IC} + X_2^{IP} \qquad (2\text{-}12)$$

where X_2^{WD} = amplitude of the slowly-varying motions due to unsteady wind with no current present and no primary motions

X_2^{IC} = increase (or decrease) in amplitude due to current

X_2^{IP} = additional increase (or decrease) in amplitude due to the primary motions.

An investigation of these different surge displacement components is presented in Appendix B. The surge displacements are computed using both the SAI and the quadratic drag formula for the 0^o heading case. The TLP is excited by maximum current, maximum regular waves (H = 80.0 feet and T = 14.0 seconds) and unsteady wind (W = 70.0 + 7.0 $\cos\omega_n t$ (knots) where ω_n is the natural surge frequency).

The computed time domain surge displacement for this wind, wave and current condition is presented in Figure 2-6. Results are shown using both the SAI drag formula and the quadratic formula. It is seen that the SAI drag formula predicts that the three main surge displacement components in this case are

Steady surge	X_o = 70.5'
Amplitude of primary motion	X_1 = 22.1'
Amplitude of slowly-varying motion	X_2 = 9.7'
Total maximum surge displacement	X_{max} = 102.4'

When the quadratic formula is used the components are

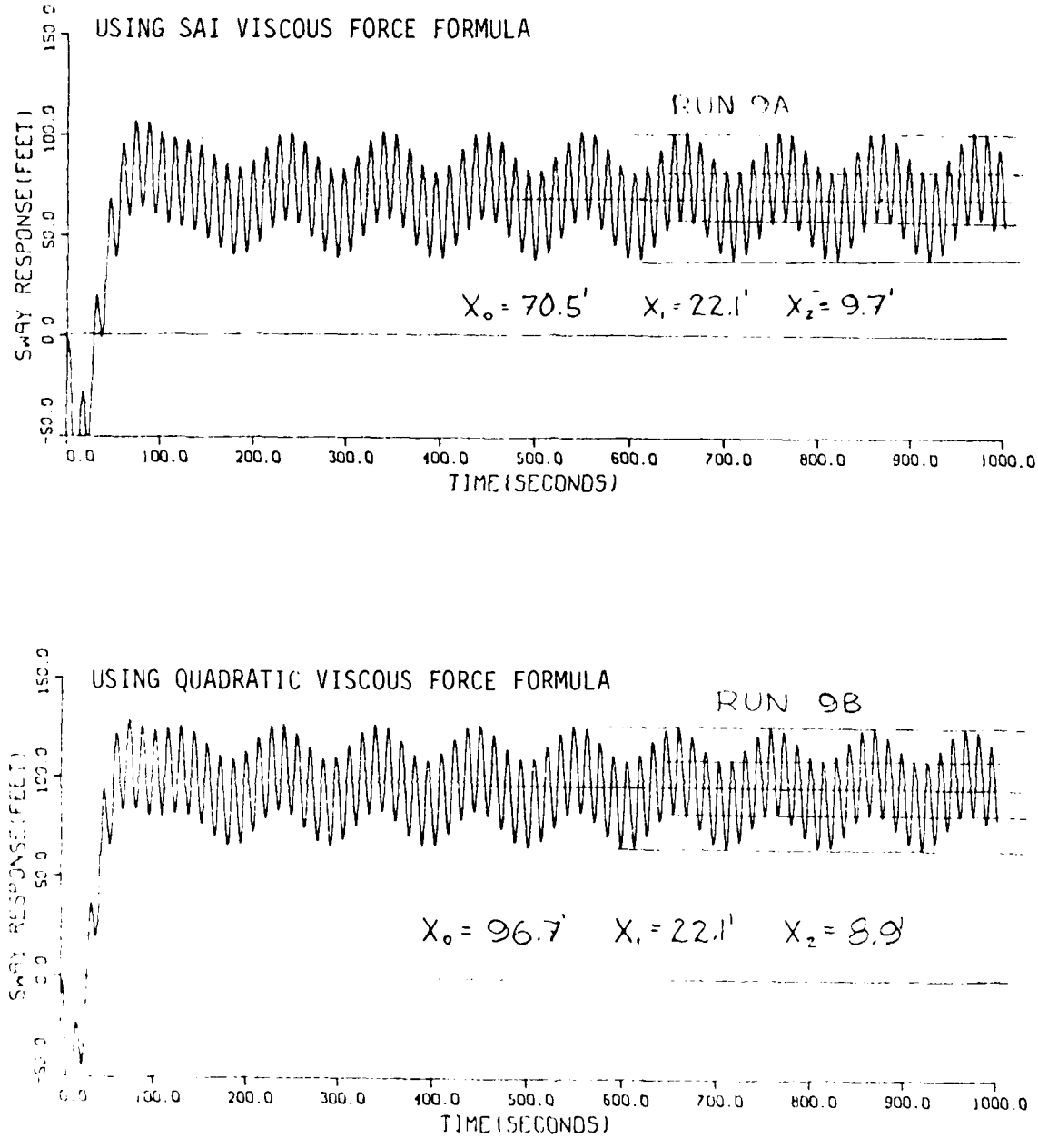

Figure 2-6. Computed nonlinear time-domain responses for TLP excited by current, unsteady wind and maximum design wave with 0° heading.

Steady surge	X_o	= 96.7'
Amplitude of primary motion	X_1	= 22.1'
Amplitude of slowly-varying motion	X_2	= 8.9'
Total maximum surge displacement	X_{max}	= 127.7'

We shall now present results for the additional individual components. The different surge displacement components have been determined by performing runs with the time domain surge motion computer program using different combinations of the above-stated current, wave and wind conditions. The results for each of these computer runs are presented in Appendix B. A summary of the results is given in Table 2-2.

The most important final conclusions which can be drawn from the results presented in Table 2-2 and in Appendix B are:

- Steady surge displacement is 14.4 feet when the TLP is excited by current alone. When the current and the maximum design wave are both present the quadratic drag formula predicts an increase of the steady displacement by 27.9 feet due to interactions between the current, the wave particle motions and the body motions. Results obtained by the SAI formula show only a 1.8-foot increase. Furthermore, the results in Table 2-2 show that if slowly-varying motions are also present, then the steady surge is unchanged when the quadratic formula is used and decreased by 0.1 feet when the SAI formula is used. Note that there is an additional steady surge component resulting from integration of the viscous forces over the instantaneous wetted surface. This component which is equal to about 3-4 feet is not included in Table 2-2.

- Amplitude of the primary wave-induced surge motions is 22.1 feet. Computations have shown that the wave-frequency motion is affected only slightly by viscous drag forces. These motions are essentially completely dominated by inertia effects. This implies that

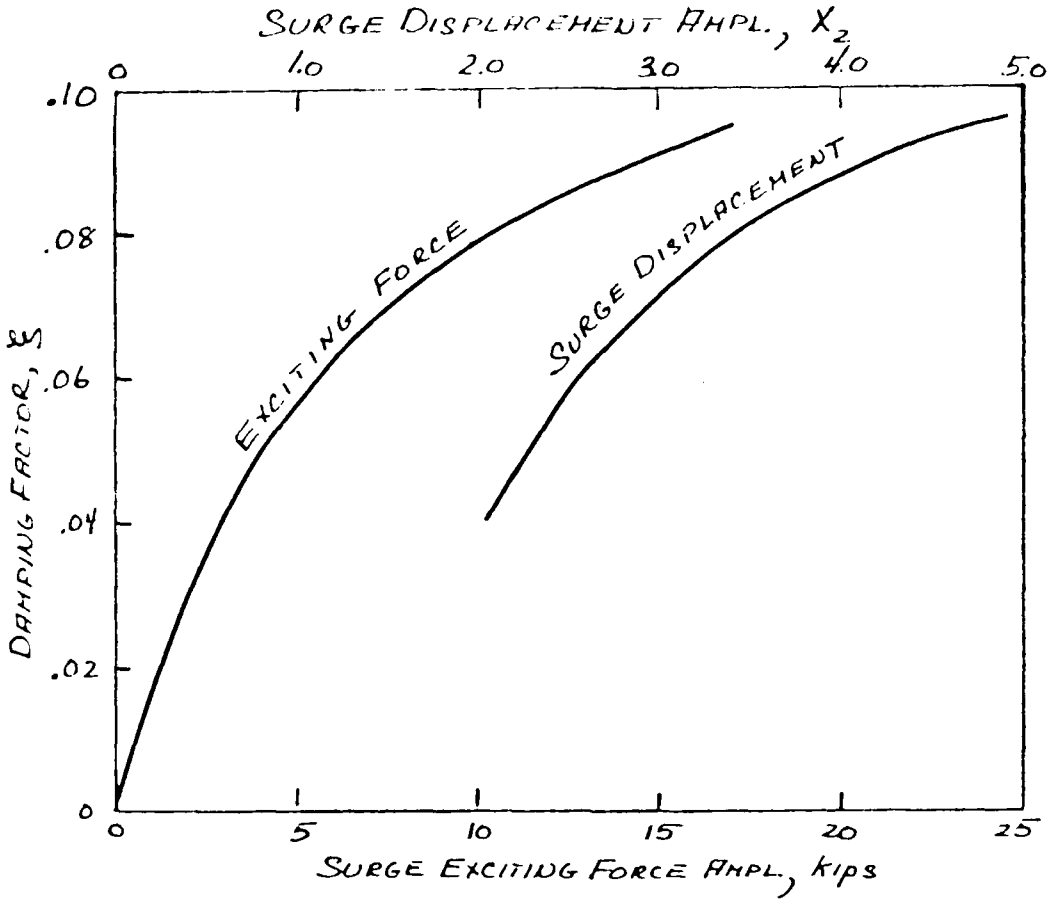

Figure 2-8. Damping factor, ζ, as function of surge exciting force amplitude and as function of surge displacement amplitude, X_2.

2.7 TLP Size Investigation

In this section we shall compare surge-motion results for the TLP #1 and TLP #2 designs. Detailed descriptions of the two TLPs are included in Appendix A. Note that TLP #2 is 1.2 times larger than TLP #1, and that TLP #1 is assumed to be designed for 2000-foot depth whereas TLP #2 is designed for 3000-foot depth.

The same HFFM potential-flow data as presented in Section 2.2 and the time-domain regular wave results as presented in Section 2.4 and Appendix B obtained for TLP #1 have also been obtained for TLP #2. However, here we shall not present all of the detailed results for TLP #2. We shall only

$$\phi_f^{(2)}(\omega^*) \quad /10 \text{ kips}^2 \cdot \text{sec.}$$

Now using Figure 2-8, equation (2-35) is easily solved by iteration and the results are

$$X_{1/3}^{(2)} = 2.6 \text{ feet and } \zeta = 0.06.$$

The final surge displacement results for the sample irregular sea condition are

Steady Displacement	
Due to wind	5.8'
Due to wave drift	2.3'
Primary wave-frequency motions	
Significant amplitude, $X_{1/3}^{(1)}$	0.9'
Slowly-varying natural-frequency motions	
Significant amplitude, $X_{1/3}^{(2)}$	2.6'
Total "significant" displacement	11.6'

If we had included maximum current, this would have resulted in an additional steady surge displacement of about 12 feet and probably have reduced the slowly-varying motion amplitude by a factor of 0.5. Hence, in the same irregular sea condition with current, the total "significant" surge displacement will be approximately 25 feet.

where $A = 0.0081\ g^2$ and $B = 33.56\ h_{1/3}^2$. The significant wave height, $h_{1/3}$ = 10 feet. The average mean period for this is $T_1 = 6.73$ seconds. We shall assume that a typical wind speed for this sea condition is

$$W = 39 \text{ ft/sec.}$$

For this sample case we shall assume that the current is zero.

By equations (2-19), (2-20) and (2-21) and numerical HFEM results given in Figures 2-2 through 2-5, we have that the significant first-order surge motion amplitude is

$$X_{1/3}^{(1)} = 2.0\ \sigma_x^{(1)} = 0.92 \text{ feet.} \tag{2-33}$$

The steady drift force is by equation (2-22)

$$F_o^{(2)} = 41 \text{ kips.}$$

By performing computations with the nonlinear surge time-domain code representing the wave-frequency surge motion by

$$x^{(1)}(t) = 0.92' \cdot \cos\frac{2\pi}{6.73}\, t \tag{2-34}$$

we have obtained the nonlinear relationship between the damping and the amplitude of the natural-frequency slowly-varying surge motions. This relationship is shown graphically in Figure 2-8.

From equation (2-28) it follows that the significant amplitude of the slowly-varying motion, $X_{1/3}^{(2)}$, for an irregular sea is

$$\left[2 \cdot X_{1/3}^{(2)}\right]^2 = \phi_f^{(2)}(\omega^*)\ \frac{\pi}{4\zeta\, A^2 \omega_n^3} \tag{2-35}$$

where by applying equation (2-25) we have that

where the first frequency component is a linear wave-frequency component and the second component is a slowly-varying second-order component with frequency equal to the natural surge frequency.

We shall assume that for an irregular seaway, an equivalent linear viscous damping factor can be used and that this damping factor is the same as the damping factor for natural frequency surge motions with amplitude equal to the significant second-order surge motion, i.e.

$$x^{(2)}(t) = X_{1/3}^{(2)} \cos\omega_n t.$$

The nonlinear relationship between the significant surge displacement amplitude, $X_{1/3}^{(2)}$, and the damping factor, ζ, can then be obtained by running the time-domain surge motion computer program for several exciting force values.

However, since the viscous damping depends on nonlinear interaction resulting from current and wave-frequency motion, the proper current and wave-frequency motions must be included in the time-domain computations. We shall, for simplicity, assume that the wave-frequency motions effect on the viscous damping can be represented by using a single wave-frequency component given by

$$x^{(1)}(t) = X_{1/3}^{(1)} \cos\omega_1 t \tag{2-31}$$

where ω_1 is the average mean frequency for the given sea spectrum and $X_{1/3}^{(1)}$ is the significant surge amplitude for the first-order motion.

2.6.2 Sample Results

We shall assume that a typical seaway is represented by a fully developed Pierson-Moskowitz spectrum

$$S_\zeta(\omega) = \frac{A}{\omega^5} e^{-B/\omega^4} \tag{2-32}$$

The variance of the second-order surge displacement is given by

$$\left[\sigma_x^{(2)}\right]^2 = \int_0^{\infty} \phi_x^{(2)}(\omega)\, d\omega. \tag{2-27}$$

Now if we assume that the second-order surge motion is a "natural-frequency motion" with a relatively small damping factor and that the surge natural frequency is "small", we may write

$$\begin{aligned}\left[\sigma_x^{(2)}\right]^2 &= \int_0^{\infty} \phi_f^{(2)}(\omega)\, |H(\omega)|^2\, d\omega \\ &= \phi_f^{(2)}(\omega^*) \int_0^{\infty} |H(\omega)|^2\, d\omega \\ &= \phi_f^{(2)}(\omega^*) \int_0^{\infty} \frac{d\omega}{(C - A\omega^2) + iB\omega} \\ &= \phi_f^{(2)}(\omega^*)\, \frac{\pi}{4\zeta A^2 \omega_n^3}\end{aligned} \tag{2-28}$$

where the damping factor is

$$\zeta = B/2A\omega_n. \tag{2-29}$$

Note that for surge motions at and near the natural frequency, the damping is nonlinear and depends on the magnitude of the surge motions. Furthermore, the surge damping depends on complicated nonlinear viscous interaction between the slowly-varying motions and the steady current and also the first-order wave-frequency motions.

We shall here obtain the nonlinear relationship between the damping factor, ζ, and the surge motion amplitude by using our nonlinear time-domain surge motion computer program. This computer program assumes that the surge motions only have two frequency components,

$$x(t) = X_o + X_1^{(1)} \cos\omega_1 t + X_2^{(2)} \cos\omega_n t \tag{2-30}$$

Note that the added mass and damping coefficients, A and B, are functions of frequency, ω, as shown in Figures 2-2a and 2-2b. The variance (i.e., the square of the RMS value, σ) of the first-order surge displacement is given by

$$\left[\sigma_x^{(1)}\right]^2 = \int_0^\infty \phi_x^{(1)}(\omega)\, d\omega. \tag{2-21}$$

The mean steady second order drift force is

$$F_0^{(2)} = 2\int_0^\infty F^{(2)}(\omega) \cdot \phi_a(\omega)\, d\omega \tag{2-22}$$

where $F^{(2)}(\omega)$ is the steady second-order drift force, RAO, for regular waves (see Figure 2-4a).

The surge force power spectrum due to second-order wave-induced excitation is

$$\phi_f^{(2)}(\omega^*) = 2\int_0^\infty \phi_a(\omega + \frac{\omega^*}{2})\ \phi_a(\omega - \frac{\omega^*}{2})\ \left|\mathcal{D}(\omega + \frac{\omega^*}{2},\ \omega - \frac{\omega^*}{2})\right|^2 d\omega. \tag{2-23}$$

Here $\mathcal{D}(\omega_1, \omega_2)$ is the second-order drift force RAO for excitation by two simultaneous waves with frequencies, ω_1 and ω_2. If ω^* is small, we may apply Newman's approximation and assume that

$$\mathcal{D}(\omega + \frac{\omega^*}{2}, \omega - \frac{\omega^*}{2}) \approx F^{(2)}(\omega) \tag{2-24}$$

and, furthermore, that

$$\phi_f^{(2)}(\omega) \approx 2\int_0^\infty [\phi_a(\omega)\ F^{(2)}(\omega)]\, d\omega. \tag{2-25}$$

The surge power spectrum due to second-order excitation is

$$\phi_x^{(2)}(\omega) = \phi_f^{(2)}(\omega)\ |H(\omega)|^2. \tag{2-26}$$

$$X_2 = 40.9 \text{ feet.}$$

Hence if wave groups with perfect tuning do occur in the ocean, they will result in slowly-varying surge motions which are considerably larger than those due to the maximum unsteady wind condition considered here.

2.6 Irregular Wave Results for TLP #1

The main objectives with the irregular wave investigation are to present a method for predicting the "average" surge motions in an irregular seaway and to present results for a typical sea condition. This method is not recommended for predicting extreme surge responses. It is believed that the extreme responses can be predicted more accurately by computing the nonlinear time-domain responses for particular extreme events which are expected to result in large surge responses.

2.6.1 Theoretical Formulation

We shall assume that the seaway is unidirectional and represented by a known power spectrum

$$\phi_a(\omega)$$

The surge displacement power spectrum due to first-order wave-induced excitation is

$$\phi_x^{(1)}(\omega) = \phi_a(\omega) \; |F^{(1)}(\omega)|^2 \cdot |H(\omega)|^2 \qquad (2\text{-}19)$$

where $F^{(1)}(\omega)$ is the first-order surge exciting force, RAO (see Figure 2-3a)

$H(\omega)$ is the "linear" surge displacement, RAO given by

$$H(\omega) = \frac{1}{(C - A\omega^2) + iB\omega} \qquad (2\text{-}20)$$

$F^{(2)}$ = second-order steady drift force for regular waves of unit wave amplitude

$^{-}F^{(2)}$ = amplitude of slowly-varying force for two wave components

$^{+}F^{(2)}$ = amplitude of the "springing" force for two wave components

The results presented in Section 2.2 show that the maximum drift force RAO is

$$F^{(2)} = 2.5 \text{ kips when } T = 9.3 \text{ sec.}$$

Hence we have that the second-order excitation for the wave-grouping condition considered here is

$$f^{(2)}(t) = 390 \text{ kips} + 390 \text{ kips} \cdot \cos\omega_n t. \qquad (2\text{-}18)$$

This exciting force will result in a steady surge displacement

$$X_o = \frac{390}{18.32} = 21.3 \text{ feet}$$

and a slowly-varying surge with an amplitude (estimated from the results presented in Appendix B)

$$X_2 \approx 58 \text{ feet.}$$

This is the estimated amplitude when there is no current and when damping due to interactions with the primary motions is ignored. If current is present the amplitude will be decreased due to additional viscous damping forces caused by interactions between the current and the oscillatory motions.

It should be recalled that the maximum amplitude for the slowly-varying motions resulting from the maximum unsteady wind condition is

Correct to the second order in wave amplitude, the exciting force due to two regular waves is

$$f(t) = f^{(1)}(t) + f^{(2)}(t) + \ldots \tag{2-13}$$

where the first-order force

$$f^{(1)}(t) = F^{(1)}\alpha_1 \cos\omega_1 t + F^{(1)}\alpha_2 \cos\omega_2 t \tag{2-14}$$

and the second-order force is

$$\begin{aligned} f^{(2)}(t) = {} & F^{(2)}(\omega_1) \cdot \alpha_1^2 + F^{(2)}(\omega_2) \cdot \alpha_2^2 \\ & + 2\alpha_1\alpha_2 \, {}^{-}F^{(2)}(\omega_1, \omega_2) \cdot \cos(\omega_2 - \omega_1)t \\ & + 2\alpha_1\alpha_2 \, {}^{+}F^{(2)}(\omega_1, \omega_2) \cdot \cos(\omega_1 + \omega_2)t \\ & + \alpha_1^2 \, {}^{+}F^{(2)}(\omega_1) \cos 2\omega_1 t + \alpha_2^2 \, {}^{+}F^{(2)}(\omega_2) \cos 2\omega_2 t \end{aligned} \tag{2-15}$$

We are here only interested in the steady and the slowly-varying part of the second-order force which may be written as

$$\begin{aligned} f^{(2)}(t) = {} & F^{(2)}(\omega_1) \cdot \alpha_1^2 + F^{(2)}(\omega_2) \cdot \alpha_2^2 \\ & + 2\alpha_1\alpha_2 \, F^{(2)}\left(\frac{\omega_1 + \omega_2}{2}\right) \cdot \cos(\omega_2 - \omega_1)t \end{aligned} \tag{2-16}$$

where the Newman approximation has been applied. The Newman approximation states that

$$-F^{(2)}(\omega_1, \omega_2) = F^{(2)}\left(\frac{\omega_1 + \omega_2}{2}\right) + O(\omega_2 - \omega_1). \tag{2-17}$$

Here $F^{(1)}$ = amplitude of first-order exciting force per unit wave amplitude

2.5 Surge Motions Due to Wave Grouping

We shall consider excitation due to "wave grouping" with perfect tuning. That is two simultaneous regular waves with difference frequency equal to the surge natural frequency and with mean frequency equal to the frequency for which the steady surge drift force is maximum. This particular wave condition will result in the largest possible slowly-varying wave-induced excitation since all of the wave energy is concentrated at the maximum wave-drift frequency. However, it must be recognized that it has not been established with any degree of confidence that wave groups with perfect tuning will actually occur in the ocean. The wave-grouping results presented here should be considered, therefore, as an estimate of the upper limit for the wave-induced slowly-varying excitation force.

We shall consider two waves:

$$\omega_1(t) = \alpha_1 \cos\omega_1 t$$

and

$$\omega_2(t) = \alpha_2 \cos\omega_2 t$$

where

$$\tfrac{1}{2}(\omega_1 + \omega_2) = \omega_{max} = \frac{2\pi}{9.3} = 0.676$$

$$\omega_2 - \omega_1 = \omega_{nat} = \frac{2\pi}{106} = 0.0593$$

Hence we have two waves with frequencies $\omega_1 = 0.646$ ($T_1 = 9.7$ and $\lambda_1 = 463.6$ ft) and $\omega_2 = 0.706$ ($T_2 = 8.9$ and $\lambda_2 = 405.9$ ft). We shall assume that the maximum slope is given by

$$h/\lambda = \frac{2(\alpha_1 + \alpha_2)}{\lambda_{mean}} = 0.08.$$

This implies that $\alpha_1 = \alpha_2 = 8.85$ feet.

Table 2-3. Surge displacements for two extreme regular wave conditions for 0^o heading.

	Maximum Design Wave H = 80.0 ft T = 14.0 sec		Maximum Drift Wave H = 46.4 ft T = 9.5 sec	
	SAI Drag	Quad Drag	SAI Drag	Quad Drag
Steady Current Displacement, X_o^C	16.1	42.3	15.2	35.5
Steady Wind Displacement, X_o^W	52.5	52.5	52.5	52.5
Steady Drift Displacement, X_o^D	2.0	2.0	64.1	64.1
Wave Frequency Amplitude, X_1	22.1	22.1	1.7	1.7
Slowly-Varying Motion Amplitude, X_2	9.7	8.9	18.8	12.8
Total Maximum Surge Displacement	102.4	127.7	152.3	166.6

The results summarized in Table 2-3 show that the largest surge displacement will occur for the 0^o heading angle with "maximum drift wave" and maximum current. When the quadratic drag formula is used, the maximum displacement is

$$X_{max} = 166.6 \text{ feet.}$$

Note that the results presented in Table 2-3 show that for the maximum design wave case the surge displacement (using quadratic drag) is

$$X_{max} = 127.7 \text{ feet}$$

which is substantially smaller than the surge displacement for the "maximum drift wave" case.

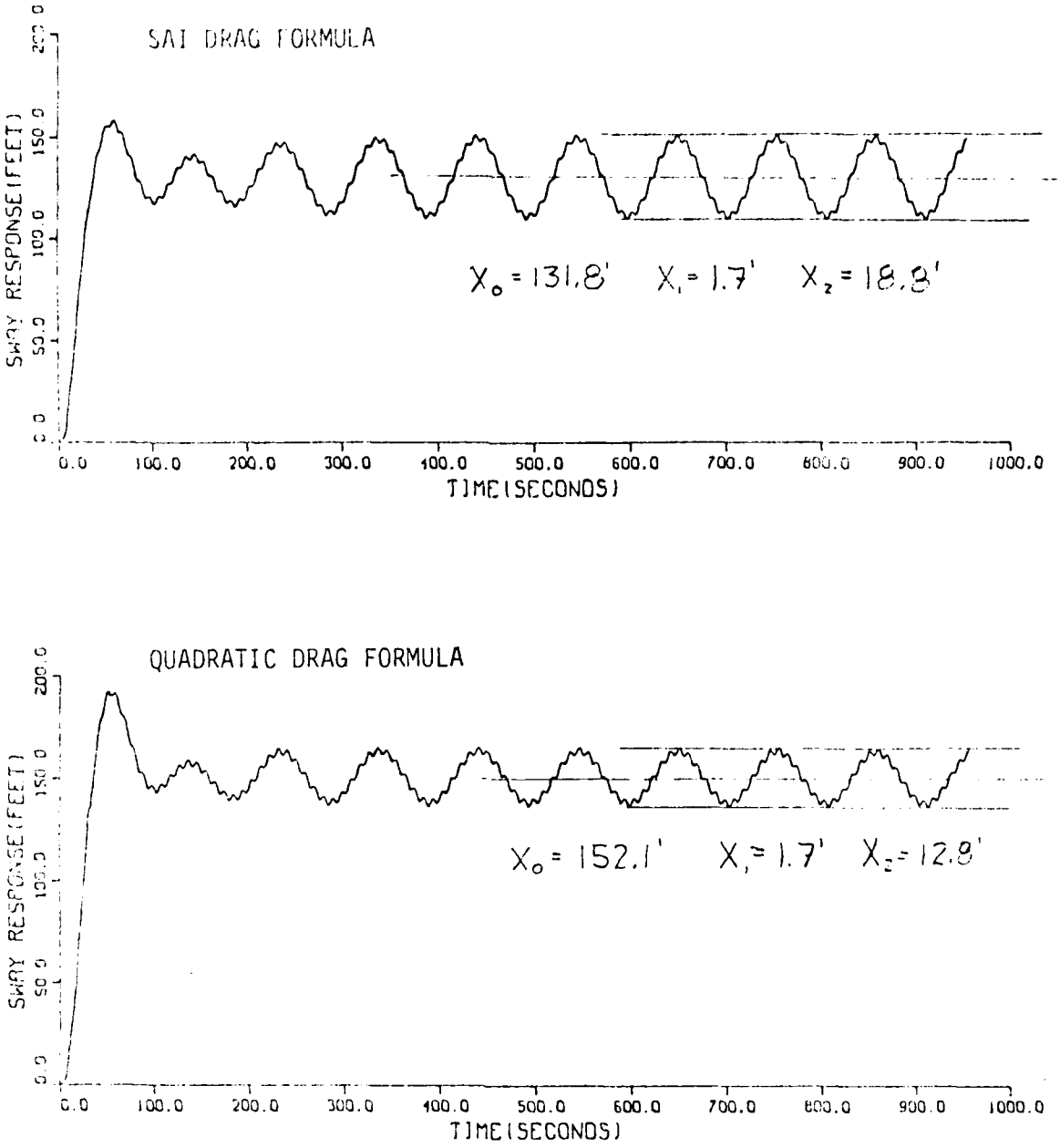

Figure 2-7. Surge displacements for "maximum drift wave" condition with 0° heading (Condition 2).

The results presented above indicate that the SAI drag formula predicts values of viscous forces due to interactions between current and wave-frequency motions that are much smaller than the values predicted by the quadratic viscous force formula. They also show that the total surge motions predicted by the SAI drag formula will, in general, have smaller steady displacements than the motions predicted by the quadratic drag formula.

It is difficult to determine the particular environmental condition and heading angle which will result in the largest maximum surge displacement. Note, for example, that the current may decrease the amplitude of the slowly-varying motions by a magnitude larger than the steady displacement due to current. In such a case, the current will actually result in a decrease in the total surge displacement. Several computer runs have been performed in order to establish the most extreme condition. Of particular interest are the following two regular wave conditions for which results are summarized in Table 2-3.

Condition 1

0^{o} heading, maximum regular wave with H = 80.0 feet and T = 14.0 seconds, maximum unsteady wind and maximum current. Motions computed by SAI and quadratic drag. Results for the surge motions as functions of time are presented in Figure 2-6.

Condition 2

0^{o} heading, "maximum drift wave" with H = 46.4 feet and T = 9.5 seconds and maximum unsteady wind. Surge motion plots for this condition are presented in Figure 2-7.

The "maximum drift wave" in Condition 2 refers to the regular wave which will produce the largest steady wave-induced drift force for the heading in question.* It is assumed in these cases that the wave amplitude is determined from the maximum wave steepness given by $H/\lambda = 0.10$. Note that the maximum theoretical wave steepness for nonbreaking waves is $H/\lambda = 0.14$ and that waves with steepness $H/\lambda \geq 0.12$ have in many cases been recorded.

* As shown in Figure 2-4b, the maximum draft force in regular wave is 1,200 kips and occurs at T = 9.5 sec.

the wave-frequency motions can be predicted very accurately by linear theory ignoring viscous damping and interactions due to current and slowly-varying motions.

- Amplitude of the slowly-varying motions due to unsteady wind excitation alone is 40.9 feet. If current is present in addition to the unsteady wind, then the amplitude of the slowly-varying motions is predicted to decrease by 15.4 feet when the SAI drag formula is used and 25.4 feet when the quadratic formula is used. If wave-frequency motions are also present, then the SAI formula predicts an additional decrease of 15.8 feet, whereas the quadratic formula predicts an additional 6.6-foot decrease. The total decrease in the slowly-varying amplitude due to current and wave frequency motion is 31.2 feet when the SAI drag formula is used and 32.0 feet when the quadratic formula is used.

Table 2-2. Surge displacement components for TLP#1 excited by current, maximum design regular waves and unsteady wind with 0^{o} heading angle (values given in feet).

	SAI Drag Formula	Morison Drag Formula
Steady displacement	70.5	96.7
Wave-frequency amplitude	22.1	22.1
Slowly-varying amplitude	9.7	8.9
Total surge displacement	102.4	127.7

	SAI Drag Formula	Morison Drag Formula
Due to current & interactions	16.1	42.3
Due to wind	52.5	52.5
Due to wave drift	2.0	2.0
Slowly-varying * excitation alone	40.9	40.9
Increase due to current	-15.4	-25.4
Increase due to wave-frequency motion	-15.8	-6.6

	SAI Drag Formula	Morison Drag Formula
Current alone	14.4	14.4
Increase due to wave-frequency motion	1.8	27.9
Increase due to slowly-varying motion	-0.1	0.0

* Slowly-varying due to unsteady wind excitation alone.

summarize the TLP #2 surge motion results and make comparisons between the two platforms. Note that no irregular wave results have been obtained for TLP #2.

Table 2-4 shows the main surge motion component for TLP #2 excited by the maximum design wave and the regular wave condition which results in the maximum steady drift exciting force (referred to as the "maximum drift wave"). Note that the maximum design wave, the maximum current and the maximum wind conditions are assumed the same for TLPs #1 and #2. Comparing the results presented in Table 2-4 with the TLP #1 results shown in Table 2-3, it is seen that the surge motions for TLP #2 are slightly larger than for TLP #1. However, if we normalize the surge motions with respect to water depth, the TLP #2 motions are in general smaller than for TLP #1. It is not possible to make any specific comparisons between the the two TLPs. We have here assumed that the dimensions for TLP #2 are 1.2 times the dimensions for TLP #1. However, it is difficult to evaluate if 1.2 is the correct scaling between a platform operating in 2000-foot depth and a platform operating in 3000-foot depth. Therefore, we must be careful in drawing any general conclusions from a comparison between the surge motions for these two platforms.

Table 2-5 shows the surge displacement components for TLP #2 excited by current, maximum design wave and unsteady wind. Comparing these results with the results presented in Table 2-2 for TLP #1 it is seen that the viscous interaction effects as computed by the Morison quadratic drag formula and the SAI drag formula are about of the same relative magnitude. However, we do note that the additional damping of the slowly-varying motions due to viscous interaction effects between the slowly-varying motions and the current are substantially larger for TLP #2 than for TLP #1. When the SAI drag formula is used this additional damping effect is 2.5 times larger for TLP #2 than for TLP #1, and when the Morison drag formula is used, it is 1.6 times larger. It is difficult to pinpoint any specific reason for these differences.

Table 2-4. Surge displacements for TLP #2 for two extreme regular wave conditions for 0^0 heading.

	Maximum Design Wave H = 80.0 ft T = 14.0 sec		Maximum Drift Wave H = 55.9 ft T = 10.5 sec		Irregular seas $h_{1/3}$ = 10 ft
	SAI Drag	Quad Drag	SAI Drag	Quad Drag	SAI Drag
Steady Current Displacement, X_o^C	18.5	53.7	17.2	46.5	0*
Steady Wind Displacement, X_o^W	66.9	66.9	66.9	66.9	5.8*
Steady Drift Displacement, X_o^D	8.0	8.0	96.9	96.9	2.3
Wave Frequency Amplitude, X_1	18.3	18.3	2.3	2.3	0.9
Slowly-Varying Motion Amplitude, X_2	9.6	7.9	21.9	14.1	2.0
Total Maximum Surge Displacement	121.2	154.6	205.0	226.6	11.6

* For the irregular seas case the current is assumed zero and the wind strength is only 39 ft/sec.

Table 2-5. Surge displacement components for TLP #2 excited by current, maximum design regular waves and unsteady wind with 0^0 heading angle (values given in feet).

	SAI Drag Formula	Morison Drag Formula		SAI Drag Formula	Morison Drag Formula		SAI Drag Formula	Morison Drag Formula
Steady displacement	93.3	128.5	Due to current & interactions	18.5	53.7	Current alone	17.1	17.1
						Increase due to wave-frequency motion	1.4	36.4
						Increase due to slowly-varying motion	0.0	0.2
			Due to wind	66.9	66.9			
			Due to wave drift	8.0	8.0			
Wave-frequency amplitude	18.3	18.3						
Slowly-varying amplitude	9.6	7.9	Slowly-varying* excitation alone	53.3	53.3			
			Increase due to current	-38.0	-40.6			
			Increase due to wave-frequency motion	-5.7	-4.8			
Total surge displacement	121.2	154.6						

* Slowly varying due to unsteady wind excitation alone.

3.0 SPRINGING TENDON LOAD INVESTIGATION*

3.1 The TLP Springing Problem

3.1.1 General Discussion of the Springing Problem

Linear and nonlinear wave-induced high-frequency springing exciting forces can result in large oscillatory loads in the tendons at the natural frequency of the TLP. The natural periods for heave and pitch motions for most deep-water TLPs are typically between 2 to 3 seconds. For the discussion in this section let us assume that the vertical motions natural period, T_n, equals 2.5 seconds.

Regular wave excitation shall be considered first. The wave-induced springing exciting forces can be divided into

- first-order forces resulting from a wave with period, T_w, equal to the natural period of the TLP:

$$T_w = T_n = 2.5 \text{ seconds}$$

- second-order forces resulting from a wave with period equal to twice the natural period of the TLP:

$$T_w = 2T_n = 5.0 \text{ seconds}$$

- third-order forces resulting from a wave with period equal to three times the natural period of the TLP:

$$T_w = 3T_n = 7.5 \text{ seconds}$$

and so on for higher order excitations.

---

* All of the springing load results presented in this section are for zero degree heading. The springing loads for 45^0 heading can be expected to be $\sqrt{2}$ times larger.

It is important to recognize that the second- and third-order excitations are caused by waves which have a larger period and consequently are much longer and have much more energy than the waves giving rise to the linear excitation. If we consider a constant wave-height/wave-length ration, H/λ, it follows that the waves causing the second- and third-order excitation have 16 and 81 times, respectively, the energy of the waves causing the linear excitation. It can be expected, therefore, that the second- and third-order springing forces may be much larger than the first-order forces.

Another important fact is that the springing loads in the tendons will mainly be caused by pitching motions resulting from horizontal wave excitation. The vertical springing excitation due to short waves is so small that it can practically be ignored.

For a typical 2000-foot depth TLP configuration excited by regular periodic waves with $H/\lambda = 0.075$, our computations show that it can be expected that the first-order surge springing exciting force is of the order of magnitude of

$$f_1^{(1)} = 50 \text{ kips}$$

and that the second-order springing force may be of the order of magnitude of

$$f_1^{(2)} = 200 \text{ kips}$$

and that both act very close to the free surface (about three feet below). The effective pitch center for a TLP can be expected to be about 20 feet below the free surface resulting in a pitch moment arm of about 17 feet. Hence, the amplitudes of the first- and second-order pitch springing moments may be of the order of magnitude of

$$f_5^{(1)} = 800 \text{ kips-feet}$$

$$f_5^{(2)} = 3400 \text{ kips-feet}$$

Note that the waves causing the first-order excitation have a period equal to the natural period, whereas the waves causing the second-order excitation have a period equal to twice the natural period of the TLP.

Another critical aspect is that there is very little viscous damping and practically no wave damping for the high-frequency pitch motions. The amplification factor is very large resulting in tendon loads which may be of the order of magnitude of 600 kips per tendon. Figure 1-3 shows schematically the total springing surge exciting force of 250 kips and the resulting 5,000 kips load on the eight left-hand side tendons and -5,000 kips load on the eight right-hand side tendons. These are approximate results for a 2000-foot depth TLP with typical dimensions as shown in the figure.

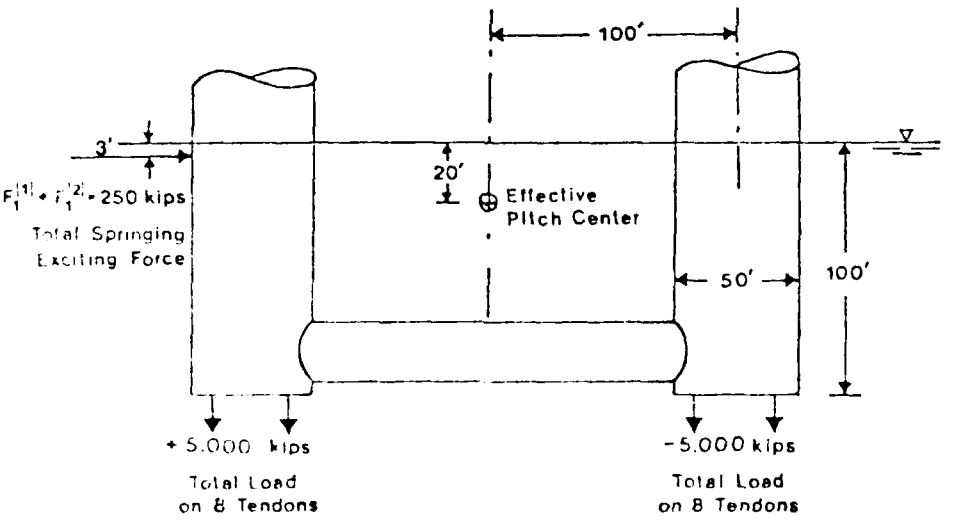

Figure 3-1. Total springing surge exciting force and resulting tendon load for TLP with typical dimensions.

We have at the present time made no attempt to predict the third- or higher-order springing excitation. It is believed that the higher-order excitations may be as important as the second-order; however, we need to have a better understanding of the second-order excitation and, in particular, as it applies to realistic irregular sea conditions before we can advance to the more complicated higher-order excitation problem.

3.1.2 Problem Formulation

We shall here refer to springing loads as the additional tendon loads caused by wave-induced vertical motions at or near the natural frequency of the TLP. Since the wave lengths for both the first- and second-order springing wave excitations are smaller or of the same order of magnitude as the depth of the TLP, it can be concluded that the heave springing excitation forces are small and can be ignored. The springing loads in the tendons at or near the natural frequency of the system must result, therefore, from a pitch moment about the virtual mass center caused by wave-induced horizontal forces acting on the four legs at a location close to the undisturbed free-surface level.

We shall here assuem that the pitch springing exciting moment for the TLP at or near the natural frequency can be obtained from the springing excitation for a single leg. In fact, we shall assume that the pitch exciting moment with respect to the virtual mass center is

$$F_5 = 4(F_5^* + z_c F_1^*) \tag{3-1}$$

where $F_5^* = F_5^{(1)} + F_5^{(2)}$ = pitch springing moment for a single leg with respect to a coordinate system located at the undisturbed free surface.

$F_1^* = F_1^{(1)} + F_1^{(2)}$ = surge springing force for a single leg.

z_c = vertical distance from undisturbed free surface to the virtual mass center.

The factor "4" in equation (3-1) has been used assuming that the springing forces for the four legs are in phase. This is a conservative estimate. Figure 3-2 shows schematically the springing excitation in the two reference systems.

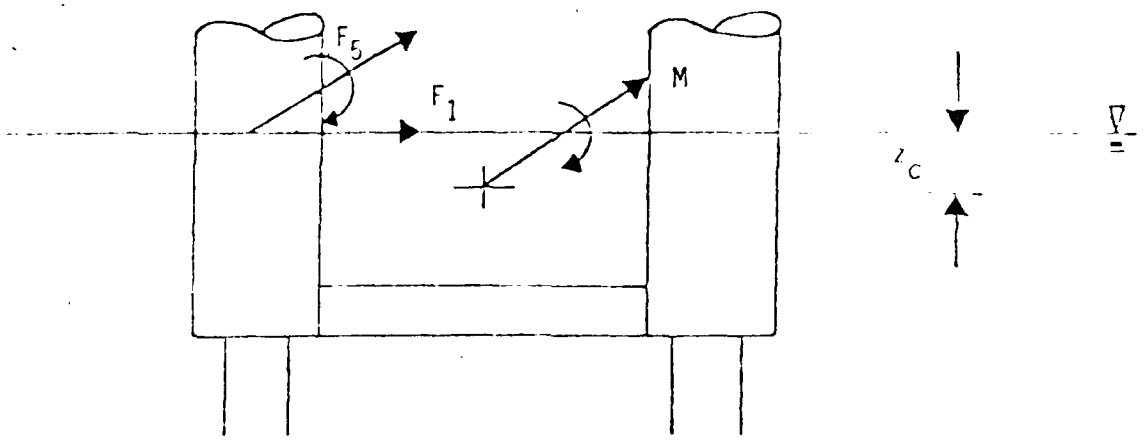

Figure 3-2. Total TLP pitch moment about effective pitch center.

A formal derivation of the first- and second-order springing forces are presented in Salvesen, et al. (1983). It is shown that both the first- and the second-order forces can be expressed in terms of the first-order velocity potential, $\phi^{(1)}$. The contribution from the second-order potnetial, $\phi^{(2)}$, can be shown to be small for the vertical cylinder case. By applying an approach similar to the method used by MacCamy and Fuchs (1954) and by assuming that the waves are short, $\lambda/H << 1$, and that the water depth is large, $\lambda/d << 1$, it can be shown that the first-order velocity potential, $\phi^{(1)}$, for the vertical cylinder case can be expressed in terns of a series expansion. Then by using this expansion it can be shown that the first- and second-order surge forces and pitch moments can be expressed in terms of the Hankel's function. By applying this approach we have been able to develop very efficient computational methods for predicting the wave-induced springing exciting forces and moments.

3.2 Regular Wave Results for TLP #1

3.2.1 Pitch Springing Moment Results

In this section we shall present wave-induced pitch springing moment results for the TLP #1 design excited by regular sinusoidal waves. The first-order springing moment is

$$F_5^{(1)}(t) = f_5^{(1)} \cos \omega_e t \tag{3-2}$$

where ω_e is the exciting frequency. Note that for first-order excitation, the excitation frequency is the same as the wave frequency. The second-order springing moment is

$$F_5^{(2)}(t) = f_5^{(2)} \cos \omega_e t \tag{3-3}$$

For the second-order excitation, the excitation frequency, ω_e, is equal to twice the wave frequency. Note that the pitch moments are about the virtual mass center which is 21.8 feet below the undisturbed free-surface level.

Figure 3-3 shows both the first-order and second-order pitch springing moment amplitudes as function of the exciting period. Results are shown for two wave steepnesses, $H/\lambda = 0.050$ and 0.075. It is seen from the figure that the second-order moment, $f_5^{(2)}$, is substantially larger than the first-order moment, $f_5^{(1)}$. This is partly due to the fact that the waves causing the first-order moment have the same period as the exciting period, $T_W = T_E$, whereas the waves causing the second-order moments have periods twice the exciting period, $T_W = 2T_E$. This implies that the wave height for the waves causing the second-order moments at a given excitation period is four times the wave height for the waves causing the first-order moment (assuming a constant H/λ value). Furthermore, it is seen from the tabulated values in Figure 3-3 that at the natural pitch period ($T_n = 2.506$ sec) and for wave steepness, $H/\lambda = 0.075$, the first-order moment is 1600

ft-kips, whereas the second-order moment is 5680 ft-kips. In other words, the second-order moment is in this case about 3.6 times larger than the first-order moment.

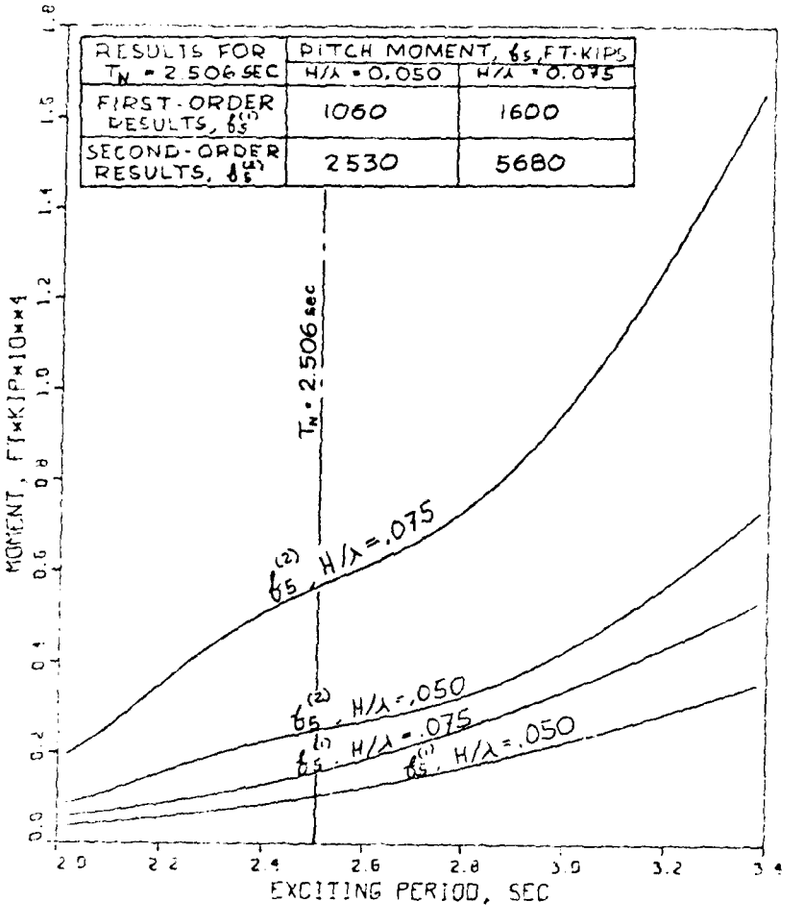

Figure 3-3. First- and second-order pitch moments, $f_5^{(1)}$ and $f_5^{(2)}$, for H/λ = .050 and H/λ = .075.

3.2.2 Equation of Motion

If we consider the pitch motion about the virtual mass center, the motion is uncoupled and the equation of motion is

$$A\ddot{\theta} + B\dot{\theta} + C\theta = f_5 \cdot e^{-i\omega t} \tag{3-4}$$

Here θ is the pitch angle, A is the virtual mass moment of inertia, B is the damping coefficient which is typically a function of the pitch angle, C is the restoring coefficient and f_5 is the pitch moment amplitude. As shown in Appendix A, for the TLP #1 design

$$A = 4.06 * 10^{10} \text{ slug-ft}^2 \tag{3-5}$$

$$C = 2.553 * 10^{11} \text{ lb-ft} \tag{3-6}$$

The pitch natural period is

$$T_n = 2\pi \frac{A}{C} = 2.506 \text{ seconds.} \tag{3-7}$$

Of interest here is the additional tendon tension load due to pitch springing motion rather than the pitch motion itself. The tendon tension load per tendon is linearly proportional to the pitch angle

$$\tau = \alpha\theta \tag{3-8}$$

where the coefficient

$$\alpha = \frac{L}{2} \cdot C_{33} \frac{1}{16} = 1.45 * 10^5 \text{ kips/rad.} \tag{3-9}$$

Therefore, the tendon tension load per tendon can be expressed as

$$\tau(\omega) = \frac{\alpha \cdot f_5}{(-\omega^2 A + C) - i\omega B} \quad . \tag{3-10}$$

The tendon tension load can also be expressed in terms of the magnification factor, n, as

$$\tau(\omega) = n(f_5 \frac{\alpha}{C}) \tag{3-11}$$

where $f_5\ \alpha/C$ is the zero frequency tendon tension. The magnification factor is defined as

$$n \equiv \frac{1}{1 - (\frac{\omega}{\omega_n})^2 - i2\zeta \frac{\omega}{\omega_n}} \tag{3-12}$$

where the damping factor is by definition

$$\zeta \equiv \frac{B}{2A\omega_n} = \frac{B}{B_c} \quad . \tag{3-13}$$

Here B_c is the critical damping coefficient.

Note that when the TLP is excited by a pitch moment at the natural frequency, ω_n, the amplification factor is

$$n = \frac{1}{-i2\zeta} \quad . \tag{3-14}$$

3.2.3 Tendon Springing Loads

By equations (3-11) and (3-14) if follows that the additional tendon tension load per tendon is

$$\tau(\omega_n) = n\ f_5 \frac{\alpha}{C} = \frac{f_5}{\zeta}\ 2.84 * 10^{-4}\ \text{kips} \tag{3-15}$$

when the TLP is excited at the natural period, T_n = 2.506 seconds. Here, the pitch exciting moment amplitude, f_5, is in kips-ft units. Note that if the damping factor, ζ, is a constant independent of the pitch motion amplitude, the tendon load, τ, is directly proportional to the pitch moment, f_5. For the TLP in the high frequency range, the damping is mainly due to

- viscous forces,
- wave generation, and
- structural damping.

In this study, we have included damping only due to viscous forces and wave generation. It is expected that the structural damping is of the same order of magnitude as the viscous damping; however, it is difficult to obtain accurate estimates for the structural damping without a complete knowledge of the details of the design of the tendons.

Figure 3-4 shows the damping factor, ζ, as a function of tendon tension load, τ (not that τ is linearly proportional to the pitch angle, equation (3-9)). Also shown in Figure 3-4 is the tendon tension load, τ, as a function of the pitch moment, f_5. These curves have been obtained by a computer program which models the viscous forces for high frequency pitch motions as well as includes the wave generation damping. Note that Figure 3-4 is only applicable to the TLP #1 design when pitching at the natural period, T_n = 2.506 seconds.

Example Results

Consider first-order regular wave excitation at the natural period and assume that $H/\lambda = 0.075$. From Figure 3-3 it follows that the first-order pitch moment amplitude is

$$f_5^{(1)} = 1600 \text{ kips-ft.}$$

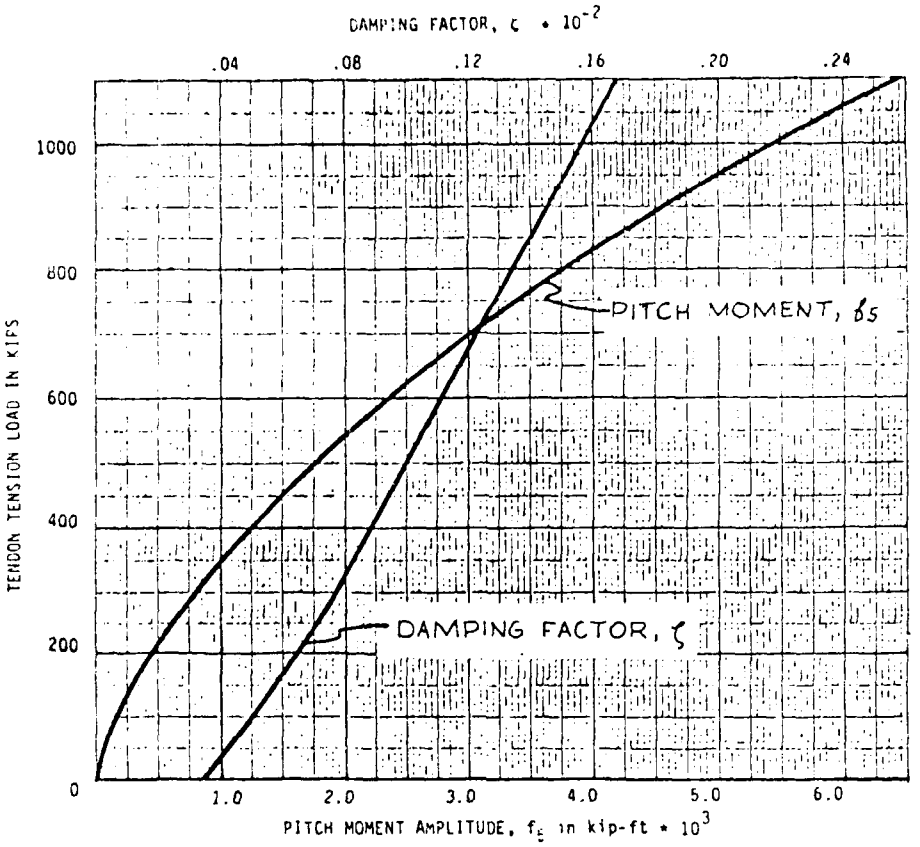

Figure 3-4. Tendon tension load, τ, as a function of pitch moment, f_5, and damping factor, ζ, as a function of tendon tension load, τ.

From Figure 3-4 we have that the additional tendon tension load is

$$\tau^{(1)} = 470 \text{ kips per tendon.}$$

Then let us consider second-order regular excitation with excitation period equal to the natural period and wave period

$$T_W = 2T_n = 5.012 \text{ seconds.}$$

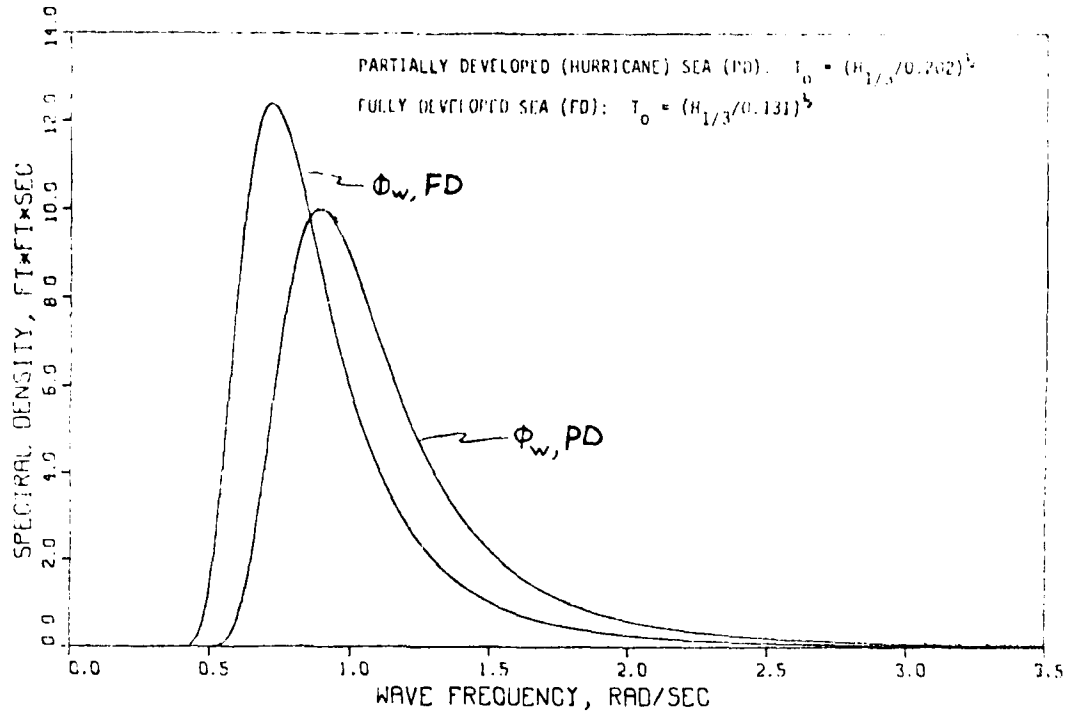

Figure 3-10. Sea spectra, fully developed (FD) and partially developed (PD).

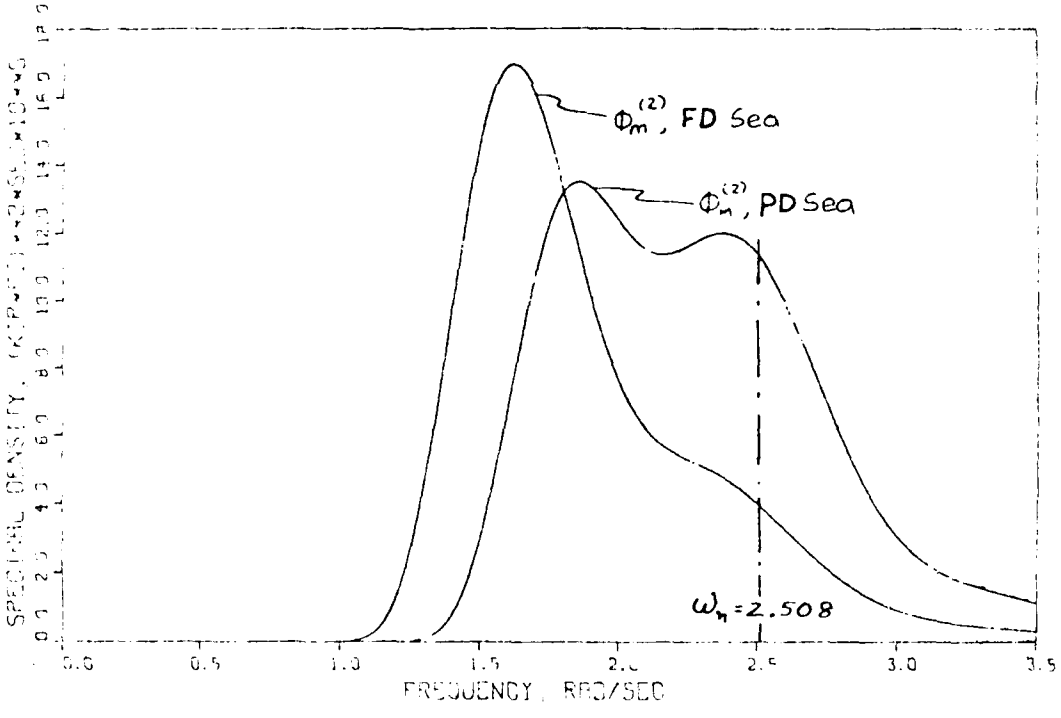

Figure 3-11. Second-order pitch exciting moment power spectra. Fully developed (FD) and partially developed (PD) sea states.

Simplified Prediction Method

The contribution to the variance (i.e., the square of the RMS value, σ^2) for second-order excitation can be estimated by the following simple procedure.

$$\begin{aligned}\sigma^2 &= \int_0^\infty |H_\tau(\omega)|^2 \cdot \phi_m^{(2)}(\omega)\, d\omega \\ &\approx \phi_m^{(2)}(\omega_n) \int_0^\infty |H_\tau(\omega)|^2\, d\omega \\ &= \phi_m^{(2)}(\omega_n) \cdot \left(\frac{\alpha}{A}\right)^2 \frac{\pi}{4}\ \frac{1}{\zeta\omega_m^3}\end{aligned} \qquad (3\text{-}36)$$

Applying this relationship to the irregular sea condition considered here, we have approximately the same result as obtained by numerical integration, namely

$$\sigma^2 \approx 1980 \ .$$

3.5 Sea State Investigation

In this section we shall present irregular sea results for TLP #1 using a fully developed (FD) Pierson-Moskowitz sea spectrum as well as the partially developed (PD) Bretschneider storm sea used in Section 3.4. For both cases the spectrum is given by equation (3-34) with $h_{1/3}$ = 10 feet. For the FD case

$$T_o = 8.73 \text{ seconds}$$

and for the PD case T_o is the same as used in Section 3.4, namely,

$$T_o = 7.04 \text{ seconds.}$$

Figure 3-10 shows the sea spectra for the two cases considered, and Figure 3-11 shows the second-order pitch exciting moment power spectrum,

- the high frequency range.

Table 3-2 shows the square of the RMS values, σ_τ^2 (see equation 3-28) for the first- and second-order tendon tension response spectrum for the high- and low-frequency ranges separately.

The results presented in Table 3-2 seem to demonstrate that the first-order contribution in the low frequency range dominates the total contribution to the RMS value for the tendon tension response. Considering only the low frequency range contribution, we find that the significant tendon tension value for this sea condition is

$$\tau_{1/3} = 2.0\,\sigma = 75 \text{ kips.}$$

If we consider only the high frequency range, we have

$$\tau_{1/3} = 2.0\,\sigma = 102 \text{ kips.}$$

It should be stressed that the main objective with this investigation has been to estimate the high frequency tendon tension load. The low frequency computations were only included to demonstrate that the low frequency tension loads may be as important as the high frequency part.

	Area and RMS values for tendon tension response spectrum, σ_τ^2 and σ_τ in kips^2 and kips			
	High Frequency Range		Low Frequency Range	
	Area	RMS	Area	RMS
First-Order Contribution	610	24.7	1420	37.6
Second-Order Contribution	1980	44.5	0	0.0
Total	2590	50.9	1420	37.6

Table 3-2. First- and second-order contributions to area and RMS values for the tendon tension response spectrum for the high and low frequency ranges.

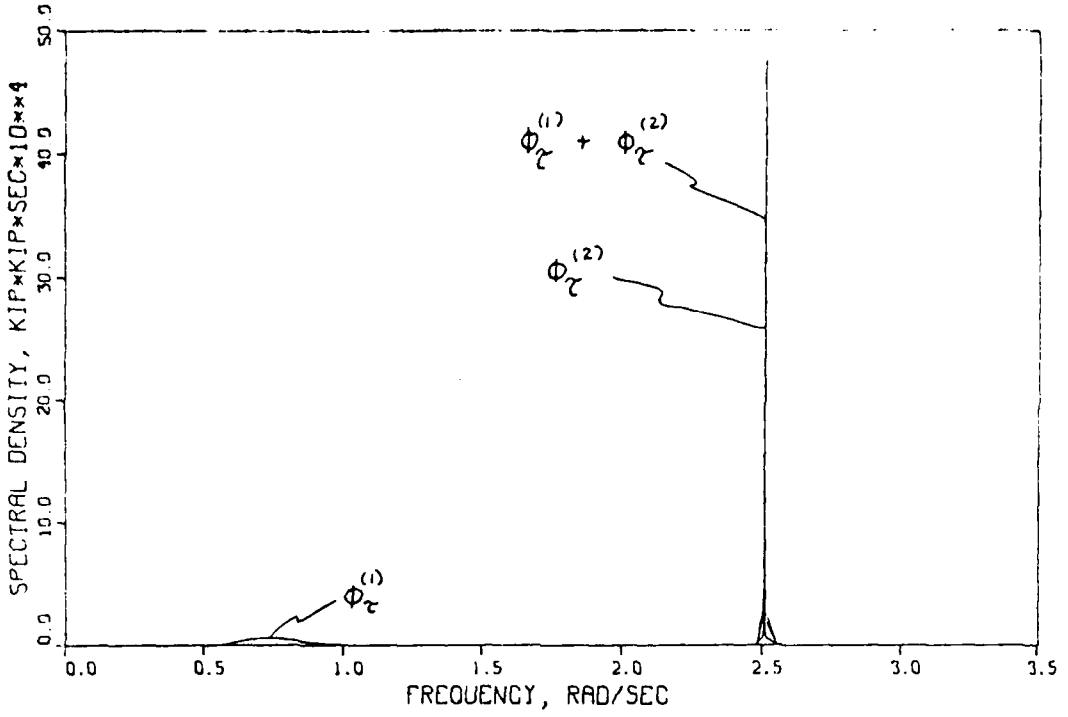

Figure 3-9a. First- and second-order tendon tension response power spectra.

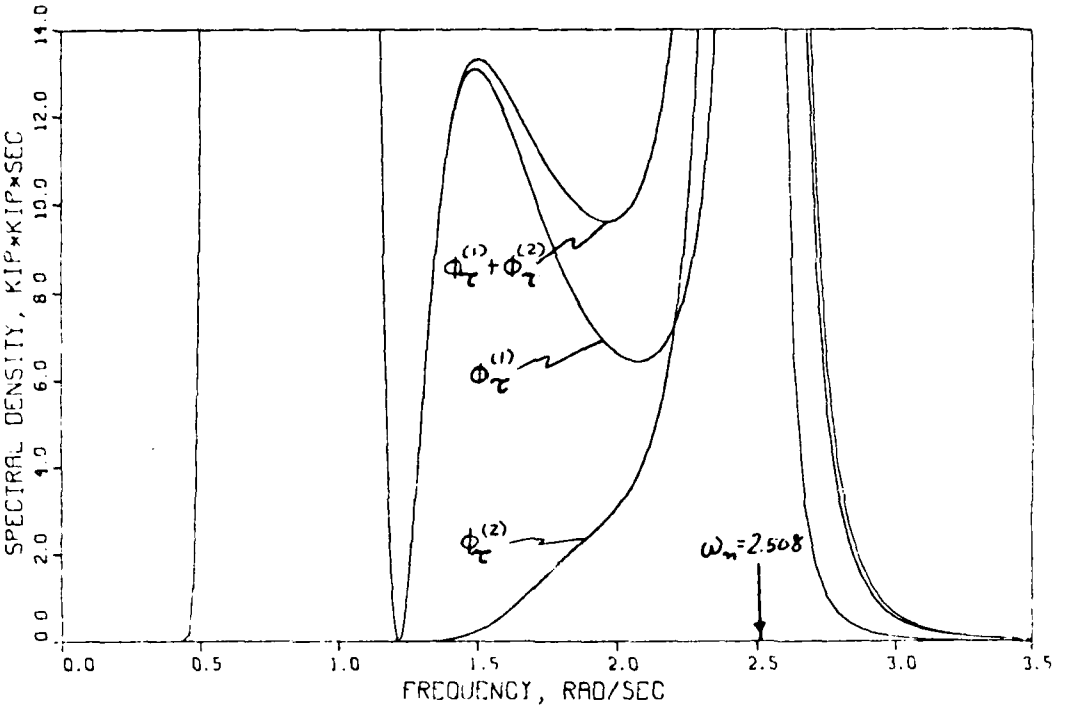

Figure 3-9b. First- and second-order tendon tension response power spectra.

$$\zeta = 0.05 * 10^{-2} .$$

Figure 3-8 shows the tendon tension RAO, $H_\tau(\omega)$, for this assumed constant damping factor.

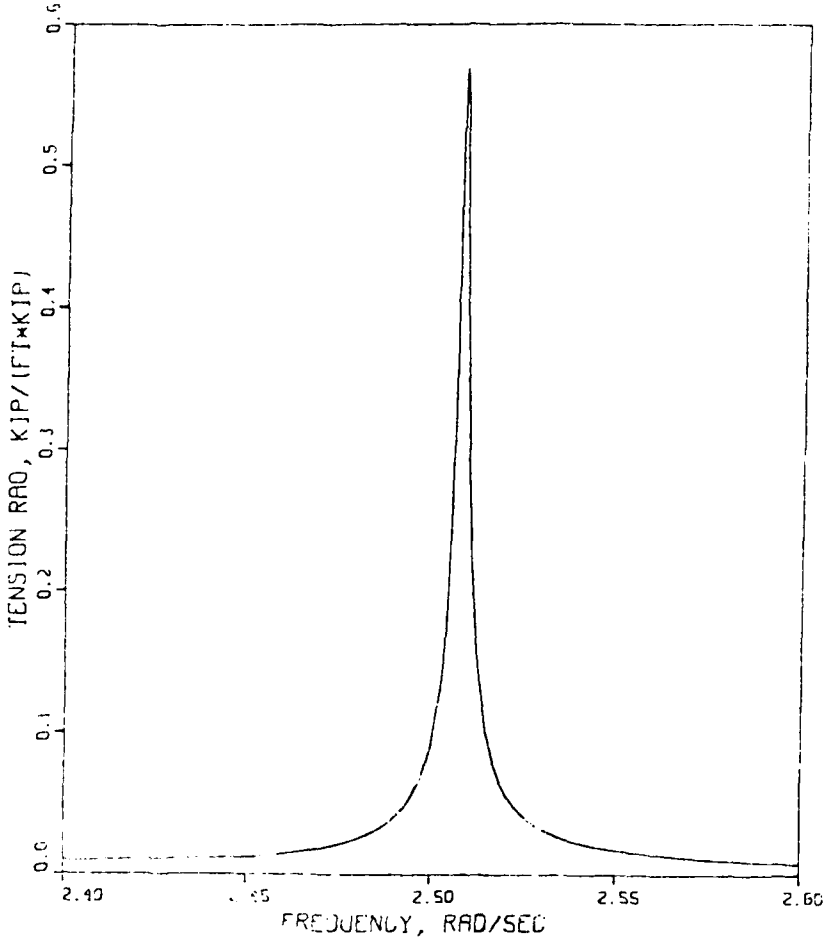

Figure 3-8. Tendon tension RAO, H_τ, for TLP #1, ω_n = 2.508 rad/sec and damping factor ζ = .0005

Figures 3-9a and 3-9b show the first- and second-order tendon tension response power spectrums. As indicated in these figures, the response power spectrum can conveniently be divided into two parts:

- the low frequency range, and

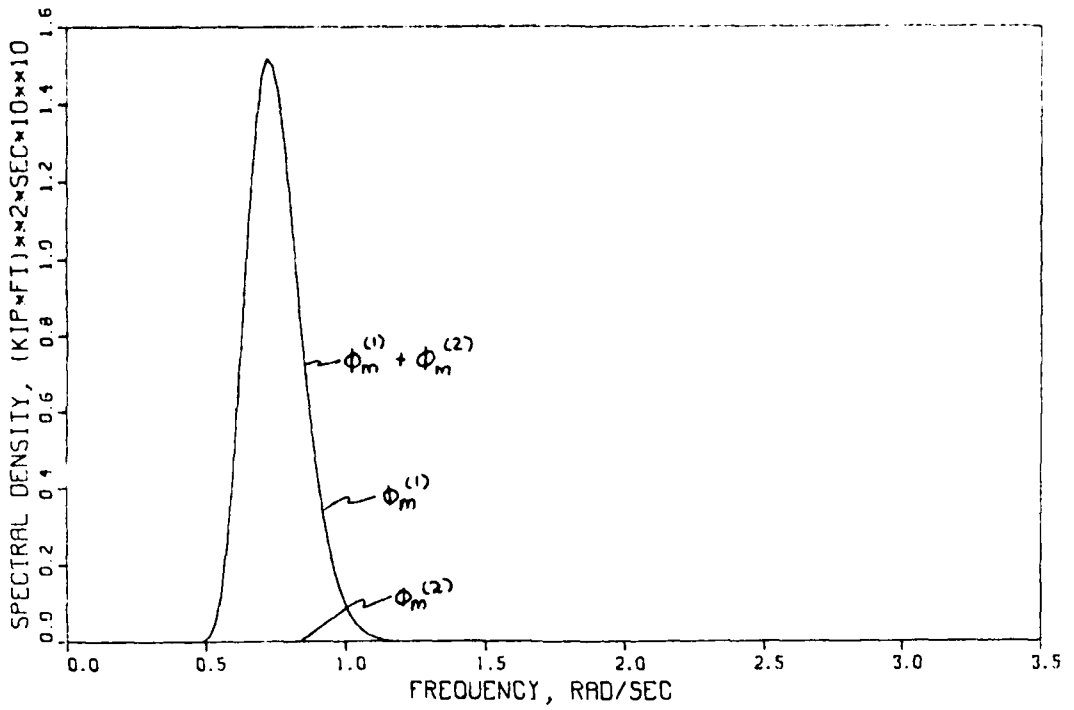

Figure 3-7a. First- and second-order pitch exciting moment power spectra.

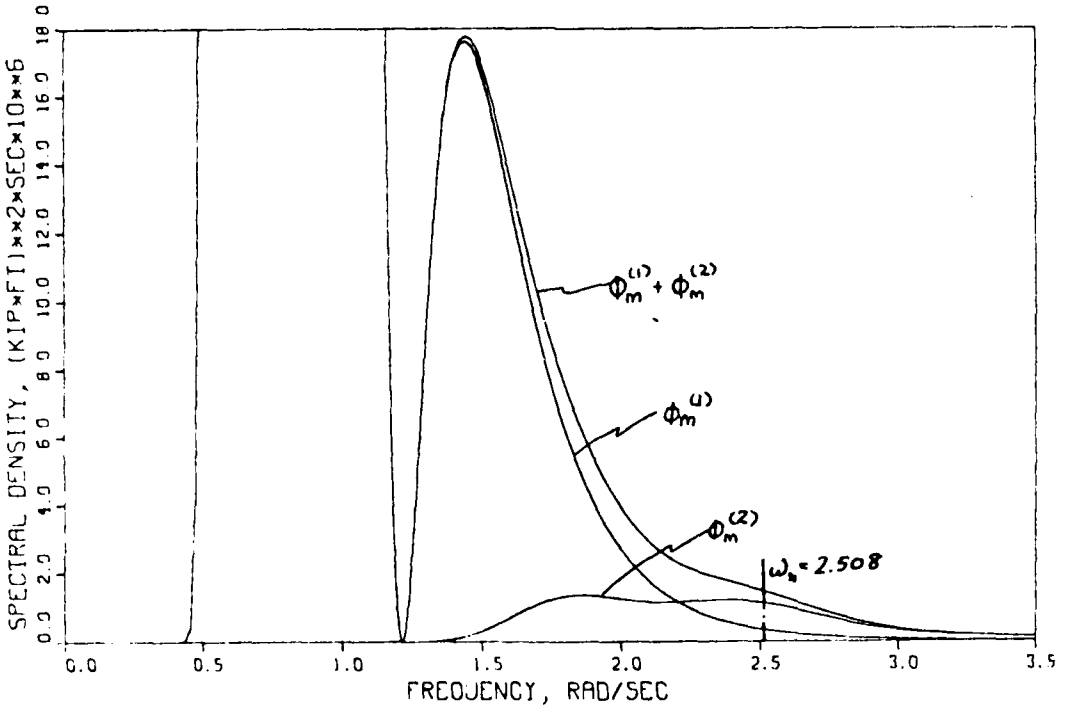

Figure 3-7b. First- and second-order pitch exciting moment power spectra

3.4.2 Computed TLP Results

In this section we shall present computed results for the TLP #1 design in an irregular seaway represented by a Bretschneider energy spectrum for a partially developed storm sea

$$\phi_a(\omega) = \frac{A}{\omega^5} e^{-B/\omega^4} \tag{3-34}$$

where $A = 486\ h_{1/3}^2/T_o^4$ and $B = 1948.18/T_o^4$. For the example case presenter here

$$h_{1/3} = 10 \text{ feet and } T_o = 7.04 \text{ sec.}$$

Figure 3-7a and 3-7b show the first- and second-order pitch exciting moment power spectrum as obtained by equations (3-23) and (3-25). Please note that for this investigation, the first-order pitch moment RAO values, $H_m^{(1)}(\omega)$, have been estimated by using single vertical leg results, the approach discussed in Section 3.1.2. This approach is only valid in the high frequency range. Therefore, any results shown here in the low frequency range should only be considered as an order of magnitude estimate. It is seen in Figure 3-7a that in the low frequency range the first-order exciting moment power spectrum, $\phi_m^{(1)}$ is as expected, an order of magnitude larger than the second-order spectrum, $\phi_m^{(2)}$. However, as seen in Figure 3-7b in the high frequency range, near the pitch natural frequency, $\phi_m^{(2)}$ is substantially larger than $\phi_m^{(1)}$.

The tendon tension load response power spectrum is given by equation (3-26) and is

$$\phi_2(\omega) = |H_\tau(\omega)|^2 \cdot \left(\phi_m^{(1)}(\omega) + \phi_m^{(2)}(\omega)\right) \tag{3-35}$$

where $H_\tau(\omega)$ is the tendon tension RAO. For simplicity we shall assume that for the irregular wave results presented here the damping factor is

and the average of the 1/10 highest amplitudes of the tendon tension load is

$$\tau_{1/10} = 2.55\,\sigma_{\tau} \quad . \tag{3-31}$$

In predicting the RMS value for the tendon tension load, it is important to recognize that the pitch damping coefficient is nonlinear. It is here suggested that the nonlinear damping can be adequately represented by using an equivalent linearization method where the damping coefficient is assumed constant and equal to the same value as for harmonic motions at the natural frequency with motion amplitude equal to the significant motion amplitude for the irregular wave case.

In other words, the following procedure is used in predicting the tendon springing load in an irregular seaway.

> First assume a value for the significant tendon tension load, which we shall label $\tau^{*}_{1/3}$. Then by using this value, the first estimated damping coefficient is obtained from Figure 3-4. The significant tendon tension load is then computed following the above steps with the estimated damping coefficient. This procedure is repeated until satisfactory accuracy has been obtained.

Note that if the free-surface elevation for the unidirectional seaway is given by

$$y(t) = \sum_{n} A_n e^{-i\omega_n t} \tag{3-32}$$

then the second-order pitch springing moment as a function of time can be expressed as

$$F_5^{(2)}(t) = \sum_{n} \sum_{m} A_n A_m \mathcal{J}(\omega_n, \omega_m)\, e^{-i(\omega_n + \omega_m)t} \quad . \tag{3-33}$$

$$H_m^{(1)} = \frac{f_5^{(1)}}{A} \quad . \tag{3-24}$$

The pitch moment power spectrum due to second-order wave-induced excitation is

$$\phi_m^{(2)}(\omega) = 2 \cdot \int_0^{\omega/2} \phi_a\left(\frac{\omega}{2} + \Delta\omega\right)\ \phi_a\ \left(\frac{\omega}{2} - \Delta\omega\right) \cdot \left|\mathcal{M}\left(\frac{\omega}{2} + \Delta\omega,\ \frac{\omega}{2} - \Delta\omega\right)\right|^2\ d(\Delta\omega) \tag{3-25}$$

where $\mathcal{M}(\omega_1, \omega_2)$ is the second-order two-wave pitch springing moment per unit wave amplitude.

The tendon tension load response power spectrum is

$$\phi_\tau(\omega) = |H_\tau(\omega)|^2 \cdot \left(\phi_m^{(1)}(\omega) + \phi_m^{(2)}(\omega)\right) \quad . \tag{3-26}$$

where the tendon tension per unit pitch moment excitation is defined by

$$H_\tau(\omega) = \frac{\tau(\omega)}{f_5} \tag{3-27}$$

and where $\tau(\omega)$ is given by equation (3-10). The variance (i.e., the square of the RMS value) of the tendon tension load is

$$\sigma_\tau^2 = \int_0^\infty \phi_\tau(\omega)\ d\omega \quad . \tag{3-28}$$

The average tendon tension load amplitude is

$$\tau_{avg} = 1.25 \cdot \sigma_\tau, \tag{3-29}$$

the significant value of the tendon tension load amplitude is

$$\tau_{1/3} = 2.00 \cdot \sigma_\tau \tag{3-30}$$

From Figure 3-5 it is seen that the RAO value for the second-order sum-frequency moment, $\mathcal{M}(\omega_1, \omega_2) = 260$ kips-ft/ft^2 for $\omega_1 = 1.054$ and $\omega_2 = 1.454$ rad/sec. Hence, the amplitude of the second-order springing moment component with exciting frequency equal to the natural frequency is

$$2\left[f_5^{(2)}\right]_{12} = 2A_1A_2\mathcal{M}(\omega_1, \omega_2) = 3620 \text{ kips-ft.}$$

From Figure 3-4 it follows that the tendon tension load for the above two-wave case is

$$\tau^{(2)} = 780 \text{ kips per tendon.}$$

3.4 Irregular Wave Results for TLP #1

3.4.1 Theoretical Formulation

We shall assume that the seaway is unidirectional and represented by a known power spectrum

$$\phi_a(\omega) \tag{3-21}$$

and that the wave-induced pitch exciting moment has a power spectrum given by

$$\phi_m(\omega) = \phi_m^{(1)}(\omega) + \phi_m^{(2)} + \ldots \tag{3-22}$$

Here the pitch-moment power spectrum due to <u>first-order</u> wave-induced excitation is

$$\phi_m^{(1)} = |H_m^{(1)}(\omega)|^2 \cdot \phi_a(\omega) \tag{3-23}$$

where the first-order pitch exciting moment amplitude per unit wave amplitude, RAO, is

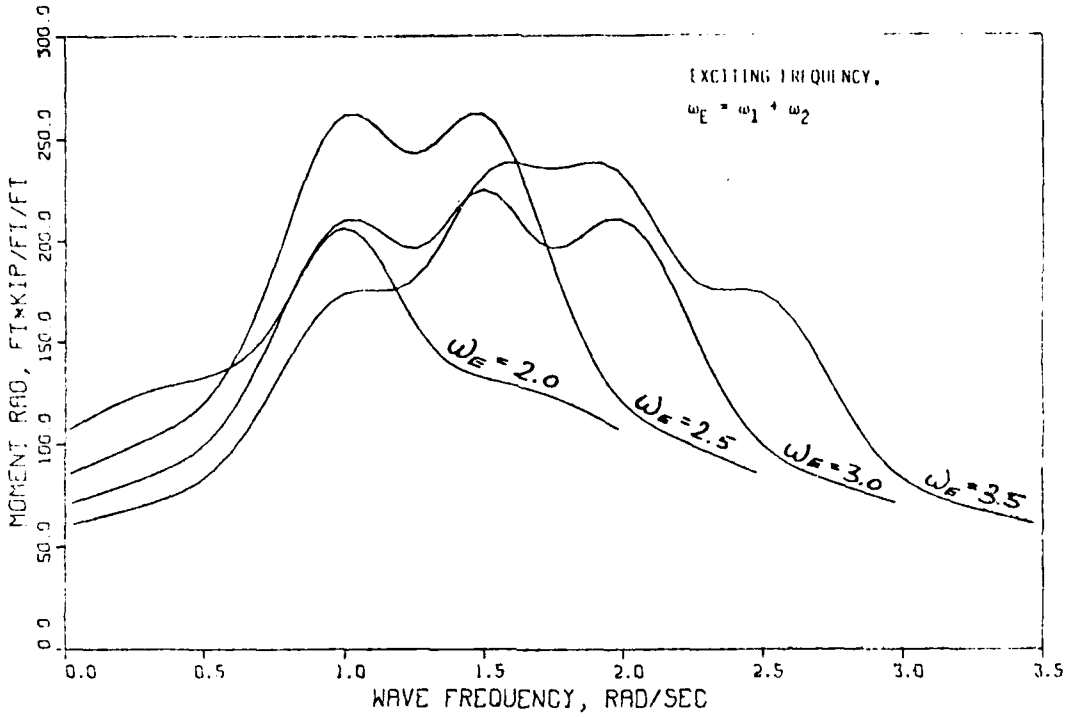

Figure 3-6. Two-wave, second-order pitch moment per unit wave amplitude, $\mathcal{J}(\omega_1, \omega_2)$.

Two-Wave Example (see Figure 3-5)

Consider two waves with frequencies

$$\omega_1 = 1.054 \text{ and } \omega_2 = 1.454 \text{ rad/sec.}$$

The sum frequency of these two waves is equal to the natural frequency for the TLP #1

$$\omega_n = \omega_1 + \omega_2 = 2.508 \text{ rad/sec}$$

Assume that they both have the same wave slope

$$H/\lambda = 0.04$$

$$2 \cdot \left[f_5^{(2)}\right]_{12} e^{-i(\omega_1 + \omega_2)t} = 2 \cdot A_1 A_2 \mathcal{S}(\omega_1, \omega_2)\, e^{-i(\omega_1 + \omega_2)t} \qquad (3\text{-}20)$$

where A_1 and A_2 are the wave amplitudes for the two waves with frequencies ω_1 and ω_2 respectively. Here $\mathcal{S}(\omega_1, \omega_2)$ is defined as the two-wave pitch springing moment amplitude per unit wave amplitude (RAO).

Figure 3-5 shows $\mathcal{S}(\omega_1, \omega_2)$ for TLP #1 for sum frequencies equal to the pitch natural frequency:

$$\omega_1 + \omega_2 = \omega_n = 2.508 \text{ rad/sec.}$$

Figure 3-6 shows $\mathcal{S}(\omega_1, \omega_2)$ for the four following sum frequencies:

$$\omega_1 + \omega_2 = 2.0,\ 2.5,\ 3.0 \text{ and } 3.5 \text{ rad/sec.}$$

Recall that for this component of the second-order pitch moment, the excitation period is equal to the sum frequency.

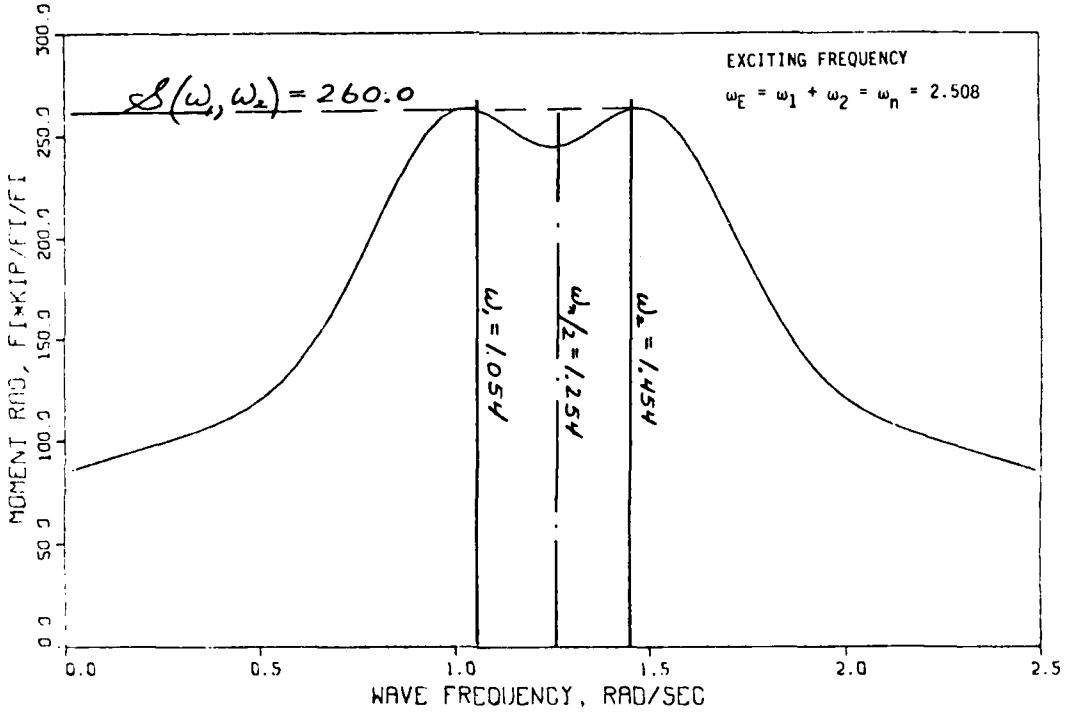

Figure 3-5. Two-wave, second-oder pitch moment per unit wave amplitude for $\omega_1 + \omega_2 = \omega_n$ = 2.508 rad/sec.

The second-order springing exciting force is given by

$$F_j^{(2)}(t) = \left[f_j^{(2)}\right]_{11} e^{-2\omega_1 t} + \left[f_j^{(2)}\right]_{22} e^{-i2\omega_2 t}$$

$$2\left[f_j^{(2)}\right]_{12} e^{-i(\omega_1 + \omega_2)t} \qquad (3\text{-}17)$$

Note that the amplitudes for the double frequency components, $\left[f_j^{(2)}\right]_{11}$ and $\left[f_j^{(2)}\right]_{22}$ are identical to the amplitude for the single regular wave case. The amplitude of the sum frequency component of the second-order springing force which is due to interactions between the two wave components is

$$2\left[f_j^{(2)}\right]_{12} = 2f_j^{(2)}(\omega_1, \omega_2) \qquad (3\text{-}18)$$

By following a formal procedure as used for the single-wave case, it can be shown that the amplitude of the sum frequency component (3-18) can be expressed in terms of the first-order potentials for the two individual waves, $\phi_1^{(1)}$ and $\phi_2^{(1)}$. By expressing these potentials in terms of series expansions a very efficient computer program has been developed for computing the two-wave amplitude, $f_j^{(2)}(\omega_1, \omega_2)$ for a single vertical cylinder. The total pitch moment for the two-wave case is obtained by equation (3-1). Note that a term containing the second-order potential, $\phi_{12}^{(2)}$, has been ignored in this approach. It is believed that this term will result in a very small contribution to the total force.

Now consider two regular waves with sum frequency equal to the natural frequency

$$\omega_n = \omega_1 + \omega_2 \qquad (3\text{-}19)$$

then the second-order sum frequency component of the pitch moment will have excitation frequency identical to the natural frequency and may be expressed as

If we assume that $H/\lambda = 0.075$, it follows from Figure 3-3 that the pitch moment amplitude is

$$f_5^{(2)} = 5680 \text{ kips-ft.}$$

From Figure 3-4 we have that the tendon tension load is

$$\tau^{(2)} = 1020 \text{ kips per tendon.}$$

The above results for first- and second-order regular wave excitation are summarized in Table 3-1.

	Pitch moment amplitudes in kips-ft	Tendon tension loads in kips
First-order regular wave excitation $H/\lambda = 0.075$	1600	470
Second-order regular wave excitation $H/\lambda = 0.075$	5680	1020

Table 3-1. Pitch moment amplitudes and tendon tension loads due to first- and second-order regular wave excitation.

3.3 Two-Wave Results for TLP #1

Consider a body excited by a wave train consisting of two regular waves with frequencies ω_1 and ω_2. The first-order exciting force is

$$F_j^{(1)}(t) = f_j^{(1)}(\omega_1)\, e^{-i\omega_1 t} + f_j^{(1)}(\omega_2)\, e^{-i\omega_2 t}. \qquad (3\text{-}16)$$

$\phi_m^{(2)}(\omega)$ for these two sea spectra. It is seen in Figure 3-11 that the pitch exciting power spectrum value at the pitch natural frequency (ω_n = 2.508 rad/sec) is almost three times as large for the PD sea as it is for the FD sea condition. According to equation (3-36), this implies that the variance, σ^2, should also be approximately three times larger for the PD case than for the FD case.

Table 3-3 shows the first- and second-order contribution to the RMS values for the tendon tension responses for the high- and low-frequency ranges both for the RD and the PD sea states. It is seen that for the high frequency range the first- and second-order RMS values for the PD sea state are about $\sqrt{3}$ times as large as they are for the RD sea state. Whereas for the low frequency range where only the first-order contribution is of a significant magnitude, the RMS values for the FD sea state are larger (by a factor of two) than those for the PD sea state.

These results seem to indicate that it is important to consider both partially developed and fully developed sea states when predicting the tendon tension responses due to wave-induced springing. In general, it can be expected that the second-order contribution will be substantially larger in a partially developed sea state than in a fully developed sea state with the same significant wave height.

	RMS values for the tendon tension response spectrum, in kips			
	High Frequency Range		Low Frequency Range	
	FD Sea	PD Sea	FD Sea	PD Sea
First-Order Contribution	16.1	24.7	75.7	37.6
Second-Order Contribution	26.3	44.5	0.1	0.0
Total	30.9	50.9	75.7	37.6

Table 3-3. First- and second-order contributions to RMS values for the tendon tension response spectrum for the high and low frequency ranges for fully developed (FD) and partially developed (PD) sea states.

3.6 Pitch Center Investigation

In this section we shall investigate the effect of the location of the pitch center for TLP #1. Note that the pitch center is defined as the virtual mass center (including both the mass of the TLP and the hydrodynamic added mass). We shall consider two pitch center locations: the actual location for the TLP #1, namely

$$z_1 = -21.8 \text{ feet}$$

and 25% of this distance,

$$z_2 = 0.25\ z_1 = -5.5 \text{ feet.}$$

3.6.1 Regular Wave Results

Figure 3-12 shows the first- and second-order pitch springing moments for TLP #1 with the two stated pitch center locations. It is seen from this figure that at the natural period the second-order pitch moment is reduced by a factor of about 10 by decreasing the pitch center to 25% of the design value. The first-order moment is reduced by a factor of about 50.

Table 3-4 shows the pitch moment amplitude values at the natural period as obtained from Figure 3-12. Also shown in Table 3-4 are the tendon tension loads due to these pitch moment values. The loads have been obtained using the nonlinear relationship between the pitch moment and tension loads as given by Figure 3-4. It is seen from the tendon tension values given in Table 3-4 that the second-order tendon tension load is reduced from 1020 kips to 240 kips by decreasing the pitch center to 25% of the design value. Similarly, the first-order tendon tension load is reduced from 470 kips to 24 kips.

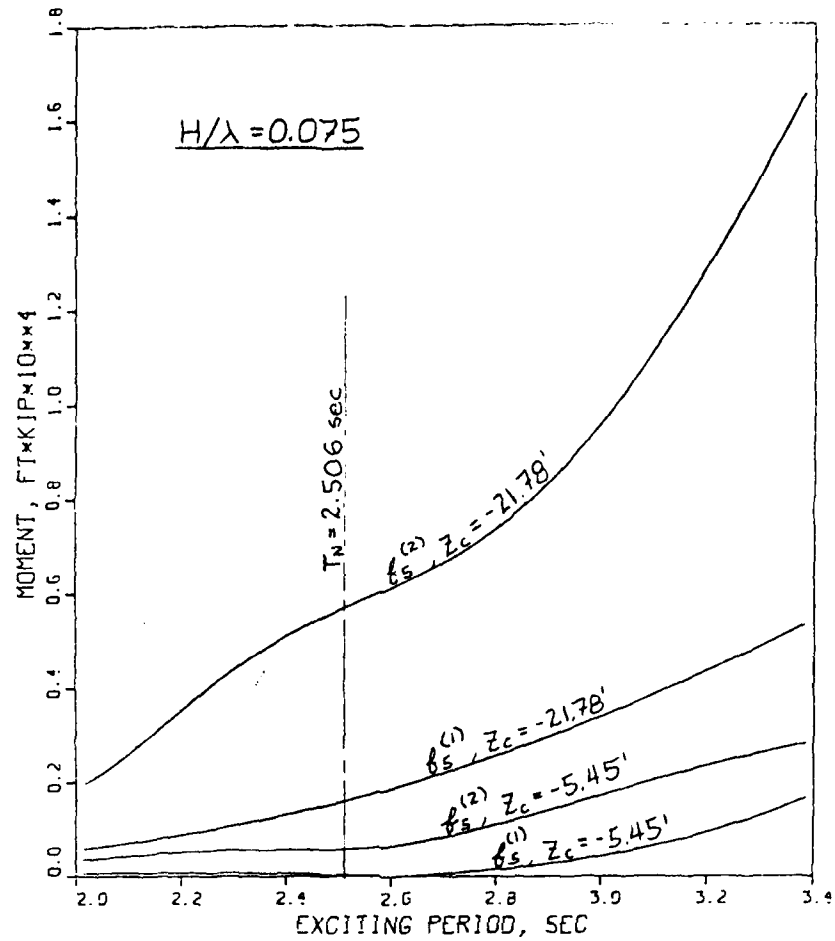

Figure 3-12. First- and second-order pitch moments for pitch center z_c = -21.78 ft and z_c = -5.45 ft.

	T_n = 2.506 sec			
	z_1 = -21.8 ft		z_2 = -5.5 ft	
	f_5, ft·kip	τ, kip	f_5, ft·kip	τ, kip
First-Order Single-Wave Excitation, H/λ = 0.075	1600	470	30	24
Second-Order Single-Wave Excitation, H/λ = 0.075	5680	1020	580	240

Table 3-4. Pitch moment amplitudes, f_5 and tendon tension loads, τ, due to first- and second-order excitation at the natural period for vertical pitch center at z_1 = -21.8 ft and at z_2 = -5.5 ft.

3.6.2 Irregular Wave Results

Figure 3-13 shows the power spectra for the second-order pitch springing exciting moments for the two pitch center locations. It is seen that the second-order power spectrum has been reduced by an order of magnitude by decreasing the pitch center to 25% of the design value.

Table 3-5 shows the RMS values for the tendon tension response for the two pitch-center locations. It is seen that there is a large reduction in the tendon tension RMS values for the contribution from the high frequency range. However, for the low frequency range, where the loads are dominated by first-order excitation, there is actually a substantial increase in the tendon tension when the pitch center is decreased to 25% of the design value. The reason for this difference between the high frequency and the low frequency range is that the high frequency range excitation is caused by short waves with exciting force locations close to the free surface, whereas the low frequency excitation is caused by longer waves with exciting force locations below the design pitch center. Hence, in the low frequency range the pitch exciting moments are actually increased when the pitch center is moved closer to the free-surface.

In summary, the pitch center investigation results show that a very effective way to reduce the second-order tendon tension springing loads is to move the pitch center closer to the free surface level. However, the first-order tendon loads in the low frequency range will most likely increase by moving the pitch center closer to the free surface. Therefore, it is very difficult to determine if it is advantageous to move the pitch center location. A careful investigation of the first- and second-order tendon load results for both the high and the low frequency ranges is required before any judgment with regard to the pitch center location can be made.

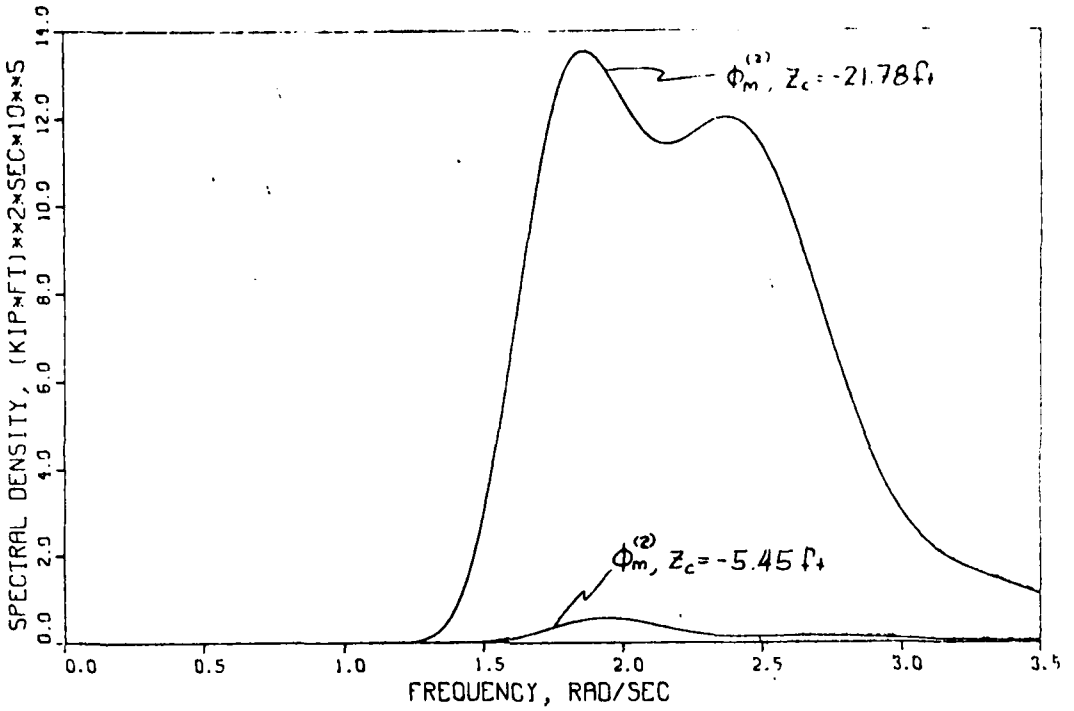

Figure 3-13. Second-order pitch exciting moment power spectra for pitch center z_c = -21.78 ft and z_c = -5.45 ft.

	RMS values for the tendon tension response spectrum, σ_τ in kips			
	High Frequency Range		Low Frequency Range	
	z_1 = -21.8'	z_2 = -5.5'	z_1 = -21.8'	z_2 = -5.5'
First-Order Contribution	24.7	5.7	37.6	59.6
Second-Order Contribution	44.5	5.0	0.0	0.0
Total	50.9	7.6	37.6	59.6

Table 3-5. First- and second-order contributions to RMS values for the tendon tension response spectrum for the high and low frequency ranges for vertical pitch center at z_1 = -21.8 ft and z_2 = -5.5 ft.

3.7 TLP Size Investigation

In this section we shall compare springing results for the TLP #1 and TLP #2 designs. A detailed description of the two TLPs is included in Appendix A. Note that TLP #2 is 1.2 times larger than TLP #1 and that TLP #1 is assumed to be designed for 2000-foot depth whereas TLP #2 is designed for 3000-foot depth.

3.7.1 Regular Wave Results

Figure 3-14 shows the first- and second-order pitch moment for TLP #1 and TLP #2 in regular waves with wave steepness, $H/\lambda = 0.075$. It is seen that the pitch moments are somewhat larger for the larger TLP. However, more importantly is the fact that the natural period for the larger, deep-water TLP #2 is 3.134 sec, whereas for the smaller TLP #1 it is only 2.506 sec. The longer waves exciting TLP #2 at its natural period have much more energy than the shorter waves exciting TLP #1 at its natural period.

The numerical values for the pitch moment amplitudes and the resulting tension loads at the natural periods are presented in Table 3-6. It is seen that the second-order pitch moment for TLP #2 is about three times as large as for TLP #1 and that the resulting tendon loads for TLP #2 are about twice as large as for TLP #1.

These results seem to indicate that the springing problem is much more critical for a deep-water TLP with a higher natural period.

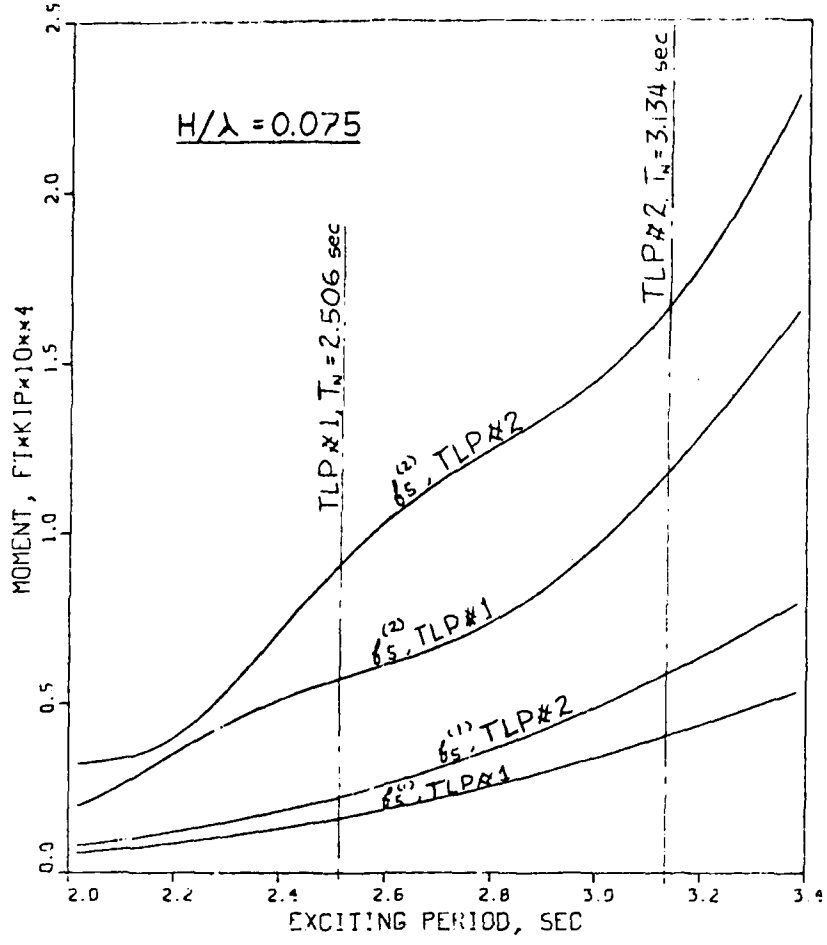

Figure 3-14. First- and second-order pitch moments for TLP #1 and TLP #2, $H/\lambda = 0.075$.

	TLP #1 T_n = 2.506 sec		TLP #2 T_n = 3.134 sec	
	f_5, ft kip	τ, kip	f_5, ft kip	τ, kip
First-Order Single Wave Excitation, $H/\lambda = 0.075$	1600	473	5820	1012
Second-Order Single Wave Excitation, $H/\lambda = 0.075$	5680	1017	16530	1883

Table 3-6. Pitch moment amplitude, f_5, and tendon tension load, τ, for TLP #1 and TLP #2 due to first- and second-order excitation at the natural periods for the individual platforms.

3.7.2 Irregular Wave Results

Figure 3-15 shows the power spectrum for the second-order pitch springing exciting moment for both TLP #1 and TLP #2. It is seen that at the natural frequencies for the two platforms the value of the power spectrum is about twice as large for TLP #2 as for TLP #1.

Table 3-7 shows the RMS values for the tendon tension response for both TLP #1 and TLP #2. It is seen that the RMS values are somewhat larger for the larger TLP, but not as much larger as the springing exciting moments.

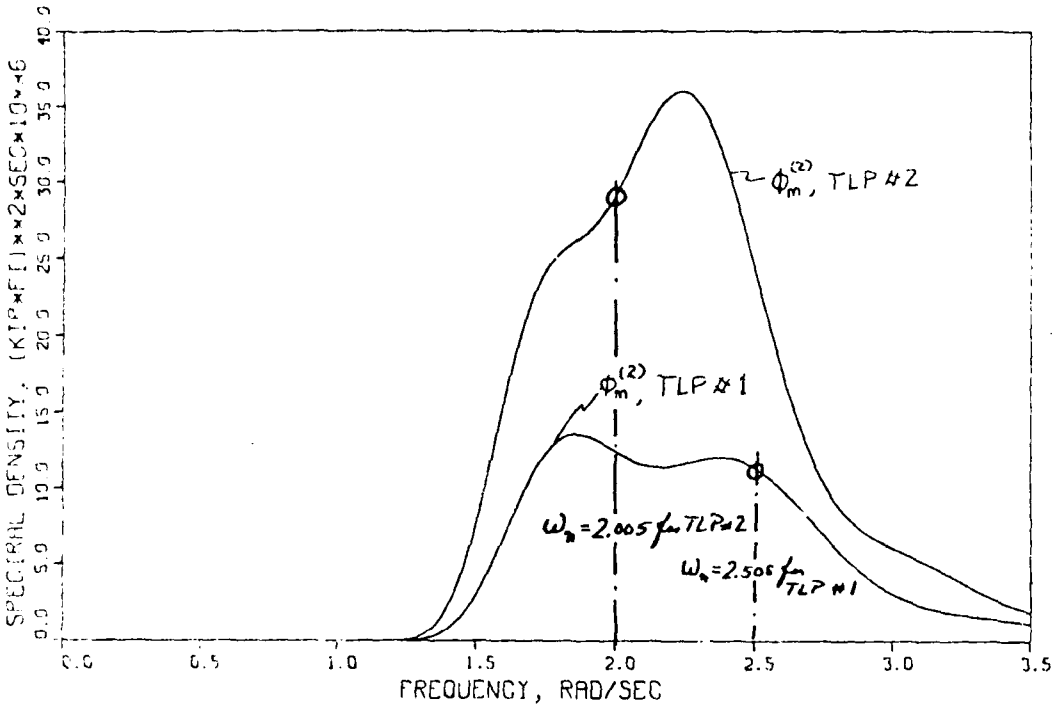

Figure 3-15. Second-order pitch exciting moment power spectra for TLP #1 and TLP #2.

	RMS values for the tendon tension response spectrum, σ_T in kips			
	High Frequency Range		Low Frequency Range	
	TLP #1	TLP #2	TLP #1	TLP #2
First-Order Contribution	24.7	71.9	37.6	40.5
Second-Order Contribution	44.5	51.8	0.0	0.0
Total	50.9	88.6	37.6	40.5

Table 3-7. First- and second-order contributions to RMS values for the tendon tension response spectrum for the high and low frequency ranges for TLP #1 (λ = 1.0) and TLP #2 (λ = 1.2).

4.0 REDUCED NUMBER OF TENDONS INVESTIGATION

4.1 Objective

The main objective of this part of the project has been to investigate the surge motions and the tendon tension loads for the case of tendon failure, i.e. only three tendons for one of the legs.

4.2 Non-Rigid TLP Structure

First, it shall be assuemd that the TLP is not completely rigid so that all of the loads from the broken tendon are taken up by the three remaining tendons at that leg.

4.2.1 Maximum External Loading

If we let t_o equal the pretension value per tendon for a normal operational condition, then the pretension value for each of the three remaining tendons is

$$t_o^* = 1.33\ t_o. \tag{4-1}$$

We shall use an asterisk to indicate that the value is for the case with one tendon removed. We shall assume that the tendons are designed to take an additional loading equal to the pretension value. This implies that the maximum total loading at the leg with three tendons is

$$3t_{max} = 6\ t_o. \tag{4-2}$$

Subtracting the pretension value for these three tendons we have that the total additional loading which can be taken up by these three tendons is

$$6t_o - 3t_o^* = 2t_o. \tag{4-3}$$

Since the total additional maximum loading at a leg with four intact legs is

$$4t_{max} = 4t_o \tag{4-4}$$

it is seen by comparing (4-3) and (4-4) that the leg with three tendons can only experience half the external loads as a leg with four tendons if it is required that the total load per tendon shall not exceed a value which is twice the pretension value.

4.2.2 Surge Motion Characteristics

If we consider the coefficients and the exciting forces for the surge equation of motion (see equation (3-1)) it is easily recognized that the mass, added mass and damping coefficient will remain about the same with one less tendon. Similarly, the excitation forces will be about the same. There will be some reduction in the viscous drag due to the elimination of one tendon; however, this effect is small compared to the total viscous force. Also note that the (linear) surge restoring coefficient which is given by

$$C_{11} = (T_o - \frac{w_t}{2}) \frac{1}{\ell} \tag{4-5}$$

will be approximately the same. Here T_o, which is the total pretension value, is unchanged and w_t, which is the weight of the tendons, is only reduced by about 6%. Note also that the $w_t/2$ term is small relative to the T_o term.

It can be concluded, therefore, that the surge motion characteristics of the TLP will remain practically the same with one less tendon. No additional computations are needed to confirm this.

4.2.3 Springing Loads

If we consider the heave restoring coefficient separately for each of the four legs, we have that the heave restoring coefficient for the leg with three tendons is 75% of the restoring coefficient for the other legs, hence

$$*C_{33}^{leg} = 0.75\ C_{33}^{leg}. \tag{4-6}$$

This implies that the natural heave period for the leg with three tendons is

$$T_n^* = T_n/\sqrt{0.75} = 1.15 \cdot T_n \tag{4-7}$$

where T_n is the natural heave period for the other three legs. Hence, the leg with only three tendons has a 15% larger natural period than the other legs.

The springing laods are caused by vertical motions at the individual legs resulting from natural frequency pitch motions of the total TLP. With three legs having a natural period of T_n and one leg having a natural period equal to 1.15 T_n, it is clear that the pitch motion will not have a single distinct natural pitch period. Therefore, it can be concluded that the springing load problem which is mainly due to a very distinct natural frequency will not be as critical as it is for the case with all of the tendons intact.

4.3 Rigid TLP Structure

It shall now be assumed that the TLP structure is completely rigid and that the load from the broken tendon is taken up by all of the remaining 15 tendons. If we use a numbering system as shown in Figure 4-1 where leg #1 is the leg with only three tendons, we have that the pretension value is increased as shown below:

	Pretension Increase
Three tendons at leg #1	25%
Eight tendons at legs #2 and #3	6.25%
Four tendons at leg #4	-6.25%

In this case the maximum external load which the total platform can experience is 56% of the load if can experience with all of the tendons intact if it is assumed that the maximum design load per tendon is twice the pretension value. This result was obtained by recognizing that the three tendons at leg #1 can only experience an additional load given by

$$3(0.75\ t_o) = 2.25\ t_o \tag{4-8}$$

whereas four intact tendons are designed for 4 t_o additional load.

Again, for the rigid TLP case the surge motion characteristics will be practically unchanged by eliminating one single tendon.

The springing problem in this case becomes a little more complicated. First, it can be shown that the pitch center will move a distance of 0.047 L (where L is the leg spacing) as shown in Figure 4-1. Furthermore, it can be shown that the pitch restoring coefficient for the case of one less tendon is

$$C^*_{55} = 0.864\ C_{55} \tag{4-9}$$

where C_{55} is the restoring coefficient with the tendons intact. The pitch natural period will be

$$T^*_n = \frac{1}{\sqrt{0.864}}\ T_n = 1.076\ T_n \tag{4-10}$$

where T_n is the intact pitch period.

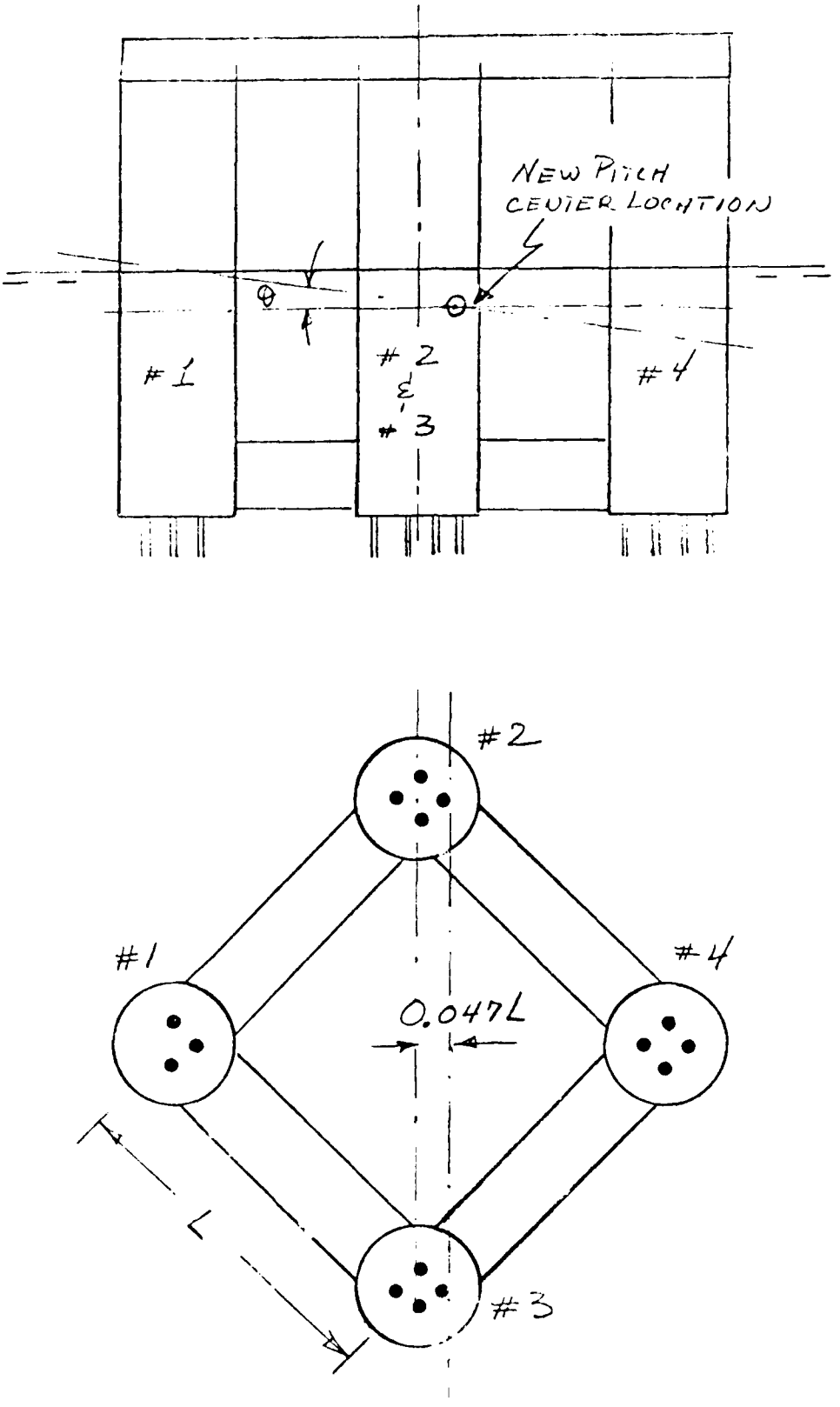

Figure 4-1. TLP with only three tendons at leg #1 and location of new pitch center.

AD-A159 778 NONLINEAR MOTIONS AND FORCES ON TENSION LEG PLATFORMS 2/2
(U) SCIENCE APPLICATIONS INC ANNAPOLIS MD
N SALVESEN ET AL. MAY 84 USCG-M-84-4 DTCG23-83-C-20064
UNCLASSIFIED F/G 13/10 NL

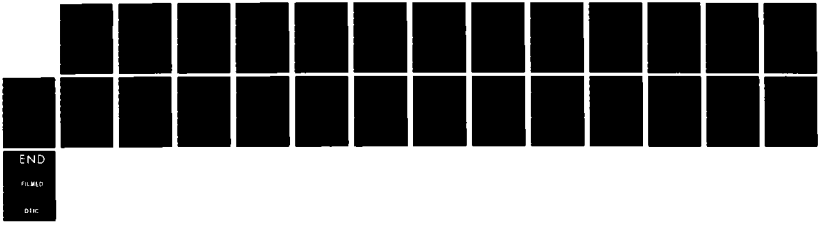

END
FILMED
DTIC

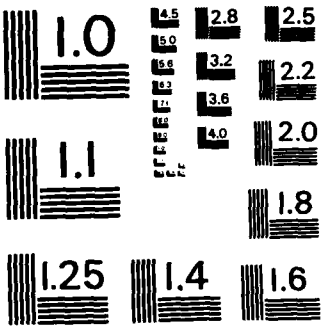

MICROCOPY RESOLUTION TEST CHART
NATIONAL BUREAU OF STANDARDS-1963-A

Consider springing tendon tension loads caused by natural frequency pitch motions excited by second-order wave-induced forces. Since the second-order excitation is proportional to the wave height squared, and the wave height is proportional to the period squared (assuming a fixed wave slope, i.e., H/ equal to a constant), it follows that the second-order pitch springing moment at a natural period equal to 1.076 T_n is approximately

$$f_5^* = (1.076)^4 \cdot f_5 = 1.34\ f_5 \tag{4-11}$$

where f_5 is the pitch moment at a natural period equal to T_n. In other words, the pitch springing moment in this case is about 34% larger.

For natural frequency motions with all of the tendons intact, the pitch angle is given by (see Section 3.2.2)

$$\theta = f_5/\omega_n\ B. \tag{4-12}$$

For the case with one tendon removed, the pitch angle is

$$\theta^* = f_5^*/\omega_n^*\ B. \tag{4-13}$$

It can be assumed that the damping, B, remains the same. Since the new natural frequency is

$$\omega_n^* = 0.929\ \omega_n \tag{4-14}$$

it follows from equation (4-13) by introducing equations (4-11) and (4-14) that

$$\theta^* = (1.34 \cdot f_5)/(0.929\ \omega_n)B = 1.44\theta.$$

Hence the pitch angle will be 44% larger than for the intact case. The loading in the tendons is proportional to the pitch angle

$$\tau = \alpha\theta$$

where the proportionality factor, α, for the case with one less tendon is

$$\alpha^* = 1.067 \cdot \frac{4}{3}\alpha = 1.42\alpha.$$

Therefore, the springing tendon tension per tendon at leg #1 will be

$$\tau^* = \alpha^* \cdot \theta^* = 1.42\alpha \cdot 1.44\theta = 2.04\tau.$$

This implies that if we consider regular wave springing excitation, the TLP with one less tendon will experience tendon laods at the leg with only three tendons which are 2.04 times the springing load in the tendons for a TLP with all of the tendons intact.

Now considering that the pretension value for the three tendons at leg #1 has already been increased by 25%, it seems as if the additional loading due to springing can become quite critical for the case with one less tendon.

5.0 REFERENCES

Aranha, J.A., C.C. Mei and D.K. Yue, "Some Properties of a Hybrid Element Method for Water Waves," International Journal for Numerical Methods in Engineering, Vol. 14, 1627-1642, 1979.

MacCamy, R.C., and R.A. Fuchs, "Wave Forces on Piles: A Diffraction Theory," Technical Memorandum No. 69, U.S. Army Corps of Engineers, Beach Erosion Board, Washington, D.C., 1954.

Maruo, H., "The Drift of a Body Floating on Waves," Journal of Ship Research, Vol. 4, 1-10, 1960.

Newman, J.N., "The Drift Force and Moment on Ships in Waves," Journal of Ship Research, Vol. 11, 51-60, 1967.

Salvesen, N., C.H. von Kerczek, D.K. Yue and F. Stern, "Computations of Nonlinear Surge Motions of Tension Leg Platforms," Paper #4394, 14th Offshore Technology Conference, Houston, Texas, 1982.

Salvesen, N., D.K. Yue, C.P. Cressy and C.H. von Kerczek, "Wave-Induced High-Frequency Springing Loads on Tension Leg Platforms," SAI Report #463-83-467-LJ, supported by SAI IR&D funds, 1983.

Yue, D.K., H.S. Chen and C.C. Mei, "Three-Dimensional Calculations of Wave Forces by a Hybrid Element Method," Proc. 11 Symp. Naval Hydrodynamics, Office of Naval Research, 1976.

Appendix A

PRINCIPAL DIMENSIONS AND NATURAL PERIODS FOR TLP #1 AND TLP #2

Two TLP designs are considered in this investigation. They are referred to as TLP #1 and TLP #2 with the following principal dimensions:

	TLP #1	TLP #2
Vertical Leg Diameter, D_1	57.0 ft	69.0 ft
Pontoon Diameter, D_2	31.0 ft	37.0 ft
Leg Centerline Spacing, L	220.0 ft	260.0 ft
Draft of Leg, H	121.0 ft	145.0 ft
Depth to Ocean Floor, d	2000.0 ft	3000.0 ft

Note that the two platforms have the same geometry with a scaling factor of approximately 1.2; however, the depth for TLP #2 is 1.5 times the depth for TLP #1. The two TLPs have a configuration as shown in Figure A-1 with four vertical legs connected with four horizontal pontoons and some kind of deck structure. In addition to this main structure, there is also an appropriate number of braces for which volume and mass are included by adding an estimated percentage factor. In the hybrid-finite-element method (HFEM) computations only the legs and the pontoons have been included. There are four vertical tendons at each of the four legs.

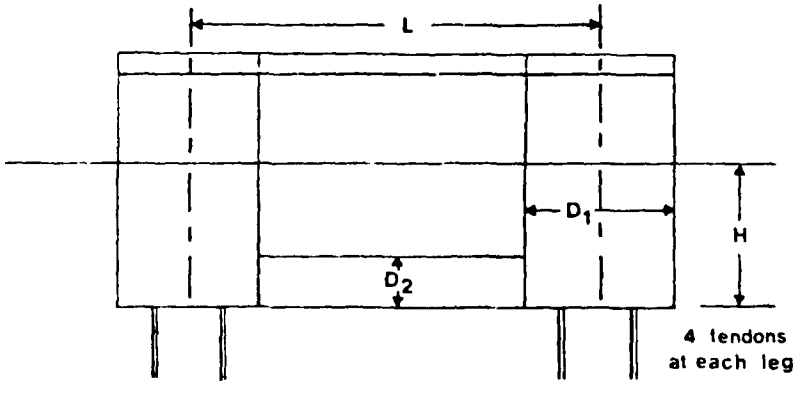

Figure A-1. TLP Geometry.

The buoyancy of TLP #1 is

$$\Delta_B = 116{,}880 \text{ kips}$$

and the total pretension value (including tendons and risers) is

$$T_o = 40{,}100 \text{ kips}$$

with the weight given by

$$W_o = \Delta_B - T_o = 76{,}700 \text{ kips.}$$

The total weight of the tendons and risers in air is

$$w_a = 13{,}900 \text{ kips}$$

and in water

$$w_w = 12{,}700 \text{ kips.}$$

The effective mass of the total TLP system is

$$M = (W_o + \frac{w_a}{2}) \frac{1}{g} = 2.60 * 10^6 \text{ slugs}$$

and the surge restoring coefficient is

$$C_{11} = (T_o - \frac{w_w}{2}) \frac{1}{\ell} = 18.32 \text{ kips/ft}$$

where

$$\ell = d - H - \varepsilon = 1840 \text{ ft.}$$

Here $\varepsilon = 39$ is the height of the bottom tendon mounting.

From the HFEM calculations presented in Figure 2-29, the surge added mass value for large periods is

$$A_{11} = 2.63 * 10^6 \text{ slugs.}$$

Hence, the surge natural period is

$$T_{11} = 2\pi\sqrt{\frac{A_{11} + M}{C_{11}}} = 106.12 \text{ sec.}$$

The heave restoring coefficient which depends on the tendon material and the tendon cross-sectional area shall be assuemd to be

$$C_{33} = 21.1 * 10^6 \text{ lb/ft.}$$

The heave added mass is

$$A_{33} = 1.44 * 10^6 \text{ slugs}$$

and the heave natural period is

$$T_{33} = 2\pi\sqrt{\frac{A_{33} + M}{C_{33}}} = 2.738 \text{ sec.}$$

The pitch restoring coefficient is approximately

$$C_{55} \approx (L/2)^2 C_{33} = 25.53 * 10^{10} \text{ ft-lb.}$$

It is assumed that the pitch center (the vertical center of the virtual mass) is

$$z_c = 21.8 \text{ feet}$$

below the water level and that the virtual pitch mass moment of inertia about this center is

$$M_{55} + A_{55} = 4.06 * 10^{10} \text{ slugs-ft}^2$$

and hence the pitch natural period is

$$T_{55} = 2\pi\sqrt{\frac{M_{55} + A_{55}}{C_{55}}} = 2.506 \text{ sec.}$$

All of the above results are for TLP #1. Table A-1 shows the results for both TLP #1 and TLP #2.

Table A-1. Mass, restoring coefficients, and natural periods for TLP #1 and TLP #2.

	TLP #1	TLP #2
Buoyancy, Δ_B (kips)	116,800	202,000
Pretension, T_o (kips)	40,100	69,000
Weight, W (kips)	76,700	113,000
Tendon weight in air, w_a (kips)	13,900	23,200
Tendon weight in water, w_w (kips)	12,700	21,900
Mass, M (slugs)	$2.60 * 10^6$	$4.44 * 10^6$
Surge restoring coef., C_{11} (kips/ft)	18.32	20.7
Surge added mass, A_{11} (slugs)	$2.63 * 10^6$	$4.28 * 10^6$
Surge natural period, T_{11} (sec)	106.12	128.96
Heave restoring coef., C_{33} (lb/ft)	$21.1 * 10^6$	$24.05 * 10^6$
Heave added mass, A_{33} (slugs)	$1.44 * 10^6$	$2.64 * 10^6$
Heave natural period, T_{33} (sec)	2.738	3.37
Pitch restoring coef., C_{55} (ft-lb)	$25.53 * 10^{10}$	$40.6 * 10^{10}$
Pitch center location, z_c (ft)	21.8	26.2
Pitch virtual mass, $M_{55} + A_{55}$ (slg-ft^2)	$4.06 * 10^{10}$	$10.1 * 10^{10}$
Pitch natural period, T_{55} (sec)	2.506	3.13

Appendix B

DETERMINATION OF SWAY DISPLACEMENT COMPONENTS BY SAI AND QUADRATIC DRAG FORMULAS

B.1 Computer Run Descriptions

A systematic series of computer runs was performed with the non-linear time-domain surge motion computer code. The individual surge displacement components were determined in order to evaluate the differences in each component using the SAI and quadratic drag formulas, and for TLP #1 and TLP #2. The following current, wind and wave conditions were selected for this investigation:

(i) Current - The current was input as a function of depth below the free surface as follows:

Z, ft	Current, knots
0.	2.70
121.	1.70
1000.	0.60
2000.	0.30

(ii) Wind - Steady wind: W_s = 70 knots
Unsteady wind: W_{us} = 7 knots $\cos\omega_n t$
where ω_n is the natural frequency of the system.

(iii) Waves - Maximum design wave: H = 80 ft, T = 14.0 sec
For this wave, the primary wave exciting force and phase are

$$F_E^{(1)} = 22{,}870 \text{ kips and } \epsilon^{(1)} = 1.596$$

The steady second-order drift force is

$$F^{(2)} = 36 \text{ kips.}$$

For the given wind conditions, with steady and unsteady components present, the wind force is

$$F_w = 960 \text{ kips} + 191 \text{ kips } \cos\omega_n t.$$

The computer runs were conducted both with the SAI drag formula (referenced by the letter "A") and the quadratic drag formula (referenced by the letter "B"). The following runs were performed:

1A and B	Current alone (no wind or waves)
2A	Maximum design wave, primary excitation only (no drift force, current or wind)
3A	Maximum design wave (primary excitation only), with integration up to the disturbed free surfece (no drift force, current or wind)
4A and B	Current and maximum design wave, primary excitation only (no wind or drift force)
5A and B	Current, maximum design wave including steady drift and steady wind (no unsteady wind)
6A	Unsteady wind only (no current, wave or steady wind)
7A and B	Current and unsteady wind (no wave or steady wind)

8A and B — Maximum design wave (primary excitation only) and unsteady wind (no drift force or steady wind)

9A and B — Current, maximum design wave including steady drift, steady and unsteady wind

The conditions stated above are tabulated in Table B-1.

Table B-1. Conditions used for surge-displacement component investigation.

Run #	Drag Formula		Current	Wave		Wind	
	SAI	Quad		Unsteady Primary	Steady Drift	Steady	Unsteady
1A			✓				
1B		✓	✓				
2A	✓			✓			
3A	✓			✓*			
4A	✓		✓	✓			
4B		✓	✓	✓			
5A	✓		✓	✓	✓	✓	
5B		✓	✓	✓	✓	✓	
6A	✓						✓
7A	✓		✓				✓
7B		✓	✓				✓
8A	✓			✓			✓
8B		✓		✓			✓
9A	✓		✓	✓	✓	✓	✓
9B		✓	✓	✓	✓	✓	✓

* Integration up to free surface

B.2 Discussion of Results

The numerical results for the cases stated above are given in Table B-2, in terms of the steady state amplitudes of surge at the wave frequency, the natural frequency and the steady surge. The corresponding time-domain plots of the surge motion are shown in Figures B-1 through B-9.

Runs 1A and 1B

Figure B-1 shows the surge response for runs 1A and 1B with current only. As should be expected, the final steady displacement is the same for both the SAI and quadratic drag formulas,

$$X_0 = 14.4 \text{ feet.}$$

The only difference between the results for the two current only cases is the transient motions die much slower with the SAI drag than the quadratic. It is believed that the quadratic drag dies out much too rapidly.

Run 2A

Figure B-2 shows the results for Run 2A, regular maximum wave only (no drift force). It is seen that the primary motion amplitude is

$$X_1 = 22.1 \text{ feet.}$$

Note that this primary motion amplitude remains the same throughout these computations which shows (as we had expected) that the primary motions are not in any way effected by the current or by the slowly-varying motions. Furthermore, viscous damping has an extremely small effect on these motions (less than 1%) and does not need to be included in primary motion predictions. The primary motions are dominated by inertia effects and hence are linear with respect to wave amplitude. This implies that linear superposition and linear statistics can be applied to the primary motions.

Run 3A

Figure B-3 shows the results for Run 3A. The only excitation is the primary wave excitation (no drift force), but in this case the hydrodynamic pressure is integrated over the instantaneous wetted surface area. It is seen that in this case there is an additional steady sway displacement

$$X_o = 7.7 \text{ feet.}$$

This is the maximum additional displacement due to integration over the instantaneous wetted surface rather than over the undisturbed wetted surface. The difference is so small that we shall not include this effect in any of the other computations.

Runs 4A and 4B

Figure B-4 shows the results for Runs 4A and 4B, current and primary wave excitation. It is seen that the quadratic damping formula predicts that the steady displacement is

$$X_o = 42.3 \text{ feet}$$

whereas the SAI drag formula predicts the steady displacement to be

$$X_o = 16.1 \text{ feet.}$$

The difference is due to the quadratic damping predicting a much larger additional drag force due to the interaction between the current and the primary and the wave-particle velocity than the SAI formula prediction.

In summary, the quadratic damping predicts that the displacement due to the current will be magnified by the primary motions by the factor

$$n = \frac{42.3}{14.4} = 2.94$$

comparisons for the linear results. It should also be kept in mind that the HFEM computations cost at least $6,000 per TLP configuration of which about $4,000 is for the computer time and $2,000 is for preparing the input data.

For the "Nonlinear Drift Forces and Surge Responses" (Part 2) extensive verification only exist for the second-order steady drift forces in regular waves (Part 2a). See for example Figure 2 of Salvesen et al. (1982) where three different theoretical approaches are compared with experimental results. Extensive comparisons between the drift forces computed for TLP configuration and experimental results have been preferred by Chevren, but these results are unpublished.

There is a great need for verification of:

- the nonlinear surge response (Part 2a), and
- the nonlinear springing forces and responses (Part 3a and b).

This is where we had hoped to perform some valuable new comparisons between theory and experiments. But there is almost a complete lack of published experimental data for controlled environmental conditions for which computations can be performed. In order that a useful validation can be performed, it is essential that not only precise geometry data be available, but also that the environmental condition be accurately known. It should be pointed out that we have not been able to locate any springing data whatsoever.

Appendix D

DISCUSSION OF COMPARISONS BETWEEN THEORY AND EXPERIMENTS

The computed TLP results presented in this report can be divided into three main parts:

Part 1: Linear Forces and Responses

Linear frequency-domain potential flow results obtained by the HFEM computer program. These results include added-mass coefficient, damping coefficient due to wave generation and first-order wave exciting forces and moments as well as the linear wave-frequency components of the motions.

Part 2: Nonlinear Drift Forces and Surge Responses

a) Second-order steady draft forces for regular waves
b) Nonlinear surge responses.

Part 3: Nonlinear Springing Forces and Responses

a) Second-order high-frequency springing forces in regular waves and in wave groups consisting of two regular waves.

b) High frequency springing response load in the tendexes.

A careful verification of all of these computed results would be desirable and in particular it would be useful to compare such results to experimental results. Fortunately, quite satisfactory comparisons have already been completed for the "Linear Forces and Responses" (Part 1). See for example the User's Manual for the HFEM Computer Program (Yue, 1982). In our opinion it would not be too valuable to perform extensive additional

For the SAI drag formula the following sectional viscous drag coefficients were used for all of the computations presented in this report. (Note that the drag coefficients were reduced due to sheltering effects in the same way as for the quadratic drag fomrula discussed on the previous page.)

Member	C_{Ds}	C_{D1}	C_{D2}
Legs	0.5	0.5	0.5
Pontoons	0.45	0.5	0.5
Horizontal Brace	0.4	0.7	0.65
Vertical Member	0.42	0.7	0.65
Diagonal Brace	0.4	0.7	0.6
Tendons: Top	0.7	0.55	0.5
Botton (1000 ft)	1.2	0.55	0.5

Appendix C

VISCOUS DRAG COEFFICIENTS

In all of the computations with the quadratic drag formula the following sectional viscous drag coefficients were used:

Legs

C_D = 0.50 for legs exposed to current

C_D = 0.25 for legs which are directly behind another leg

Pontoons

C_D = 0.45 for pontoons exposed to current

C_D = 0.45/2 for pontoons which are behind other pontoons

C_D = 0.20 for the smaller 10' horizontal member between the pontoons

Vertical Member

C_D = 0.42

Other Small Members

C_D = 0.40

Tendons and Risers

C_D = 0.60 at free surface for the risers

C_D = 0.60 at the bottom of the legs for the tendons

C_D = 1.20 at 1000-ft depth for both tendons and risers

The drag coefficient varies linearly from top to 1000-ft depth and is constant from 1000-ft depth and down to the bottom.

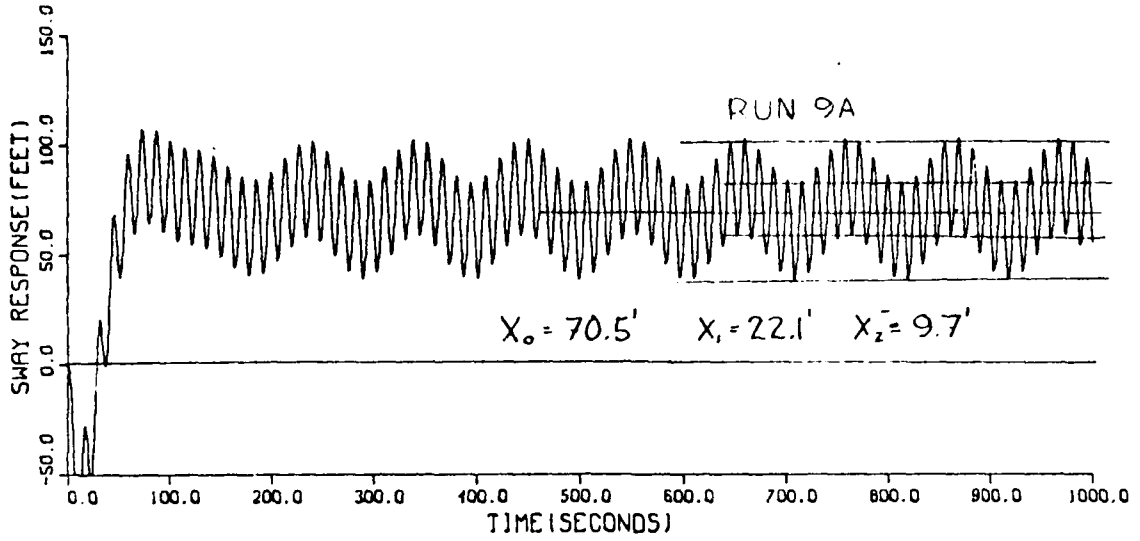

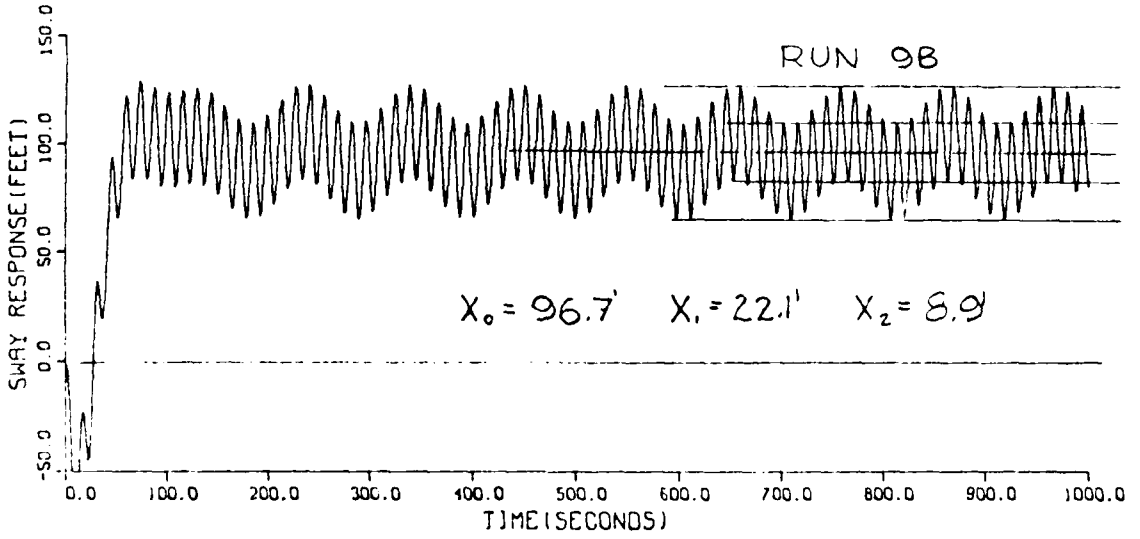

Figure B-9. Sway displacement for maximum regular wave, current, steady and unsteady wind and wave drift.

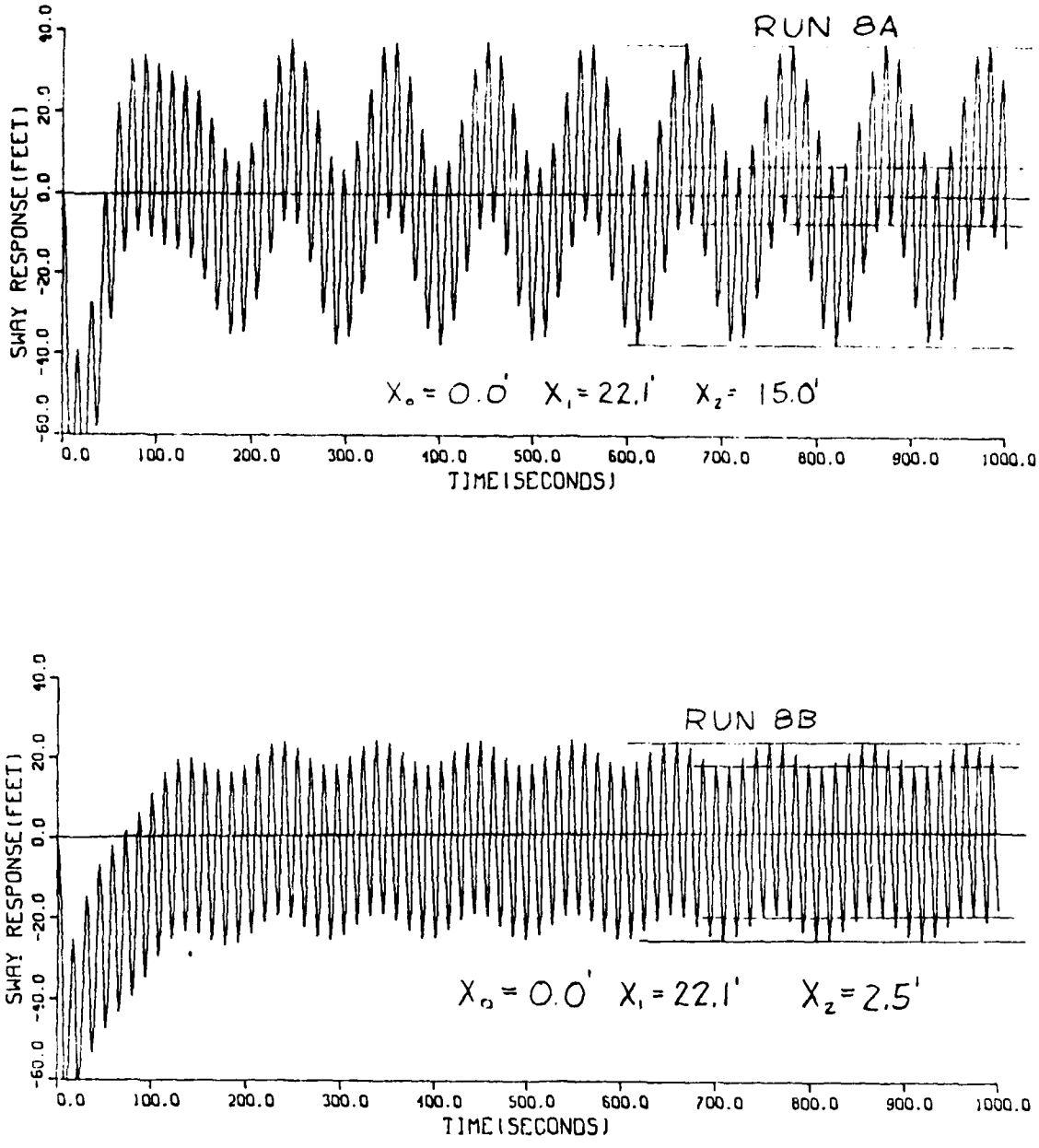

Figure B-8. Sway displacement for maximum regular wave and unsteady wind (no current, drift or steady wind).

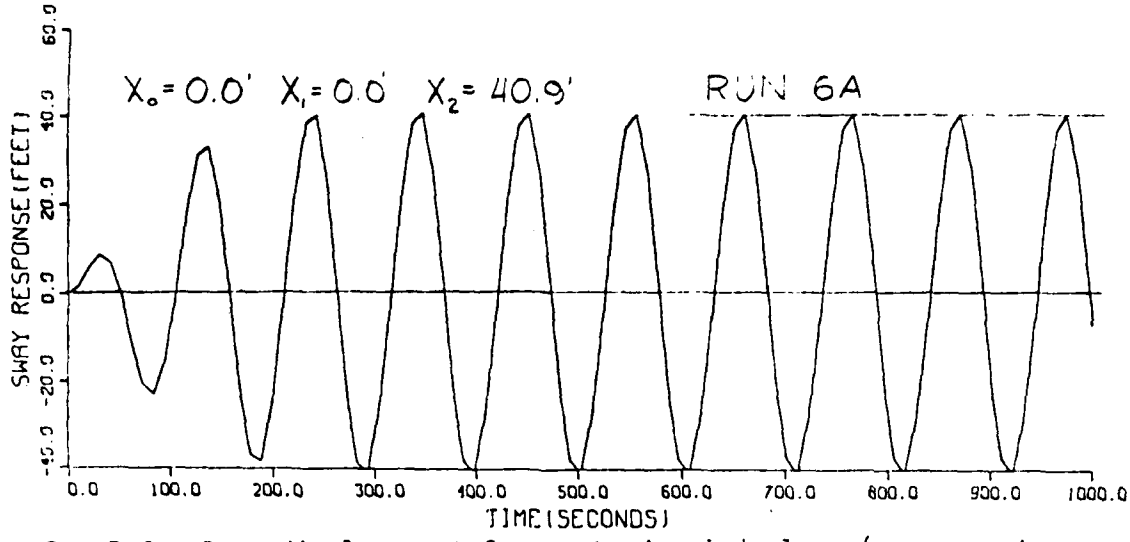

Run B-6. Sway displacement for unsteady wind alone (no current, waves or steady wind).

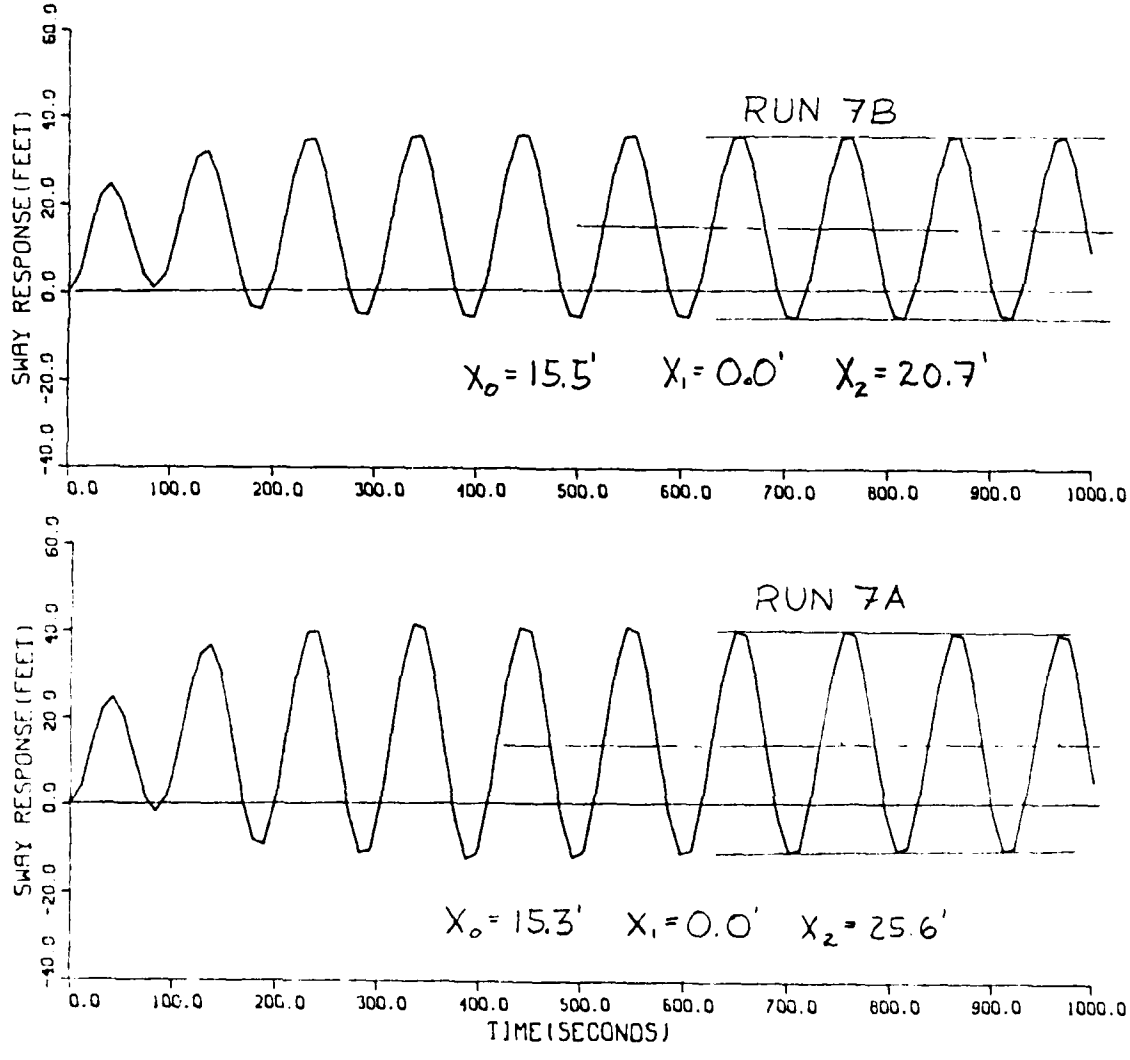

Figure B-7. Sway displacement for current and unsteady wind (no wave or steady wind).

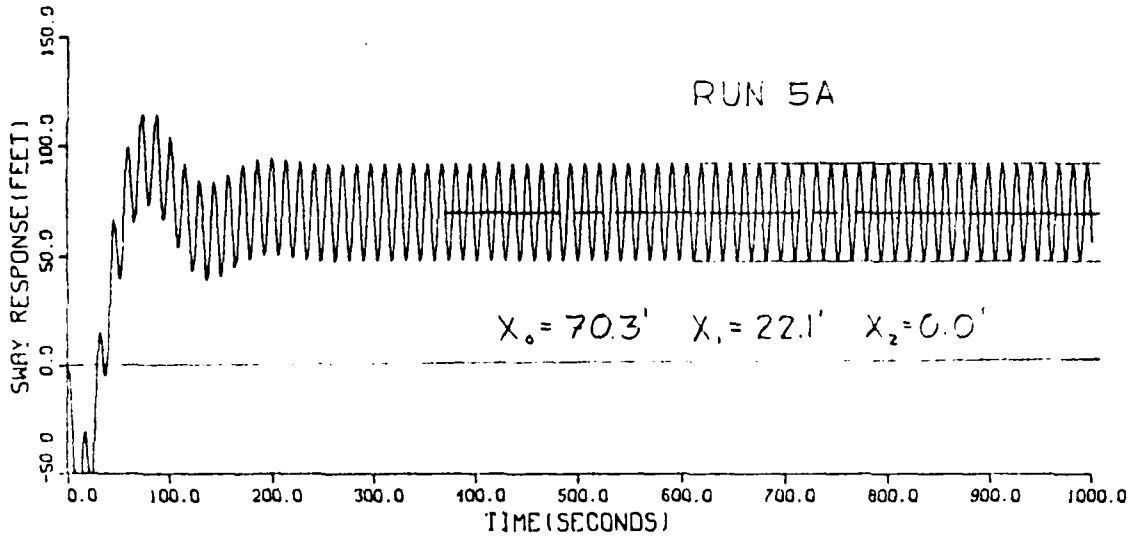

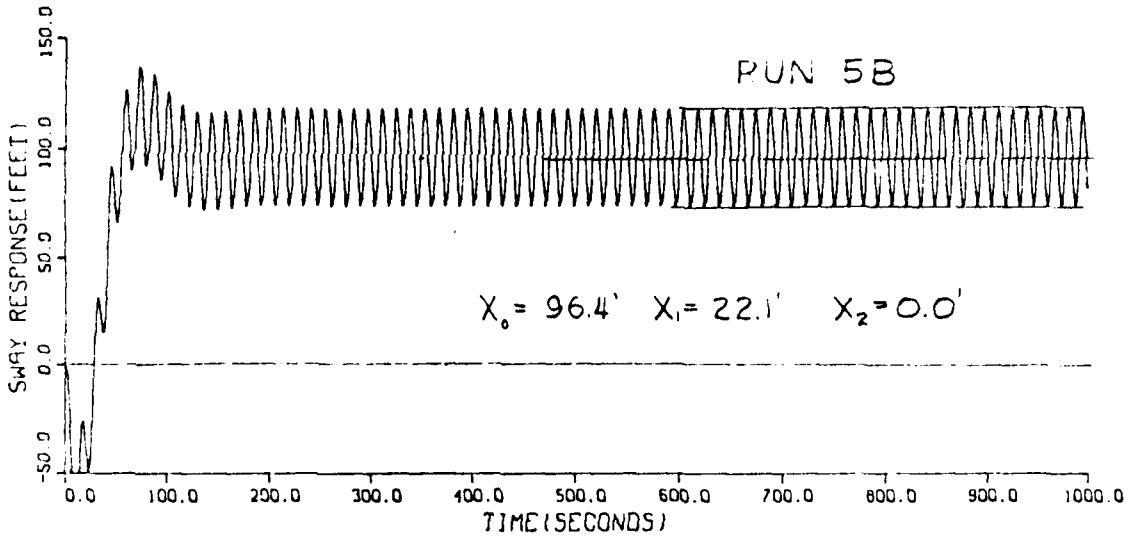

Figure B-5. Sway displacement for maximum regular wave, current, steady wind and wave drift force.

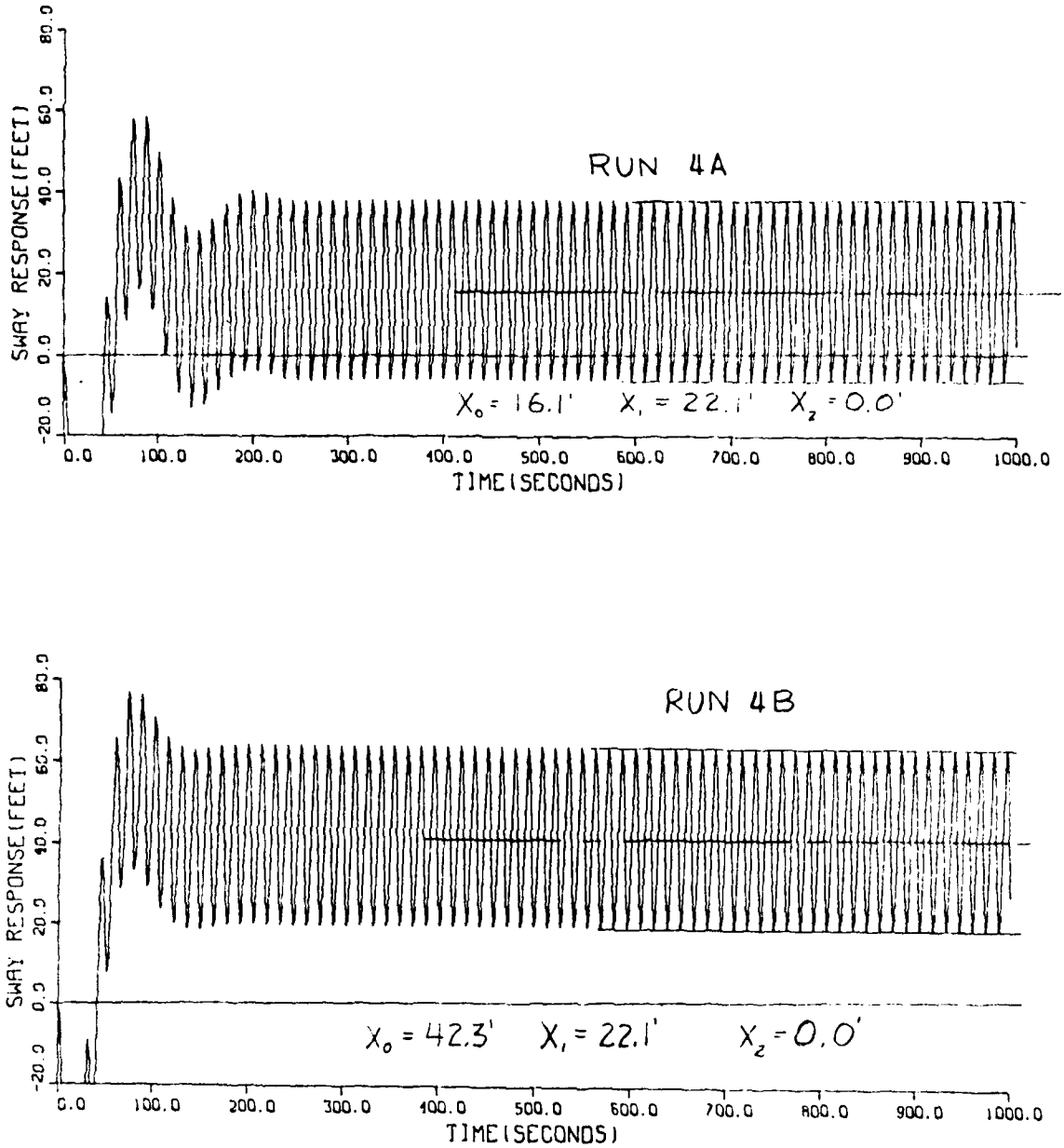

Figure B-4. Sway displacement for current and maximum regular wave (no wind or wave drift).

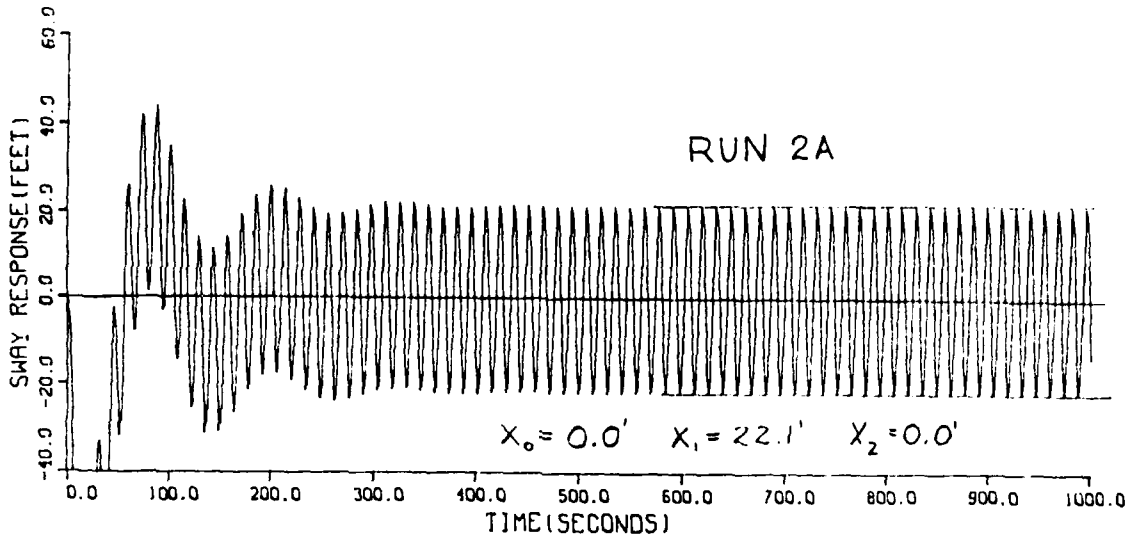

Figure B-2. Sway displacement for maximum regular wave only (no wind, current or wave drift force).

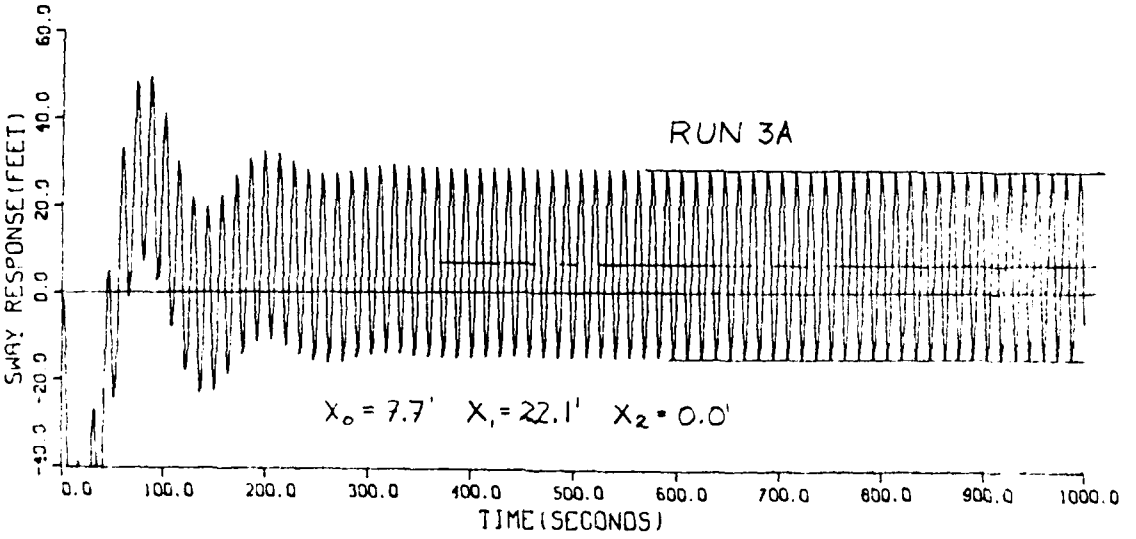

Figure B-3. Sway displacement for maximum regular wave only, with integration up to disturbed free surface level (no wind, current or wave drift force).

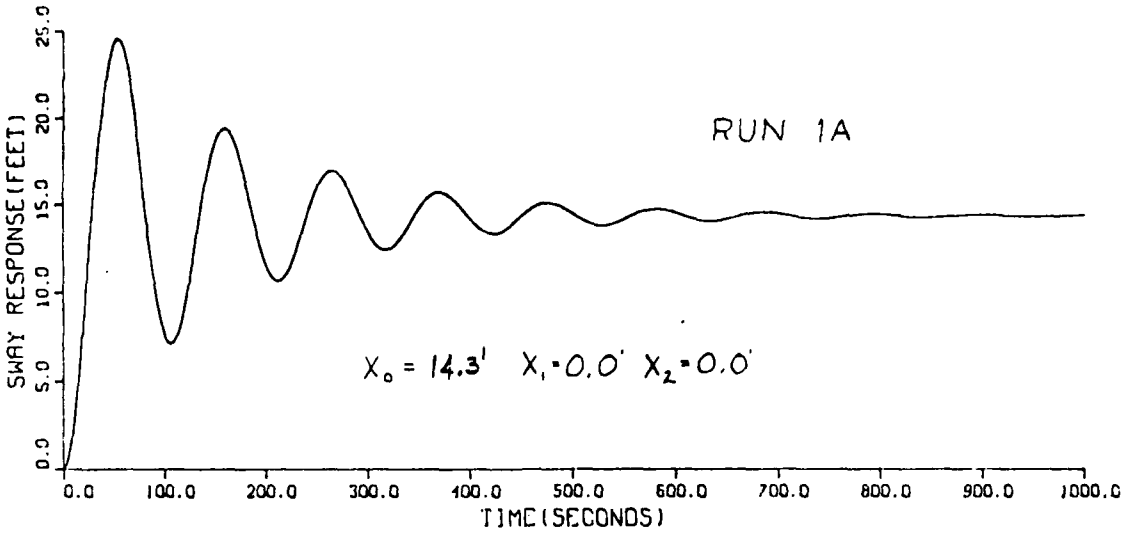

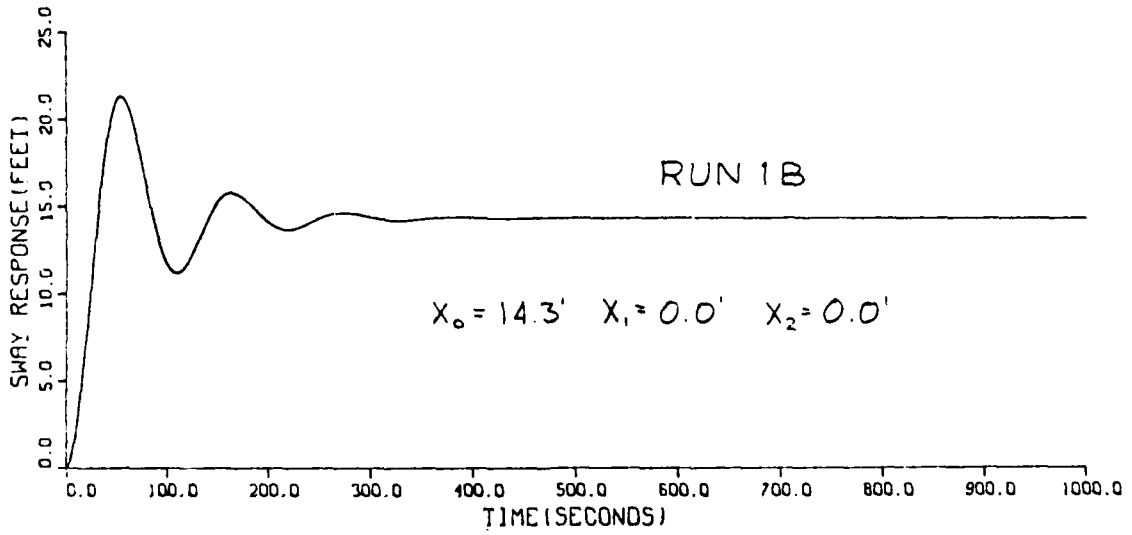

Figure B-1. Sway displacement for current alone (no wind or waves).

Table B-2. Surge displacement components

Run #	X_o, ft*	X_1, ft**	X_2, ft***
1A	14.4	0.0	0.0
1B	14.4	0.0	0.0
2A	0.0	22.1	0.0
3A	7.7	22.1	0.0
4A	16.1	22.1	0.0
4B	42.3	22.1	0.0
5A	70.3	22.1	0.0
5B	96.4	22.1	0.0
6A	0.0	0.0	40.9
7A	15.3	0.0	25.6
7B	15.5	0.0	20.7
8A	0.0	22.1	15.0
8B	0.0	22.1	2.5
9A	70.5	22.1	9.7
9B	96.7	22.1	8.9

* X_o = steady displacement
** X_1 = first-order (wave frequency) amplitude
*** X_2 = second-order (natural frequency) amplitude

Wave frequency = .450 rad/sec

Natural frequency = .600 rad/sec

smaller for the interaction between the low frequency motion and the current than for the high frequency motion and the current (see Runs 4A and 4B).

Runs 8A and 8B

The results for Runs 8A and 8B, with the maximum regular wave and the unsteady wind, are shown in Figure B-8. These runs show the interaction between the low and high frequency motions. Comparing with Run 6A, it can be seen that the low frequency motions are much reduced by the presence of the high frequency motions. For the SAI drag formula, the change in the low frequency amplitude is

$$X_2^1 = 15.0 - 40.9 = -25.9 \text{ feet (SAI drag)}$$

and for the quadratic drag,

$$X_2^1 = 2.5 - 40.9 = -38.4 \text{ feet (quadratic drag).}$$

Runs 9A and 9B

Figure B-9 shows the results for Runs 9A and 9B, including the maximum design wave, steady and unsteady wind, current and wave drift. By comparing with Run 5B, it can be seen that the low frequency motion has little effect on either the high frequency or the steady surge.

whereas the SAI displacement only shows a small increase. It is believed that the quadratic drag fomrula may be inadequate in predicting this interaction effect.

Runs 5A and 5B

Figure B-5 shows the results for Runs 5A and 5B, current, steady wind and maximum design wave, including the steady second-order drift force.

As expected, the increase in steady displacement is the same for both drag formulas,

$$\Delta X_o = 54.1 \text{ feet.}$$

The increase due to the wave drift force was about 2.0 feet, or approximately 9% of the primary motion amplitude.

Run 6A

Figure B-6 shows the motions for the unsteady wind only, Run 6A. The amplitude of the motion at the surge natural frequency is

$$X_2 = 40.9 \text{ feet.}$$

Runs 7A and 7B

Figure B-7 gives the results for Runs 7A and 7B with current and unsteady wind. Comparison with Run 6A shows the change in the low frequency motion due to the current. For the SAI drag formula, this change is

$$\Delta X_2^C = 25.6 - 40.9 = -15.3 \text{ feet (SAI drag)}$$

and for the quadratic drag the change is

$$\Delta X_2^C = 20.7 - 40.9 = -20.2 \text{ feet (quadratic drag).}$$

It can be seen that the discrepancy between the two methods is considerably

END

FILMED

11-85

DTIC